ALMA MATER STUDIORUM · UNIVERSITÀ DI BOLOGNA

Scuola di Scienze
Corso di Laurea Magistrale in Fisica

Climatological characterization and dynamics of barrier winds in the Italian region

Relatore:
Prof. Andrea Buzzi

Presentata da:
Enrico Di Muzio

Sessione III
Anno Accademico 2012/2013

Contents

List of Figures

Sommario

Il vento di barriera è un fenomeno meteorologico a mesoscala che interessa il flusso nei bassi strati atmosferici ed è dovuto all'interazione con un'orografia sufficientemente alta, quale una catena montuosa. In un'analisi adimensionale l'altezza dell'orografia viene quantificata tramite il numero di Froude orografico $\mathrm{Fr} = U/NH$, dove N rappresenta la stratificazione e U la velocità del flusso incidente. Se tale numero è sufficientemente piccolo si genera una sostanziale deviazione orizzontale del flusso incidente, associata a un aumento di pressione sul fianco sopravvento della catena montuosa. In taluni casi si può raggiungere uno stato quasi-stazionario, nel quale si riscontra un intenso vento parallelo all'orografia nei bassi strati, detto appunto vento di barriera, mentre più in alto il flusso incidente tende a superare la montagna.

Nel presente lavoro si è innanzitutto sviluppata una climatologia degli eventi di vento di barriera nella regione italiana su un periodo biennale. Gli eventi sono stati identificati e classificati principalmente sulla base della velocità del flusso incidente e della velocità e direzione del vento di barriera a 950 hPa, e per il numero di Froude valutato sopravvento. Si è poi realizzata una statistica per caratterizzare la distribuzione degli eventi rispetto al numero di Froude. La climatologia è risultata in buon accordo con la teoria idealizzata dei flussi sopra l'orografia, nei limiti della sua applicabilità ai casi reali, per la quale a numeri di Froude minori di 1 sono associati episodi di blocking e vento di barriera, mentre a numeri di Froude maggiori di 1 sono associati episodi di *flow-over* (flusso sopra l'orografia).

Tre casi di studio sono stati successivamente isolati e simulati utilizzando i modelli meteorologici BOLAM e MOLOCH, sviluppati presso l'istituto CNR–ISAC di Bologna. La caratterizzazione di ognuno degli eventi include il calcolo del numero di Froude upstream e dei parametri principali riguardanti il vento di barriera, quali velocità, spessore verticale ed estensione orizzontale, temperatura ecc. Per uno dei tre casi, riguardante le Alpi orientali e in particolar modo il Veneto, le simulazioni dei modelli sono state confrontate con dati osservati di vento, pressione, temperatura e precipitazione. Sono poi stati condotti dei *sensitivity tests* su ognuno degli eventi, alterando l'orografia gradualmente fino alla scomparsa del vento di barriera. In tal modo si è cercato da una parte di verificare l'importanza dell'effetto dell'orografia, dall'altra di associare l'intensità del fenomeno del vento di barriera al numero di Froude upstream, quantificando l'applicabilità della teoria idealizzata a casi reali. Un indice, denominato Barrier Wind Index (BWI) è stato ideato a tale scopo.

Le simulazioni effettuate hanno mostrato di essere in buon accordo con la teoria, indicandone i limiti di applicabilità all'atmosfera reale dovuti alla complessità, eterogeneità e mutevolezza che la caratterizzano rispetto ad una idealizzata. In particolare, è risultato che il Barrier Wind Index aumenta all'incirca linearmente al diminuire del numero di Froude al di sotto della valore soglia di 1. Le simulazioni hanno inoltre evidenziato l'elevata influenza del vento di barriera sulla circolazione atmosferica a mesoscala, sulla distribuzione e intensità della precipitazione e sull'avvezione di quantità di importanza meteorologica quali temperatura e umidità.

Abstract

Barrier wind is a meteorological mesoscale phenomenon generated by the interaction of low-level atmospheric flow with a sufficiently high orography, such as a mountain range. The height of the orography is expressed via a non-dimensional analysis through the orographic Froude number $\mathrm{Fr} = U/NH$, where N is stratification and U the speed of the incoming flow. If the Froude number is small enough the incoming flow undergoes a significant horizontal deflection, associated to a pressure increase on the windward side of the mountain range. In some cases a quasi-stationary state can be established, with an intense low-level wind blowing parallel to the orography that is referred to as barrier wind, while the incoming flow tends to cross the mountain aloft.

In the present work, a two-year climatology of barrier wind events in the Italian region has been carried out at first. The events have been identified and classified mainly on the basis of the speed of the incoming flow, the speed and direction of the barrier wind at the 950 hPa level and the upstream orographic Froude number. A statistic has been subsequently developed in order to characterize the events distribution with respect to the Froude number. The climatology has been shown to be in good agreement with the idealized theory of a flow interacting with the orography, within the limits of its applicability to realistic cases; according to the theory, upstream blocking and barrier wind events are associated to Froude number values smaller than 1, whereas flow over the orography occurs when the Froude number is greater than 1.

Three case studies have been selected and simulated using the BOLAM and MOLOCH meteorological models, which were developed within the CNR–ISAC institute in Bologna. Each case study has been analyzed via the calculation of the upstream Froude number and the principal parameters relating to barrier wind, such as velocity, horizontal width and vertical depth, temperature etc. For one of the events, concerning the eastern Alps and especially the Veneto region, the model simulations were contrasted with wind, pressure, temperature and precipitation observational data. *Sensitivity tests* were conducted on each event afterwards, by gradually lowering the orography up to the point that barrier wind is no longer predicted. In this way the significance of the orography effect has been assessed, while the extent of the barrier wind has been associated to the upstream Froude number, evaluating the applicability of the idealized theory to realistic cases. A Barrier Wind Index (BWI) has been devised for this analysis.

The case studies simulations are in a good agreement with the idealized theory, whose applicability limits due to the complexity, heterogeneity and variability of the real atmosphere with respect to an idealized one have been highlighted. In particular, the Barrier Wind Index has been shown to increase in an approximately linear way as the Froude number decreases, starting from the value of 1. Furthermore, model simulations emphasized the significant influence of barrier wind on the surrounding mesoscale atmospheric circulation, on precipitation distribution and intensity and on the advection of important meteorological quantities such as temperature and humidity.

Introduction

It is well known that if Earth were shrunk to the size of a pool ball, it would be smoother than a real one. This means that the height of mountains is remarkably small compared to the diameter of the Earth, much more than the tiny imperfections on the surface of a pool ball are with respect to its diameter.

It seems quite incredible, then, that mountains can have such a great influence on atmospheric circulation. However, we have to keep in mind that the atmosphere itself is very shallow compared to the size of our planet; for instance, the average depth of the troposphere is roughly one thousandth of the Earth's diameter. Thus, mountains are comparable in size to the atmosphere and that is one of the reasons why they are so efficient in modifying the airflow patterns.

But there is another fundamental factor helping mountains in their task, and that is stratification. The atmosphere is stably stratified, so that every parcel of air which is displaced vertically from its equilibrium position tends to restore its previous state by moving back to where it was. This means that it is quite difficult for a parcel of air to get past a very high mountain, unless further factors intervene (a remarkable exception to this occurs during thunderstorms, when such a strong instability may develop that a single parcel of air can move upwards by several kilometers, due to the action of strong updrafts).

The influence of mountains on the atmospheric circulation is quite a complicate matter, as it involves several phenomena on multiple scales, from the large, synoptic scale (of the order of 1000 km) to the microscale (of the order of 1 km). The Earth's rotation is of course the primary factor in determining the behaviour of the airflow, introducing an asymmetry between left and right direction due to Coriolis force. The shape of the mountain, its height, its orientation with respect to the airflow and its position on the Earth are all fundamental factors in determining the overall effects on the airflow. The presence of a large amount of moisture in the lower levels of the atmosphere may originate moderate or even intense rainfall on the windward side of the mountain, as the air is brought to saturation during its ascent; as a consequence, *föhn*-like winds may occur on the leeward side. Another remarkable phenomenon triggered by topography

is wave formation; indeed, waves have been observed on both the upwind and the downwind flank of mountains and may propagate in either direction. On a much larger scale, mountains have been shown to be able to affect planetary waves and cyclone formation, thus influencing climate in a somewhat permanent way.

Additionally, mountains can affect the upstream airflow up to notable distances; that is, the presence of the orography will not only change the airflow pattern on its downwind flank, but it may trigger a modification in the very airflow impinging on it, even far upstream of the mountain. Such a phenomenon is named *upstream influence* and may occur in various ways and to various extents, depending on wind intensity, mountain height and shape, Coriolis parameter and numerous other factors such as temperature, stratification, moisture content, etc.

Upstream influence often occurs in the form of *upstream blocking*, when low-level winds decelerate because of the mountain and are eventually brought to stagnation. A threshold level is commonly observed, so that winds below it tend to decelerate more than winds above it; such threshold is usually the mountain top level. For instance, the ALPEX experiment highlighted that while low-level winds tend to flow mainly around the Alps, currents above the mountain top level are able to cross them quite easily (Pierrehumbert and Wyman, 1985).

This seems to be a general feature of airflow interacting with steep orography, nonetheless it is worthwhile to investigate thoroughly in order to understand what are the factors playing a significant role in producing and maintaining upstream blocking. In particular, one may wonder how high and wide the mountain has to be for blocking to occur; what non-dimensional parameters it depends on; how deep and wide is the blocked region and how long it takes for it to fully develop (Coriolis force plays a critical role in limiting the growth of the blocked region, as pointed out by Pierrehumbert and Wyman, 1985).

Upstream blocking in a rotating atmosphere interacting with relatively wide mountains is strictly connected with *barrier winds*, which we are going to discuss in detail in the present work. In Chapter 1 the phenomenon is illustrated and reviewed from a theoretical viewpoint. In Chapter 2 a two-year climatology of barrier winds in the Italian region is presented. In Chapter 3 the BOLAM and MOLOCH meteorological models, which we employed throughout the present work, are described. In Chapters 4, 5 and 6 three selected case studies are described and discussed and the Barrier Wind Index (BWI), characterizing barrier winds events, is introduced. In Chapter 7 the results of our work are illustrated, while in Chapter 8 we present our final considerations and conclusions.

Chapter 1

Barrier winds

Barrier winds, which we will be henceforth refer to as BWs, originate from stable air masses directed towards a somewhat steep orographic barrier which is roughly perpendicular to the airflow. The more stable the air is, the more difficult for it to ascend the barrier; therefore, the air will tend to flow around the mountain. For the airflow to change direction from perpendicular to parallel to the barrier, a deceleration is required with the wind component normal to the mountain decreasing and the parallel one increasing at the same time. This deceleration is produced by the pressure increase on the windward side of the mountain caused by low-level convergence exceeding upper-level divergence (the so-called "piling up" or "damming up" of air against the mountain). A horizontal gradient of temperature is created and a pressure gradient opposite to that due to earlier synoptic conditions is thereby formed.

If this pattern persists for long enough (from few hours to one day or even more, depending on environment conditions), Coriolis effect becomes significant and the air is deflected to the left – to the right in Southern Hemisphere. This happens because the previous geostrophic equilibrium is broken, as pressure gradient force prevails on Coriolis force (in other words, the Rossby number becomes comparable or larger than 1). Since this modification is caused by the presence of the orography, it only occurs in the lower levels of the atmosphere, roughly those below the mountain top. After some time a new geostrophic equilibrium is established due to the changed pressure field and a *barrier wind* may form.

Barrier winds – henceforth referred to as BWs – are strong low-level winds on the windward side of the mountain, blowing parallel to it and reaching distances quite far from their starting point, up to several hundreds of kilometers. These winds are usually several tens of kilometers wide and the maximum speeds, which are generally located at an intermediate height between mountain top and mountain foot, can reach 30 m/s. BWs can develop into strong low-level jets in some circumstances and are sometimes

referred to as *barrier jets* (see, for instance, Loescher et al., 2006).

Schwerdtfeger (1984) explained BWs in the Antarctic in terms of thermal wind, whose equation is as follows:

$$\mathbf{v}_\mathrm{T} = \frac{R}{f} \ln\left(\frac{p_0}{p_1}\right) \mathbf{k} \times \nabla_p \bar{T} \tag{1.1}$$

As in the Antarctic region there is nearly always a strong temperature inversion in the lower levels of the atmosphere, air is very stable so that winds have little or no chance to cross the steep and high orographic barrier constituted by the Antarctic mountains. Thus, the air piles up against the barrier and the inversion layer gets slanted in the proximity of the mountains. An isobaric temperature gradient is established at intermediate levels, with colder air next to the mountains, and this produces a thermal wind parallel to the mountain. Since the geostrophic wind at some level p_0 is equal to the geostrophic wind at an upper level p_1 minus the thermal wind $\mathbf{v}_\mathrm{T}$, there has to be a swift turning to the right of lower levels geostrophic winds as they approach the mountains (we have to keep in mind that f is negative in Southern Hemisphere). This is illustrated in figure 1.1.

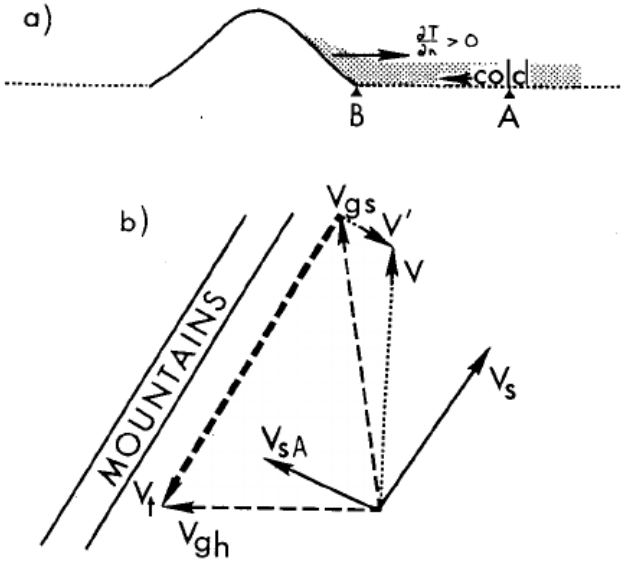

Figure 1.1: Barrier winds in the Antarctic, explained via the thermal wind equation; figure from Schwerdtfeger (1984). **a)** The inversion layer is represented in gray; A is a place far upstream from the mountains. **b)** V_{sA} is the wind near the surface at point A; the other vectors are all relative to point B: V_{gh} is the geostrophic wind above the inversion layer, V_{gs} is the geostrophic wind near the surface, V_t is the thermal wind, V_s is the wind near the surface, V is the same wind without friction and V' is the ageostrophic wind component due to the curvature of trajectories.

Although this interpretation is valid, in principle, only for Ro $\ll 1$, it has been later supported and confirmed by several observations (for instance by Marwitz (1987); see section 1.1), thus extending to any region or mountain. Nevertheless, BWs can be simply explained by pressure gradient force considerations as well, as remarked by Schwerdtfeger (1984). In any case, we assume that a steady state is finally established after some time from the beginning of the event, during which the presence of the mountains influences and modifies the large-scale airflow pattern, low-level blocking

occurs and readjustment takes place between pressure gradient, Coriolis, frictional and inertial forces, which eventually balance out.

As the preexisting synoptic-scale geostrophic equilibrium is broken by the onset of barrier winds and given that their typical scale lengths are ~ 100 km, they constitute a mesoscale feature. Nevertheless, BWs may interact with, and even modify, large-scale conditions, for instance via heat and moisture advection.

1.1 BWs history and locations

Since the early 20th century, BWs occurrences have been observed and reported by numerous authors, starting from Ficker (1906), who analyzed the piling up of cold northerly air against the Alps and the resulting surface pressure increase. This phenomenon is reported in Wegener (1911) as well. It was in the Antarctic continent, anyway, that the first systematic investigation of BWs took place, starting from Simpson (1919) who elaborated the meteorological observations performed during Scott's second expedition (1910-1913) at the winter quarters (Cape Evans) on Ross Island.

There are two regions in the Antarctica where BWs quite often occur: the western Weddell sea, along the eastern coast of the Antarctic Peninsula, and the western part of the Ross Ice Shelf, east of the Transantarctic Mountains. Although easterly winds prevail at these latitudes, strong southerly winds are regularly observed, particularly in the vicinity of the eastern flanks of mountains. These winds can originate by intense low pressure systems situated respectively over the Weddell Sea or the Ross Ice Shelf (see for instance O'Connor et al., 1994); nevertheless, their frequency is much larger than it would be if cyclones were their only source (King and Turner, 2007). Schwerdtfeger (1975) first connected such wind pattern in the western Weddell Sea to the Antarctic Peninsula, whose topography is sufficiently high and steep to block the westward airflow, deflecting it northwards and producing intense low-level jets quite frequently.

The Antarctic continent has pretty unique features that are not easily found elsewhere on the Earth – extremely cold and stable air with strong temperature inversions near the ground, remarkably high and steep topography that can block completely the low-level flow – allowing BWs to occur more frequently than anywhere else on Earth (King and Turner, 2007). Nonetheless, BWs have been observed at several other places all over the world. Smith (1982) cites New Zealand, the Alps, Taiwan, Iceland and the Front Range (the Rocky Mountains easternmost range, between Colorado and Wyoming) among the places where they most frequently occur. The Brooks Range (Alaska) was studied by Schwerdtfeger (1974), while BWs in the southern coastal region of Alaska have been analyzed by Loescher et al. (2006). BWs in the Sierra Nevada region have been addressed by Parish (1982) and Marwitz (1987). van den Broeke and Gallee (1996) and Moore

and Renfrew (2005) studied BWs in Greenland. In the present work we are going to deal with barrier winds in the Mediterranean and, more specifically, in the region around the Italian peninsula.

1.2 BWs characterization and features

(Schwerdtfeger, 1979) roughly estimated, for the Antarctic Peninsula BW, a 100 km width and a 4-8 hPa increase in pressure on the windward flank of the orography owing to the damming up of the cold air. Subsequent simulations performed by Parish (1983) using a two-dimensional hydrostatic mesoscale model with a 15 km horizontal resolution confirmed Schwerdtfeger's inferences about the pressure increase, while the BW width was found to be larger, up to 300 km depending on the initial conditions imposed in the model (typical winter temperatures with varying easterly geostrophic winds were used for the initialization). In any case, the BW maximum speeds were found between 200 and 1000 m above the ground, that is halfway between mountain foot and mountain top. Complete blocking was observed in the lowest levels.

Parish's experiments first indicated that a two-dimensional hydrostatic model with relatively low horizontal resolution ($\gtrsim$ 10 km) is sufficient, to a certain extent, to successfully simulate BWs – at least as far as their general features are concerned. Further experiments (see e.g. Parish, 1982, O'Connor et al., 1994 and Buzzi et al., 1997) confirmed this assumption. Nonetheless, more accurate simulations are obviously needed to account for complex topography, latent heat release effects and to discern side effects and microscale features. For instance, Schwerdtfeger (1984) noted that, in addition to BWs and to southerly winds originating by low pressure systems over the Ross Ice Shelf, there is another type of southerly winds blowing on the eastern flank of the Transantarctic Mountains, which must not be confused with the previous two. These are fast katabatic winds coming from the mountain transverse valleys; after arriving at the end of the valleys, they lose their previous topographic guide and are forced to turn left due to the Coriolis acceleration.

In fact, it is not always simple to distinguish "pure" barrier winds from winds having a somewhat mixed origin – that is, orographic barrier, cyclone forcing plus other side effects, possibly microscale ones. Different reasoning has to be made for every case, taking into consideration as more factors as possible (see also Chapter 2).

Aside from the obvious differences between BWs occurring at various places and periods of the year, owing to heterogeneity in temperature, stability, moisture content, wind and pressure patterns, possible instability etc. there are some basic features that they always exhibit – regardless of the above-mentioned factors – all of which are found on the windward flank of the mountain:

- a more or less pronounced pressure increase, due to the incoming flow cooling because of its rising motion (see e.g. Smith, 1982);
- a considerable departure of the flow from the large-scale geostrophic equilibrium, as remarked before (see Marwitz, 1987);
- a strong vertical wind shear of both signs particularly evident for the mountain-parallel wind component, with a maximum located roughly halfway between mountain foot and mountain top and lighter winds above and below it;
- a somewhat sharp turning of the incoming flow as it approaches the mountain, that is, a large horizontal shear of the mountain-parallel wind component as well.

The last two features are especially noticeable in the lower levels of the atmosphere, as BWs are usually low-level winds. Thus, winds at higher levels may be completely different from those at lower levels, the boundary being roughly the mountain top level, as discussed earlier. However, the transition between the blocked layer and the non-blocked one may be quite smooth, with winds gradually veering – or backing, in the Southern Hemisphere – from (almost) completely parallel to the mountain to approximately normal to it above; in such a case it is difficult to estimate the BWs vertical depth. In case a well-formed barrier jet is achieved, its maximum wind speed (up to 30 m/s, as reported in the first place by Schwerdtfeger, 1984) can be much larger than wind speeds far above the mountain top level.

There is one further feature not infrequently associated with BWs, even though it is not regularly observed: the presence of a *cold pool* generated primarily by the evaporation of hydrometeors on the windward side of the mountain; this effect enhances the damming up of the incoming airflow discussed earlier. The cold pool can be determinant in influencing the airflow and rainfall pattern (see section 1.3).

1.3 BWs influence on weather and climate

Barrier winds can have a strong impact on weather and even on climate – although the latter case is more unlikely, since a really large frequency of BWs occurrences is required for their influence to be of a long temporal scale (an example of this is discussed later in this paragraph). The simplest way BWs can affect weather is by the very act of transporting air from a place to another, that is by advecting cold air, warm air and/or moisture. As a result, air masses with different temperatures and moisture contents can interact with each other and produce further weather phenomena such as intense precipitation.

BWs are commonly coupled with the presence of a *cold pool*, a layer of colder air near the surface that can be generated by several factors: it can be produced by adiabatic cooling of the incoming flow; it can be pre-existing as an inversion layer; or it can originate by the evaporation of hydrometeors falling as precipitation – in this case, it is referred to as *evaporative* cold pool. This enhances the low-level blocking caused by the incoming flow damming up against the mountain. As a result, the whole blocking situation is reinforced, since the upper portion of the incoming flow, being warmer than the blocked layer below, is forced to ascend over it and possibly cross the mountain, thus being unable to displace the cold pool from its position (and to interrupt the development of BWs as well). This may allow the low-level blocking to last much more than it would otherwise.

The evaporative cold pool is a typical feature of rainy BWs episodes – that is, episodes with significant precipitation associated. The inversion cold pool is more commonly found (it is a very frequent occurrence in the Antarctic continent, where strong temperature inversion are often found in the lower atmosphere). BWs can extend the cold pool to a certain extent by advecting it along the mountain. Rainfall patterns are usually shifted when a cold pool is present, with maxima located on the windward side of the mountain rather than near the mountain top, as the incoming flow is forced to ascend further upstream than it would in the absence of the cold pool, causing clouds and precipitation to form earlier.

The presence of a cold pool associated to BWs episodes was highlighted, for instance, by Marwitz (1987) who analyzed two storms hitting the western flank of the Sierra Nevada, both featuring a strong, persistent BW with a cold pool associated, whose primary origin was the melting of snowflakes above the blocked layer. The incoming flow was forced to rise above it, thus generating precipitation and enhancing the low-level blocking by cooling and stabilizing the lower layer, with a positive feedback.

A somewhat different example of this kind of blocking characterized the infamous 1994 Piedmont flood, as pointed out by Buzzi et al. (1998) and later by Rotunno and Ferretti (2001). It has been suggested that the westward deflection of southerly subsaturated flow directed towards, and blocked by, the eastern Alps enhanced the low-level convergence with southerly saturated flow directly impinging on the western Alps. The warmer – in terms of equivalent potential temperature θ_e – saturated flow was forced to rise above the colder subsaturated one, producing intense rainfall. In this case the difference in θ_e between the two airflows produced quite a similar effect to that of a cold pool. Indeed, in both cases the incoming flow is forced to ascend further upstream than it would otherwise, as though the shape of the mountain were changed.

The mechanism described above does not always end up to intensify rainfall, it may also reduce it depending on the situation. Bousquet and Smull (2003) analyzed

an upstream blocking event which also occurred in Piedmont, during MAP (Mesoscale Alpine Programme) IOP 8, on October 21st, 1999. Both the operational Swiss Model (SM) and the experimental Mesoscale Compressible Community model (MC2) had forecast heavy rainfall, with associated flooding, on the southern side of the western Alps for that day; however, only moderate precipitation eventually occurred, with total rainfall far smaller than forecast and maxima located over the Po Valley, significantly upstream of the mountains. The authors claimed the reason of such unrealistic forecasts was the underestimation of the depth and extension of the blocked flow, which acted to displace rainfall maxima and – in this case – had the ultimate effect of reducing the total rainfall.

Bousquet and Smull (2003) also highlighted another impact of upstream blocking, occurring quite far from the region where it originated and developed. The blocked flow, initially directed westwards, was deflected southwards by the western part of the Alps and eventually escaped the Po Valley via the Ligurian Apennines numerous valleys, outflowing into the much warmer Ligurian Sea. As a consequence, low-level convergence over the Gulf of Genoa was influenced and probably enhanced – a cold front was coincidentally sweeping that region, so that the two effects concurred. Such a phenomenon is not uncommon in Liguria (see, for instance, Buzzi et al., 2013), even though its origin is not always upstream blocking caused by the Alps. The cold, northerly wind blowing from the Ligurian valleys is called *tramontana scura*.

Finally, barrier winds impact may extend in time too, affecting not only weather but climate as well. Schwerdtfeger (1979) highlighted the crucial role played by barrier winds along the eastern side of the Antarctic Peninsula in determining the climate of the Weddell Sea region. These winds drive a great amount of ice northwards, which accumulates in the northwestern Weddell Sea and cools down the climate of the whole region, whose average annual temperature is much cooler than that of other maritime regions surrounding the Antarctica at the same latitude.

Moreover, since the Antarctic Peninsula and its topography extend much more northward than any other Antarctic orographic feature, the BWs are driven well beyond the Antarctic Circle, right into the circumpolar westerly winds region. Ice and cold water are transported from the Weddell Sea to the southern Atlantic Ocean and even – albeit to a lesser extent – to the southern Indian Ocean. Thus, the Antarctic Peninsula BWs climatic influence turns out to be much greater than one would expect. As the Transantarctic Mountains do not extend as northward as the Antarctic Peninsula, there is no such strong ice drift in the western part of the Ross Ice Shelf, despite the fact that intense barrier jets regularly occur in this region as in the western Weddell Sea.

In the Northern Hemisphere, van den Broeke and Gallee (1996) studied BWs on the western coast of Greenland and suggested that the advection of warm and moist air northwards by these winds could favour the melting of the ice sheet. On the other

hand, Moore and Renfrew (2005) suggested that the BWs frequently blowing along the southeastern coast of Greenland could play a significant role in driving the East Greenland Current and transporting cold air over the Irminger Sea, triggering convection in the whole region.

1.4 Theory and significant parameters

Two non-dimensional parameters are relevant when it comes to characterizing an airflow and determine whether BWs can occur or not: the Rossby number $\mathrm{Ro} = U/fL$ and the orographic Froude number $\mathrm{Fr} = U/NH$, where U is the incoming wind, f is Coriolis parameter, N is Brunt-Väisälä frequency, L is the mountain horizontal length scale and H is the mountain height. The Rossby number can be interpreted as the ratio of inertial to Coriolis force, the Froude number as the ratio of incoming kinetic energy to the potential energy needed to climb the mountain (Sheppard, 1956).

The influence of the Earth's rotation on upstream blocking was first studied by Queney (1948) in two dimensions, using linear theory. Afterwards, Smith (1980, 1982) analyzed the flow splitting with a three-dimensional model, again with hydrostatic linear theory. As pointed out by Smith (1979), the linear theory starts failing as soon as the height of the orography is comparable with the vertical wavelength of the hydrostatic disturbances $2\pi U/N$. This is consistent with observations, as mountains higher than 1 km have been shown to be able to generate nonlinear phenomena, such as wave steepening/breaking and upstream blocking.

The Froude number is thus useful as a diagnostic parameter to discern cases in which linear theory is suitable for from the others. The threshold value is not clearly defined, as it distinctly depends on the situation, owing also to the intrinsic difficulty in estimating the Froude number in conditions that are far from ideal. Nonetheless, $\mathrm{Fr} = 1$ is generally recognized as an approximate threshold, with linear domain at $\mathrm{Fr} > 1$ and nonlinear domain at $\mathrm{Fr} < 1$. This is, for instance, what Sheppard (1956) found using Bernoulli's equation to estimate the speed that an incoming flow must have to overcome the background stability and reach the mountain top. However, that is just a qualitative estimate, as pointed out by Smolarkiewicz and Rotunno (1990), who conversely noted that the theory developed by Smith (1980, 1988) represents adequately the tendency for flow reversal and upstream stagnation/blocking in the $\mathrm{Fr} < 1$ regime. These features are a consequence of the positive density anomaly situated on the windward side of the mountain and not of the parcel's loss of kinetic energy against the mountain as interpreted by Sheppard (1956).

Drazin (1961) found that when $\mathrm{Fr} \ll 1$ – in the strongly nonlinear regime – low-level air tends to flow around the orography, following horizontal trajectories; Smith (1980)

later confirmed this findings, showing that as the Froude number increases – that is, moving towards the linear regime – larger vertical velocities are attained, with low-level airflow still exhibiting the tendency to be around the mountain instead of over it.

In any case, upstream blocking has been found to be coupled with lower Froude numbers (see, for instance, Chen and Smith, 1987 and Pierrehumbert and Wyman, 1985). That said, some considerations have to be made about the degree of uncertainty associated to the Froude number estimation and its relationship with upstream blocking:

- as Chen and Smith (1987) noticed, identifying a blocked flow is never straightforward, due to uncertainties in the degree and depth of blocking, the blocking by only one portion of a mountain, and the upstream deceleration, which might be attributed to the synoptic system rather than the mountain;
- Froude number – as well as Rossby number – is easily calculated in *ideal conditions*, while assuming to deal with, for instance, an uniform flow with speed U, a stratification N constant with height and a simply shaped mountain of height H; in real-life conditions, it may be tricky to decide what values have to be assigned to these quantities; one can either take a rough estimate or calculate them in some way, for instance by averaging them over a certain area (the latter procedure is especially suitable whenever there is a large spectrum of scales to deal with).

Generally speaking, the application of an idealized theory to a realistic atmosphere is to be taken *cum grano salis*, as a theory that has been devised for an idealized flow over a simple shaped topography cannot accurately account for the heterogeneity and variability which are typical of the real atmosphere.

The orographic modifications to airflow and their relationship with the Rossby number and the Froude number are well summarized by the regime diagram in figure 1.2, taken from Rotunno and Ferretti (2001), which gathers model results from previous works on the argument. The flow is assumed to be adiabatic and on a f-plane and the latent heat release effect is neglected. As we can see:

- for $U/N < L < U/f$, the Earth's rotation can be neglected (Ro > 1); mountain waves occur in the linear case Fr > 1 (Queney, 1948); the nonlinear case Fr < 1 has been analyzed with two different approaches: with a two-dimensional orography, blocking occurs upstream and wave breaking downstream of the mountain (Pierrehumbert and Wyman, 1985); with a three-dimensional orography, the airflow splits and vortices with quasi-vertical axes are found on the leeward side of the mountain (Smolarkiewicz and Rotunno, 1989);
- for $L > U/f$, the Earth's rotation influence is dominant (Ro < 1); quasi-geostrophic theory results (Buzzi and Tibaldi, 1977; Smith, 1979) exhibit an anticyclonic flow

perturbation over the mountain region, with strong asymmetry (the flow turns to the left) which is larger the higher the mountain.

Substituting the typical midlatitude values $U = 10$ m/s and $N = 10^{-2}$ s^{-1}, it is evident that when L is much larger than 1 km we can assume that the airflow is hydrostatic within a good approximation. This will be valid for every barrier wind event we are going to analyze.

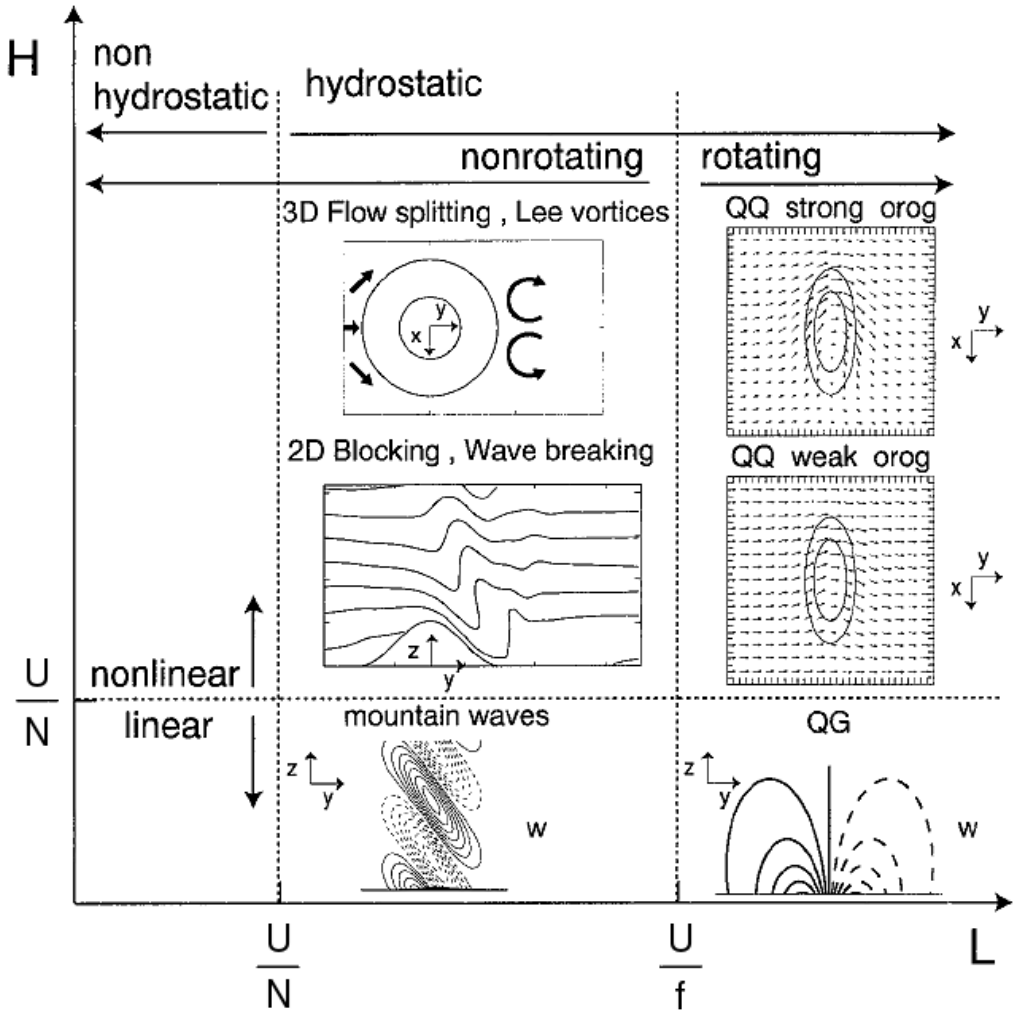

Figure 1.2: Regime diagram for dry-adiabatic airflow of constant speed U and uniform stratification N impinging on a mountain of height H and breadth L on an f-plane. Typical Northern Hemisphere midlatitude values for N and f are assumed, such that $N \gg f > 0$. The abscissa is logarithmic.

As the theories summarized in figure 1.2 are only valid when latent heat release effect is negligible, we must use caution whenever this assumption is no longer appropriate – obviously when convective instability occurs. Even when stratification is stable and the

diabatic contribution due to latent heat release is neglected, as soon as the air reaches saturation the *moist Brunt-Väisälä frequency* N_m has to be used instead of the dry one N_d. As a result, the Froude number increases, because $N_m < N_d$. Throughout the present work we have always used the dry Brunt-Väisälä frequency N_d, which will be simply referred to as N. This approximation will be satisfactory, albeit not particularly accurate, for the mesoscale climatology in Chapter 2, as it will provide us with a first estimate of the Froude number distribution of BW events in the Italian region. A much more precise estimation of N will be employed while analyzing the case studies in Chapters 4, 5 and 6: in this case the virtual potential temperature θ_v will be used for the calculation in order to account for the effect of the presence of water vapour; the absence of saturation will be checked at every instant before carrying out the calculation.

A dimensional parameter associated with upstream blocking and barrier winds is the *Rossby radius of deformation* $d = NH/f$, which was found to determine the maximum width of BWs during a blocking situation over time (Pierrehumbert and Wyman, 1985). It is the Coriolis force, indeed, that prevents upstream blocking from indefinitely developing away from the mountain, arresting its growth at some point as soon as the width of the blocked flow equals d.

In the following chapter a two-year climatology of BWs events in the Italian region will be illustrated. We have estimated the Froude number for each episode and then calculated the average one for all episodes, aiming to assess the distinction between blocked and non-blocked airflow in terms of the upstream Froude number.

Chapter 2

Barrier winds in the Italian region: a mesoscale climatology

In order to get an idea of how frequently barrier winds occur in the Italian region and what are their distinguishing features, a two-year climatology has been developed using the BOLAM and MOLOCH meteorological models daily forecasts, available at `http://www.isac.cnr.it/dinamica/projects/forecasts/`. These models, developed at the CNR–ISAC Institute in Bologna, were tested in various project contexts and have shown high forecasting skills (see Chapter 3 for references and a detailed description of the two models).

BOLAM is a limited-area hydrostatic model based on primitive equations; convection is parameterized. Daily forecasts are for 72 hours ahead; runs are initialized at 00 UTC, deriving initial and boundary conditions from NOAA–NCEP GFS model (USA) 00 UTC analysis and subsequent forecasts. Horizontal resolution is 0.10 degrees in rotated coordinates (approximately 11 km) and 50 vertical levels are employed. The integration domain is displayed in figure 2.1.

MOLOCH is a non-hydrostatic, fully compressible, convection resolving model developed more recently than BOLAM and optimized for short-range, high detailed forecasts. Daily forecasts are for 48 hours ahead; runs start at 03 UTC, retrieving initial and boundary conditions from BOLAM forecasts, into which MOLOCH is usually nested. Horizontal resolution is 0.0207 degrees in rotated coordinates (roughly equivalent to 2.3 km) and 50 vertical levels are employed. The integration domain is displayed in figure 2.1 within the one of BOLAM.

Several output maps are available from BOLAM and MOLOCH daily forecasts, including: m.s.l. pressure, 3-hours precipitation accumulation, cloud cover and snow height; wind, temperature, potential temperature, equivalent potential temperature and relative humidity at various heights; geopotential height, CAPE, 0 °C level and PV (on both isobars

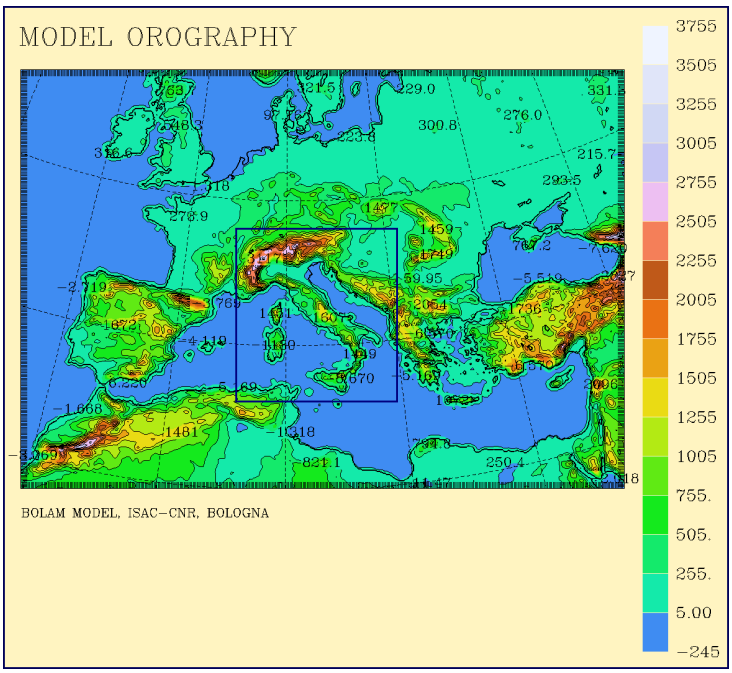

Figure 2.1: BOLAM and MOLOCH daily forecasts integration domains (respectively the larger one and the smaller one within the blue frame); the altitude is expressed in meters.

and isentropes) for BOLAM only; cloud water and vertical velocity for MOLOCH only. All meteorological variables are displayed every three hours; 12-hours rainfall and snowfall accumulation maps are also available.

As BOLAM and MOLOCH models are quite accurate and optimized for short-range forecasting, the agreement between forecasts and real values is generally good, especially for dynamical quantities as those considered here (wind, temperature etc.). For this reason we chose to use model forecasts rather than observational data – such as satellite data, ground data etc. – to develop our climatology, thus attaining much larger spatial and temporal resolutions that let us investigate upstream blocking and BW episodes with greater accuracy. Of course, daily analyses used by BOLAM and MOLOCH models as initial and boundary conditions were also employed to study the BW episodes in this climatology.

2.1 Methodology and criteria

For our climatology, we analyzed meteorological conditions over the Italian region in a two-year period: from July 1, 2010 to June 30, 2011 and from July 1, 2012 to June 30, 2013. Our aim is to characterize BW episodes in terms of their geographical distribution, preferential season(s) of occurrence, duration, related large-scale patterns, upstream wind speed, Froude number. Additional features, such as thermodynamic variable patterns, rainfall distribution and BW maximum speeds, were also investigated,

although they were not included in the final categorization since they exhibited high variability.

Additionally, we also included *flow-over* episodes in the final categorization: that is, events not featuring BWs, whose low-level incoming winds flow over – and cross – the mountains, as in contrast with upstream blocking. Our target is to contrast their properties and their Froude number distribution with those of BW events. We expect the average Froude number of flow-over events to be significantly higher than the one of BW events. For the sake of convenience, we are going to make use of the inverse orographic Froude number NH/U (henceforth referred to as NMH, *Non-dimensional Mountain Height*) instead of the Froude number itself.

BOLAM maps have been especially used to get an overview of each BW episode, given the model's larger domain; 500 hPa geopotential height maps were particularly useful to examine synoptic conditions and identify the large-scale circulation patterns that are more likely to lead to upstream blocking and BW events.

The wind at the 950 hPa level has been chosen as the most suitable field for representing the low-level flow, because the BW maxima are generally situated around this altitude (as we saw in the previous Chapter) and boundary layer effects are (nearly) negligible at this level. For each episode an estimate of both upstream (U) and barrier winds (W) has been inferred from MOLOCH 950 hPa wind maps by averaging the wind over appropriately selected areas (see below for details).

The average dry Brunt-Väisälä frequency for the low-level upstream flow has been estimated from temperature at 950 hPa and 850 hPa as follows:

$$\begin{aligned} N^2 = \frac{g}{\theta}\frac{d\theta}{dz} = \frac{g}{\theta}\frac{d\theta}{dp}\frac{dp}{dz} \simeq \frac{g}{\theta_1+\theta_2}\frac{\theta_1-\theta_2}{p_1-p_2}\left(\rho_1+\rho_2\right)g = \\ = \frac{g^2}{R\Delta p}\frac{\theta_1-\theta_2}{\theta_1+\theta_2}\left(\frac{p_1}{T_1}+\frac{p_2}{T_2}\right) = \frac{g^2}{R\Delta p}\frac{T_1-\Pi T_2}{T_1+\Pi T_2}\left(\frac{p_1}{T_1}+\frac{p_2}{T_2}\right) \end{aligned} \tag{2.1}$$

where $1,2$ indices denote quantities at $p_1 = 950$ hPa and $p_2 = 850$ hPa levels (hence $\Delta p = p_1 - p_2 = 100$ hPa) and the following relations have been used to derive the final form of equation 2.1:

$$\textit{hydrostatic equation} \qquad \frac{dp}{dz} = -\rho g \tag{2.2}$$

$$\textit{ideal gas law} \qquad p = \rho R T \tag{2.3}$$

$$\textit{potential temperature} \qquad \theta = T\left(\frac{p_0}{p}\right)^{\frac{R_d}{c_p}} \tag{2.4}$$

$$\Pi = \left(\frac{p_1}{p_2}\right)^{\frac{R_d}{c_p}} \tag{2.5}$$

Naturally, calculating the average N of the 950–850 hPa layer by using only the temperature values at its lower and upper boundaries may be an oversimplification; nonetheless, if θ varies in an approximately linear way along the layer this method can provide us with an acceptable estimate (let's say, within 20%) of the real N, which is good enough to let us associate BW episodes with some interval of Froude number values, as we aim to do in our conclusive categorization.

There is more than one reason why such an estimate is reasonable for our purposes. First, as we said before, BWs are usually associated with stable atmospheric conditions, far from both convective instability and strong temperature inversions; hence, our assumption of a roughly linearly varying stratification is generally well satisfied. Furthermore, wind speeds and temperatures have been averaged (visually) over a large area – at least 100 km in both width and length, depending on the case – about 200 km upstream of the mountain, thus increasing the accuracy of the estimate. In most cases it has been straightforward to do so, as wind speed and temperature fields were quite uniform, especially during long-lasting, slowly-evolving events, that are the ones we focused on.

The NMH, or inverse Froude number, has been calculated using the above-mentioned N and U and the estimated mountain height H. A different height was used for each episode, the same mountain range being assigned varying values depending on which portion the incoming flow impinges on.

Finally, we set some thresholds for distinguishing the BWs from other winds. *If* a low-level (950 hPa) "wind belt" is found on the windward side of a mountain and: its width is at least 10 km; its winds are extensively (that is, over at least 50% of the total area) larger than 10 m/s and their maximum speed is at least 15 m/s; the angle between the winds and the mountains is smaller than 20°; *then*, the winds will be referred to as BWs. Winds that are not BWs but whose parameters are close to the ones above will be referred to as "pseudo" BWs. An additional threshold of 12 hours[1] has been chosen for episode duration: events featuring a BW for less than 12 hours were not included in the final categorization.

Had we not used such thresholds to separate the "strong" BW episodes from the "weak" ones, there would have been an excessive number of events in the final categorization, as the highest Italian mountains (especially the Alps and the Apennines) tend to deflect the upstream airflow quite often. For our purposes, we are only interested in significant, long-lasting events featuring a somewhat steady barrier wind, which is established after some readjustment has taken place and considerably influences the surrounding circulation.

[1] equivalent to 5 output maps, as these are displayed every 3 hours.

2.2 Locations

A topographic map of the region included in the present work is displayed in figure 2.2. The major mountain ranges have been highlighted, together with a sketch of the BW they may generate and the corresponding upstream winds required for them to occur.

Figure 2.2: Topographic map of the Italian region; the major mountain ranges – the ones that are most likely to generate BWs – have been highlighted; the corresponding BW is sketched as dashed arrows, the upstream wind as solid arrows.

2.2.1 The Alps

The Alps are the largest and highest mountain range in Italy. Even though the major peaks (*Monte Bianco*, 4810 m; *Monte Rosa*, 4634 m) are located in their western part, which is also the highest one, the eastern Alps are much wider than and almost as high as the western Alps, reaching 4049 m at *Piz Bernina*. The envelope of the Alps is well above 2000 m.

The eastern Alps can originate strong barrier winds provided suitable conditions are met. These episodes will be henceforth referred to as Alpine, for the sake of conciseness. In order for BWs to occur, there has to be a southerly to southeasterly flow coming from the Adriatic Sea,[2] as shown in figure 2.2. The conformation and arrangement of Italian and Balkan orography facilitates the occurrence of BWs, as the airflow starting from the southern Adriatic Sea may be driven – and possibly accelerated – along the "sea-aisle" shaped by the Apennines to the west and the Dinaric Alps to the east; once the flow reaches the eastern Alps, it dams up against them and is (may be) deflected westwards due to the increased pressure on the southern side of the Alps, generating BWs. These are also driven by the presence of the Alps to the north and the northern Apennines to the south and are possibly accelerated while moving westwards through the narrowing Po Valley.

All Alpine episodes identified in our climatology are rainy, probably due to a couple of concomitant factors: the remarkable height of the Alps, which forces the upper portion of the incoming flow to ascend considerably, thereby causing a massive amount of water vapor to condense and form clouds; and the fact that the incoming flow has usually collected much moisture while travelling a long distance over the sea (see for instance Bertò et al., 2004). All flow-over events are also rainy, the main difference between them and the BW ones being in rainfall distribution rather than in the total amount of precipitation – maxima are located near the mountain top in the first case, further upstream in the second case.

A 2200 m height has been attributed to the eastern Alps when estimating the average NMH of the Alpine events.

An example of Alpine event is shown in figure 2.3. A deep cyclone centered over the Ligurian Sea – whose presence is revealed by intense, counter-clockwise rotating winds over Sardinia – generates strong southeasterly winds over the Adriatic Sea; these are sharply deflected to the left about 100 km upstream of the eastern Alps, blending into an intense and wide barrier wind (figure 2.3a, which extends more than 200 km westwards

[2] As the present work deals with BWs in the Italian region, we will not consider northerly airflow impinging on the northern flank of the Alps, which is another flow pattern to frequently produce blocking and BWs (Ficker, 1906; Chen and Smith, 1987).

in the Po Valley and all the way from the Alps to the Adriatic coast.[3]

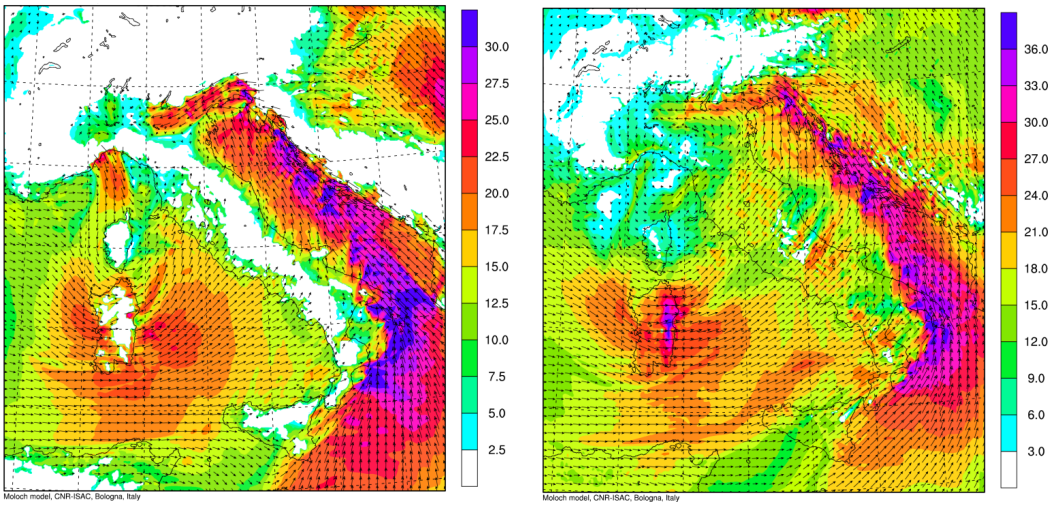

(a) Wind at 950 hPa (m/s). **(b)** Wind at 850 hPa (m/s).

Figure 2.3: Alpine BW episode, wind at 950 hPa and at 850 hPa; MOLOCH forecast for November 1, 2012, 00 UTC, initial time October 31, 2012, 03 UTC.

A glance at the 850 hPa wind map (figure 2.3b) confirms that it is a low-level jet, as there is no band of intense winds blowing parallel to the orography at that height, even though the incoming winds turn slightly to the left in the vicinity of the mountains.

The upper-level synoptic situation for this event is displayed in figure 2.4. Most Alpine episodes are associated with a large-scale pattern similar to that, with a mid-tropospheric trough over the western Italy and intense southerly airflow upstream of the eastern Alps. As this pattern occurs more frequently during wintertime, Alpine BW events mostly occur from mid-October to mid-April, whereas they are quite rare during summertime (due also to the low stratification typical of summer conditions). Air moisture content can be a critical factor to determine whether the low-level southerly airflow will cross the Alps or get blocked, possibly causing BWs.

Most Alpine events are similar to the one that we have depicted so far. Nonetheless, BWs may originate from any southerly airflow, even one coming from the central portion of northern Apennines, for instance; however, in such a case there is not enough space to the west for a barrier flow to fully develop, so that intense BWs will never occur. The western, north-to-south-oriented portion of the Alps may also generate BWs; this actually happens quite often when moderate to strong easterly winds blow over the Po Valley, as they are deflected southwards by the Alps and end up in the cul-de-sac in Piedmont

[3] In most cases, the incoming winds make a more gentle turn and appear to merge into BWs few kilometers downstream; in other words, BWs are primarily generated to the left of the incoming winds, while “mixed” winds are found directly in front of them (see section 2.3).

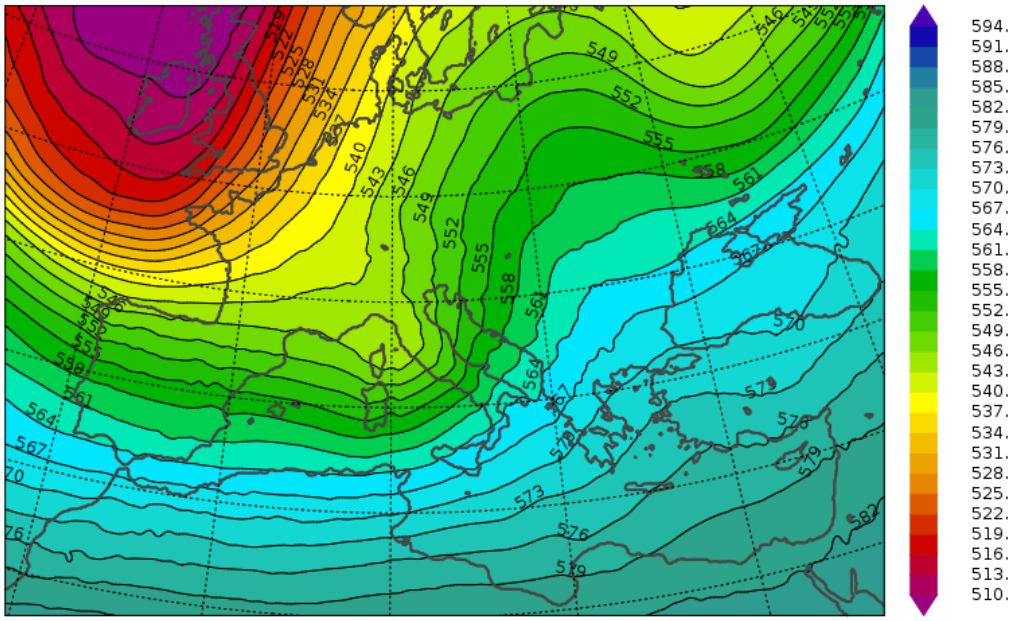

Figure 2.4: Alpine BW episode, 500 hPa geopotential height (dam); initial condition at 00 UTC for the November 1, 2012 BOLAM run.

(near Cuneo), where they accumulate and eventually escape the Po basin through the numerous Ligurian valleys (see e.g. Bousquet and Smull, 2003). However, intense BWs will not occur in such a situation, since there is no sufficient space for them to develop, as in the previous example. On the other hand, the low-level outflow from the Po Valley can be a determinant factor in generating BWs off the Ligurian coasts (see subsection 2.2.4 and Chapter 6).

2.2.2 The Apennines

The Apennines are the second-highest mountain range in Italy, extending throughout the peninsula from Liguria to Calabria. The highest peaks (*Corno Grande*, 2912 m; *Monte Amaro*, 2793 m) are all located in the Abruzzo region, which features the highest terrain among all regions in the peninsular Italy.

The Apennines can produce BWs mainly in two cases: when northeasterly airflow impinges on their eastern side and when southwesterly airflow impinges on their western side. In the following, the first case will be referred to as Adriatic, while the second case will be referred to as Tyrrhenian.

Adriatic episodes, as we will see, are the most frequent ones, especially during wintertime; the Adriatic coast is well exposed to northeasterly winds coming from the Balkans, particularly right after the passage of a cyclone over the Italian region, during the rising pressure stage; these winds are generally quite stably stratified and dry, so they

cannot easily cross the Apennines, especially the Central Apennines which are the highest; BWs are thus generated as the incoming winds turn eastwards. Since northeasterly winds blowing over the Adriatic Sea tend to be quite dry, few Adriatic events included in this climatology are rainy. For the same reason, almost a half of the Adriatic flow-over events are also rainless.

An example of Adriatic episode is displayed in figure 2.5. The incoming flow consists of multiple streaks of strong wind separated by areas of weak wind. Such a pattern is typical of Adriatic episodes. The origin of the incoming winds may explain this difference. While in most cases they come from the sea, in this case they come from the Balkans – and specifically from the Dinaric Alps – that are a complex terrain, generating inhomogeneity in wind speeds.

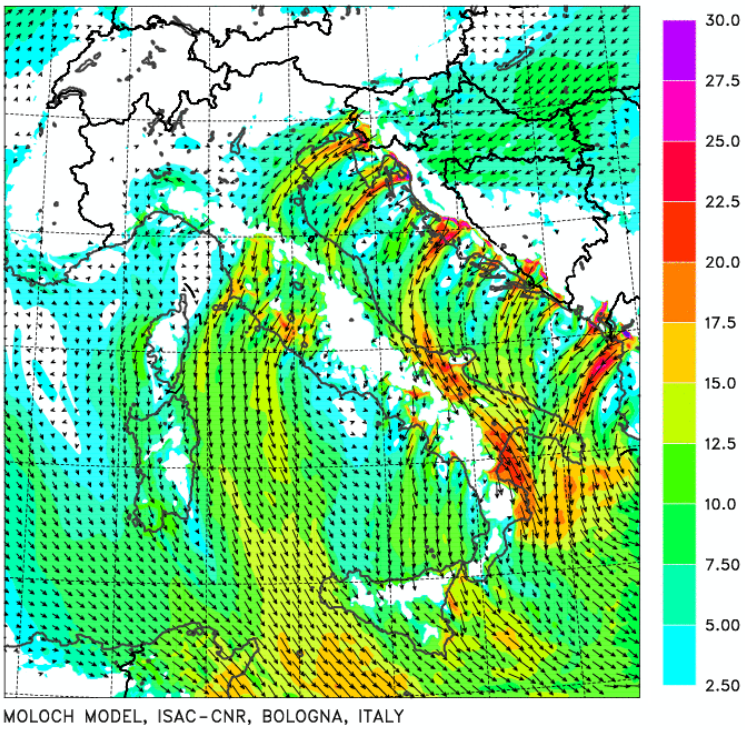

Figure 2.5: Adriatic BW episode, wind at 950 hPa (m/s); MOLOCH forecast for October 28, 2010, 00 UTC, initial time October 27, 2010, 03 UTC.

It is worth to point out the significant role played by the central Apennines. Being much higher than the rest of the range, they are much more effective at deflecting the incoming winds. An actual barrier wind is thus established only in the southern half of the peninsula, whereas winds impinging on the northern half of the range are able to cross it, as we can notice in figure 2.5. This occurs quite frequently indeed.

The upper-level synoptic situation for this episode is shown in figure 2.6. That is the typical large-scale configuration associated with BW occurrences in the Adriatic Sea; after a cyclone has passed over Italy, pressure rises and cool, dry northeasterly winds blow over the sea, damming up against the Apennines. As this pattern is most commonly

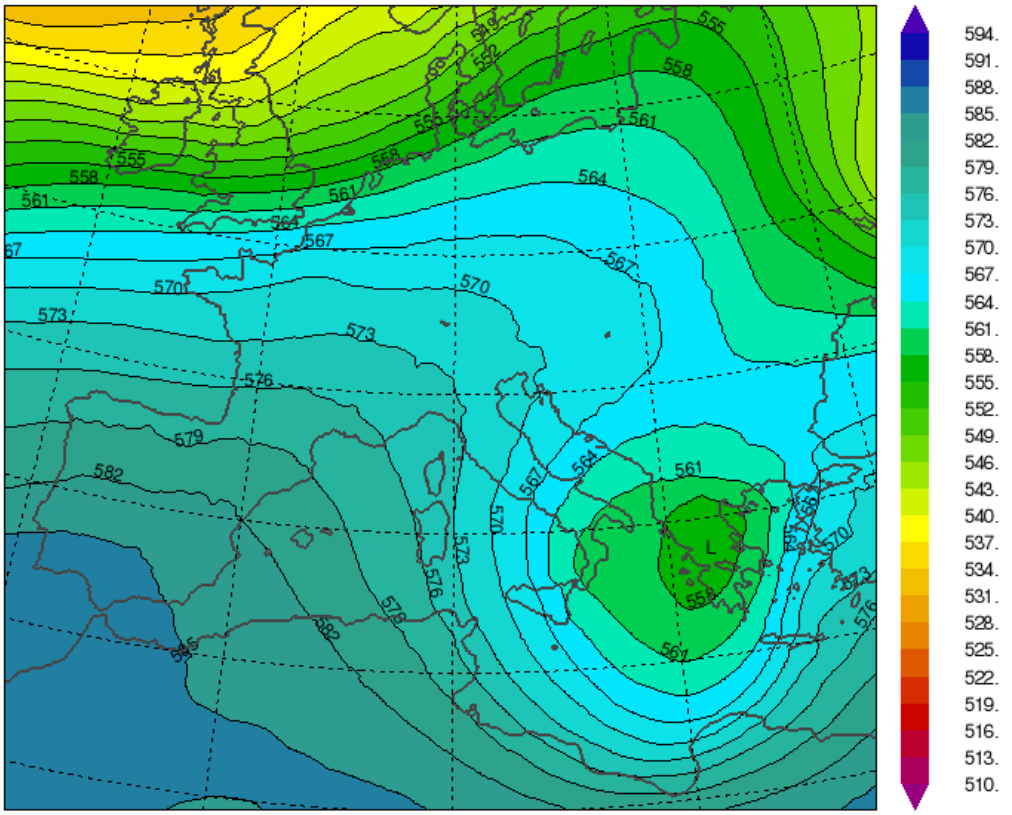

Figure 2.6: Adriatic BW episode, 500 hPa geopotential height (dam); initial condition at 00 UTC for the October 28, 2010 BOLAM run.

observed during wintertime, Adriatic events preferentially occur from October to April, while they are very rare during summertime.

Another feature that is peculiar of most BW events throughout the world can be observed in figure 2.7: a pressure ridge (sometimes referred to as "pressure nose"), first noticed by Ficker (1906) and later cited by several authors (for instance by Smith (1982), as said earlier). Surface pressure is higher on the windward side of the Apennines than it is on their leeward side, the difference being about 1-2 hPa. This effect, albeit modest, is evident and its cause is low-level convergence exceeding upper-level divergence due to the "damming up" of the incoming flow against the mountains, as already noted in Chapter 1.

Tyrrhenian events are less frequent than Adriatic ones, as southwesterly (westerly to southerly) winds blowing over the Tyrrhenian Sea are generally warmer and moister than Adriatic northeasterly winds, hence they tend to cross the Apennines rather than being deflected northwestward due to latent heat release effects.[4] On the other hand, the

[4]Latent heat release effects are considerable, modifying greatly the stratification of a flow and shifting nonlinear regimes to lower values of the Froude number, as noted by Miglietta and Buzzi (2004).

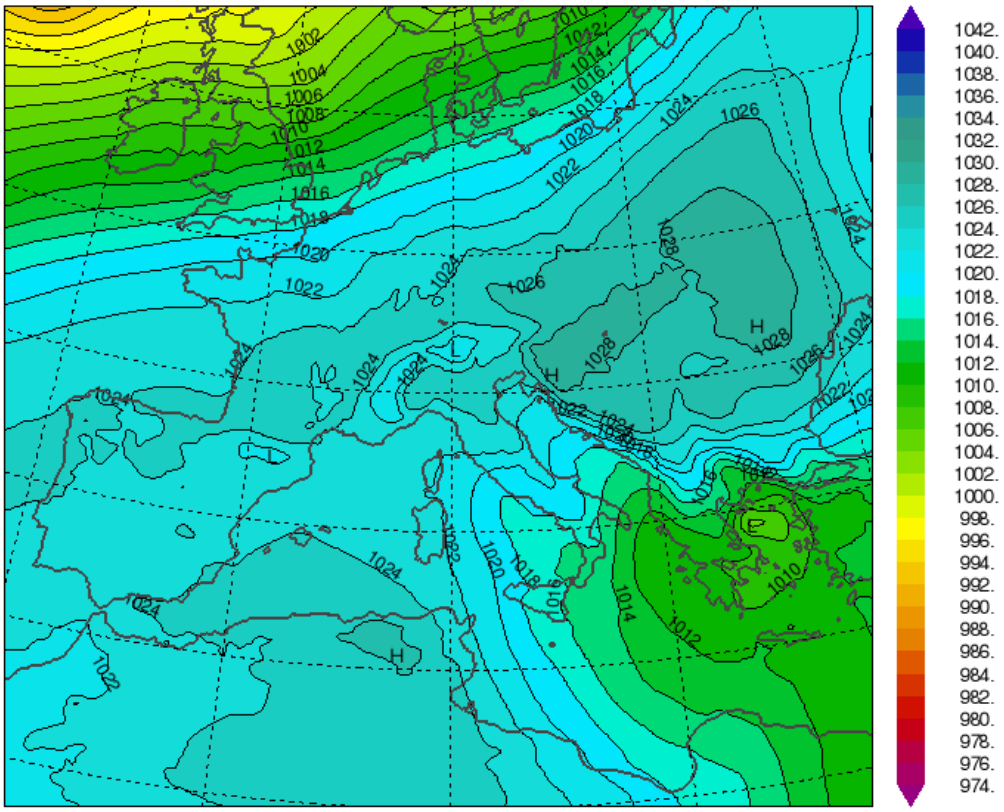

Figure 2.7: Adriatic BW episode, m.s.l. pressure (hPa); initial condition at 00 UTC for the October 28, 2010 BOLAM run.

central Apennines are so effective at deflecting winds that most events in our climatology feature a split incoming flow, its northern part being deflected and generating BWs, while its southern portion crosses the southern Apennines. Most Tyrrhenian BW episodes included in this climatology are rainless, while all flow-over events are rainy.

An example of Tyrrhenian episode is displayed in figure 2.8. Unlike the previous Adriatic event, in this case the upstream airflow consists of a wide band (about 300 km) of moderately intense winds blowing over the sea; hence, wind speed is quite uniform over a large area. A barrier wind is found about 100 km to the left and downstream (in this case, northwestward) with respect to the middle of the incoming flow band. This is the usual pattern for events in the Italian region, whereas BWs extending in front of the whole band of incoming flow (such as that of the Alpine episode we discussed earlier) are almost exclusively found for the Alpine events (see also section 2.3 for a detailed discussion).

Whenever moderate to deep cyclones are present over the Tyrrhenian Sea, it is not straightforward to discern whether it is the cyclonic circulation of the depression or the orography to make the incoming flow turn left; in other words, we may wonder what is

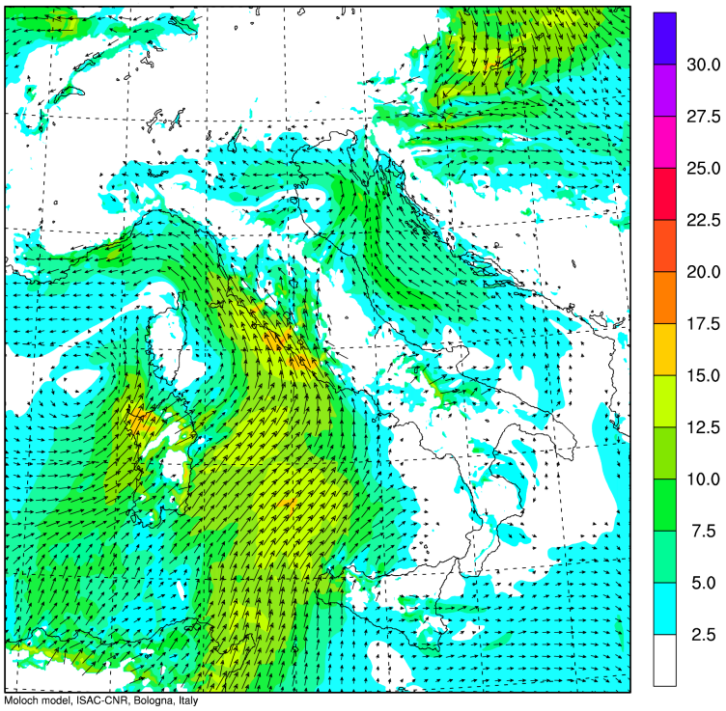

Figure 2.8: Tyrrhenian BW episode, wind at 950 hPa (m/s); MOLOCH forecast for September 23, 2012, 00 UTC, initial time September 22, 2012, 03 UTC.

the prevailing effect in determining wind trajectories and whether a BW event is "pure" or not. Since cyclones occur quite frequently in the Tyrrhenian region and westerly airflow is usually very moist, Tyrrhenian BW events turn out to be the most infrequent ones – there are only 8 of them in our climatology.

In order to overcome the issue of determining whether the event we are dealing with is pure or influenced by a cyclone, we have to take into consideration several key features. *If*: the incoming flow is somewhat straight, turning left more or less sharply – in few tens of kilometers; a sort of transition level is found, such that the incoming flow below it turns left, while the one above it does not; a pressure ridge is found, with higher pressure on the windward side of the mountain; *then*, it is plausible that it be a pure BW event.

If, conversely, incoming winds turn left gradually (all the way along their path); they do that at every level (at least, let's say, in the lowest 3000 m of the atmosphere); there is no trace of a "pressure nose" on the windward side of the mountain and there is a somewhat deep cyclone nearby; *then*, the cyclone influence on wind circulation is predominant and it is quite unlikely that it be a pure BW event.

2.2.3 The Dinaric Alps

The Dinaric Alps, also called Dinarides, are the principal Balkan mountain chain and one of the highest in Europe, reaching 2694 m at *Maja Jezerce* (Albania). When southwesterly to southerly flow is blowing over the southern Adriatic Sea, the Dinaric Alps are likely

to deflect it northwestward, generating southeasterly BWs. Since, as said earlier, the Adriatic Sea is bordered on both sides by high mountains, thus resembling a natural corridor, these BWs may develop into strong jets under suitable circumstances, also due to the small roughness of sea with respect to land. For the sake of conciseness, these episodes will be henceforth referred to as Dinaric. Most Dinaric BW events included in this climatology are rainless, while all flow-over events are rainy.

An example of Dinaric event is displayed in figure 2.9. It is worthwhile to note that most Dinaric episodes feature a very similar incoming flow to this one, due to the southern Italian and Albanian topography, which shapes and channels the airflow so that wind speed maxima are found in the Ionian Sea, off the Calabrian coast.

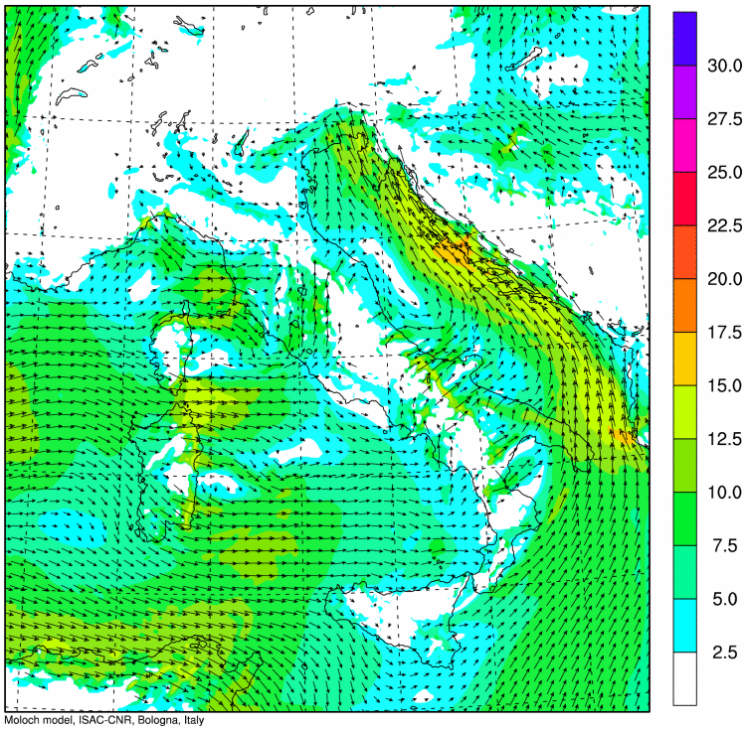

Figure 2.9: Dinaric BW episode, wind at 950 hPa (m/s); MOLOCH forecast for January 11, 2011, 00 UTC, initial time January 10, 2011, 03 UTC.

The upper-level synoptic situation for this episode is shown in figure 2.10. This is quite a similar large-scale pattern to that producing Alpine events: this resemblance is not occasional but is often found, as an upper-level geopotential trough over Italy is likely to produce southerly low-level winds. Dinaric events also occur preferentially during wintertime, while they are quite rare during summertime. It has to be noted that BWs have occasionally occurred at two distinct locations at the same time, although that is quite rare, due to the multiple conditions that have to be met for a BW to be established – in terms of temperature, stability, moisture content, wind speed and so on.

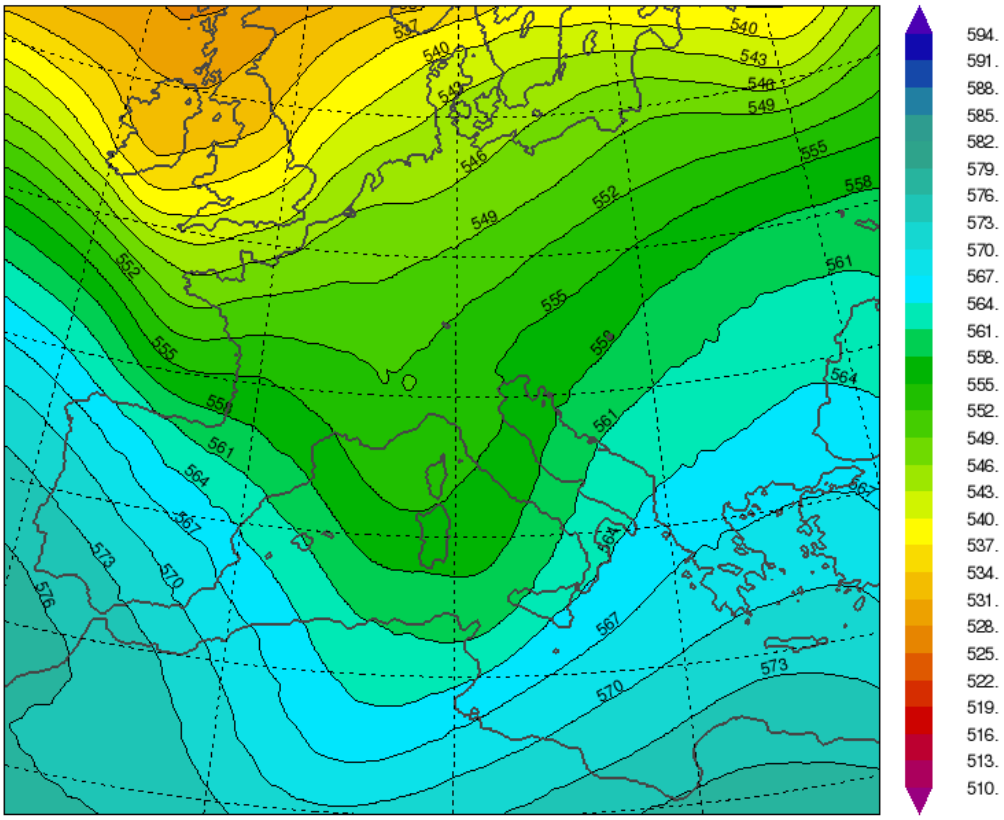

Figure 2.10: Dinaric BW episode, 500 hPa geopotential height (dam); initial condition at 00 UTC for the January 11, 2011 BOLAM run.

2.2.4 The Maritime Alps

The Maritime Alps are the southernmost portion of the western leg of the Alps, between France and the Italian regions of Liguria and Piedmont; they are remarkably high, reaching 3297 m at *Monte Argentera*. The Maritime Alps may originate BWs when southerly flow is blowing over the Mediterranean Sea west of Sardinia and Corsica, as well as when southeasterly flow is blowing over the Tyrrhenian Sea. Sardinia and Corsica constitute an obstacle to these flows, so that winds tend to be channeled between Corsica and Tuscany and guided along the orography, thus turning left even before reaching the Maritime Alps. Such an effect contributes to generating BWs. For the sake of conciseness these events will be henceforth referred to as Ligurian. Unlike the other BW events, Ligurian ones especially occur in autumn and spring.

Low-level convergence between the incoming flow and colder northerly winds coming from the Po Valley through the Ligurian valleys significantly contributes to enhance convection over Liguria and the Ligurian Sea (see, for instance, Buzzi et al., 2013). As a consequence, most Ligurian events, both BW and flow-over ones, are rainy.

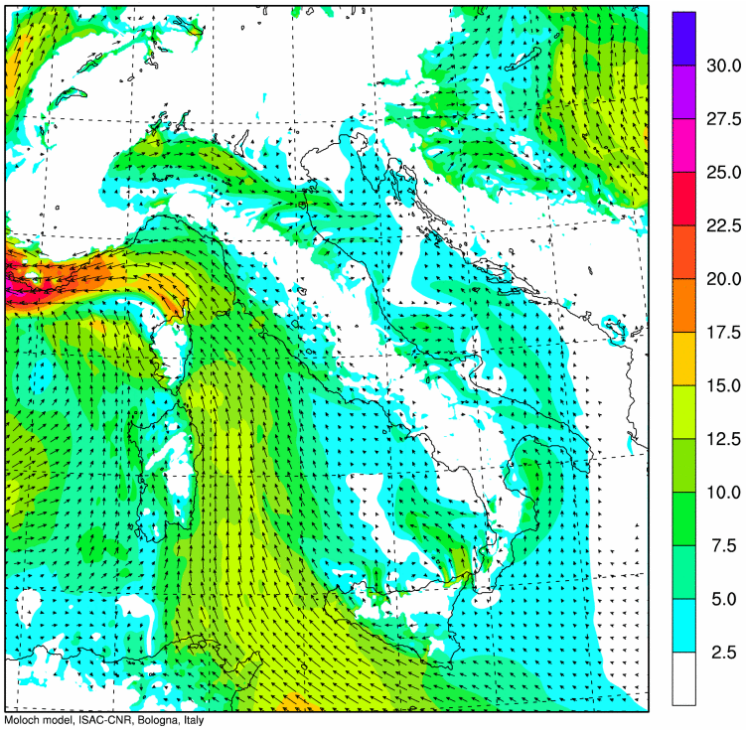

Figure 2.11: Ligurian BW episode, wind at 950 hPa (m/s); MOLOCH forecast for April 23, 2011, 00 UTC, initial time April 22, 2011, 03 UTC.

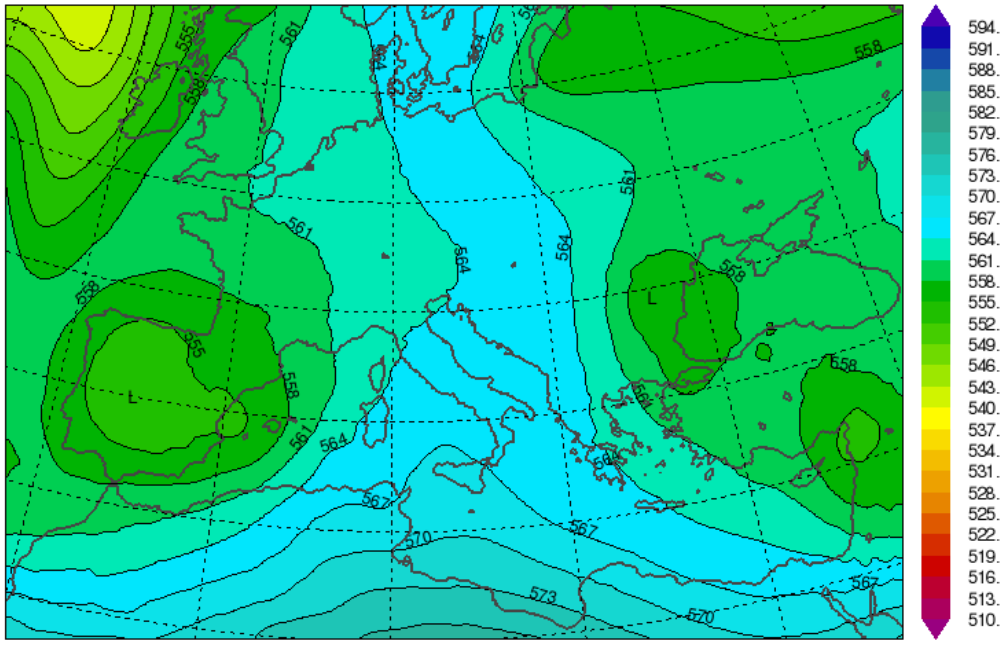

Figure 2.12: Ligurian BW episode, 500 hPa geopotential height (dam); initial condition at 00 UTC for the April 23, 2011 BOLAM run.

An example of Ligurian event is displayed in figure 2.11, while the synoptic situation related to it is shown in figure 2.12. As we can see, this is an anticyclonic episode (hence a totally rainless one). The incoming flow maxima are found east of Sardinia and Corsica, since their orography constitutes an obstacle to the wind, as remarked before. This is quite a pure event, while several episodes in this region turn out to be "mixed" ones, as cyclones are often found and somewhat centered over the Tyrrhenian Sea, making it difficult to assess whether winds turn left because of the Maritime Alps effect or due to the cyclone.

Finally, we have to mention further mountain ranges that can also generate BWs, albeit occasionally: the southernmost part of the Apennines, Sicilian, Sardinian and Corsican mountains, the latter being the most effective at deflecting the incoming flow. In fact, we did not include them in our climatology because they only caused few minor events during the two-year period we investigated. It seems reasonable that these mountains cannot produce long-lasting, extensive BWs since they are not as extensive as the major Italian mountains, albeit being considerably high; moreover, their orientation is such that the incoming flow is hardly normal to them, hence the distinction between incoming and barrier winds is unclear in most cases.

2.3 First-type and second-type events

We deem it necessary to point out a significant distinction among barrier winds events. The events similar to the Alpine one in subsection 2.2.1 (see also figure 2.3a), featuring a BW extending all the way in front of the incoming flow, will be henceforth referred to as *first-type* events; the others, featuring a BW located to the left and downstream of the incoming flow, with no BW in front of it – hence more comparable to the Tyrrhenian event (subsection 2.2.2, figure 2.8) or to the Dinaric one (subsection 2.2.3, figure 2.9) – will be referred to as *second-type* events.

First-type events are typically Alpine ones. This pattern is hardly seen elsewhere in the Italian region, possibly due to the unique conformation of the Adriatic Sea which constitutes a sort of "sea-aisle", framed on both sides by high mountains – the Apennines and the Dinaric Alps – and ending with even higher mountains – the Alps. The airflow is thus guided along this corridor up until its dead end, where it may either cross the Alps or be deflected. However, the presence of the Alps easternmost portion is such a constraint that the damming-up effect is enhanced, so that a BW can be established in front of the whole incoming flow. This pattern is associated with low-level flow separation: the BW tends to be divided from the incoming flow by an area of sharp horizontal wind shear (see also the Alpine case study in Chapter 4).

On the other hand, winds impinging on other mountains, such as the Apennines, are

much more free from topographic constraints. Second-type events occur in this case: as for a BW to be established a certain extent of pressure increase has to be attained due to the airflow damming up against the mountain, this condition will only be satisfied in the left part, that is downstream, of the incoming flow. Therefore, incoming winds will appear to make a gentle turn to the left and merge into a more or less pronounced barrier wind.

A first-type event will be examined in Chapter 4, while a second-type event will be discussed in Chapter 5.

2.4 Results of the climatological analysis

The findings of our two-year climatology are summarized in table 2.1, where BW and flow-over episodes are classified by the location of occurrence. The overall results are also shown. Several significant parameters have been calculated for each episode set: average NMH with its standard deviation, average upstream wind speed $\overline{U}$, average BW maximum speed $\overline{W}$, number of episodes and percentage of rainy ones.

Location	*type*	$\overline{NMH}$	σ	$\overline{U}$	$\overline{W}$	*# evs.*	*% rainy*	t	*p-value*
Alpine	**BW**	1.7	0.2	15	12	7	100%	3.4	$2 \cdot 10^{-3}$
	FO	1.4	0.1	21	—	5	100%		
Adriatic	**BW**	1.3	0.3	13	11	21	29%	7.1	$< 10^{-3}$
	FO	0.7	0.2	18	—	12	58%		
Tyrrhenian	**BW**	1.3	0.3	13	10	8	12%	4.3	$< 10^{-3}$
	FO	0.7	0.3	16	—	11	100%		
Dinaric	**BW**	1.5	0.2	14	11	12	33%	8.9	$< 10^{-3}$
	FO	0.8	0.2	16	—	13	100%		
Ligurian	**BW**	1.3	0.4	13	11	16	62%	4.6	$< 10^{-3}$
	FO	0.8	0.2	13	—	8	88%		
OVERALL	**BW**	1.4	0.3	13	11	64	44%	12.1	$< 10^{-3}$
	FO	0.8	0.2	16	—	49	88%		

Table 2.1: Results of the climatology. **BW** designates BW episodes, **FO** flow-over episodes. For each episode set, $\overline{NMH}$ is the average Non-dimensional Mountain Height (or inverse Froude number), σ is the associated standard deviation; $\overline{U}$ is the average upstream wind speed and $\overline{W}$ is the average BW maximum speed, both of them being expressed in m/s; t is the significance test statistic, while the p-value is the associated probability threshold.

As we can observe in the table:

- The average NMH considerably differs between BW episodes and flow-over ones, the latter exhibiting much lower values than the former – more precisely, NMH values greater than 1 for BW events and smaller than 1 for flow-over events, as we would expect. Moreover, flow-over episodes clearly feature stronger average upstream winds than BW ones. Both these differences are in good agreement with the theory discussed in Chapter 1, for which the stronger the incoming flow – that is, the larger the upstream orographic Froude number U/NH – the more easily the flow crosses the mountain.

- The percentage of rainy episodes is also much larger for flow-over episodes than for BW ones. This may be interpreted as due to the deeper layer of upstream airflow managing to cross the mountain in flow-over cases, meaning that a larger amount of moisture is condensed, hence clouds are more easily formed.

- The largest values of NMH are found for the Alpine events (both BW and flow-over ones), due to the considerable height of the Alps. Aside from the fact that we would possibly need a larger number of Alpine episodes for our categorization to be more accurate, the NMH of the Alpine rainy events could have been possibly overestimated owing to the fact that we have used the dry Brunt-Väisälä frequency N_d throughout, instead of the moist frequency N_m. Since the flow impinging on the Alps is forced to ascend much more than the one impinging on lower mountains, it is likely that the flow is soon brought to saturation – also because in flow-over cases also the low-level part of the flow, which is usually the moister one, ascends the mountain. This could have caused an overestimation of N and of the NMH as a result.

Nonetheless, the use of N_d is sufficient to yield an estimate of the Froude number distribution of BW and flow-over events, as already discussed in section 2.1. In order to check the distinction in the Froude number distribution between the two types of events and to rule out potential errors, we conducted Welch's t-test, a statistical significance test and an alternative version of Student's t-test, on every episode set.

This test is used when dealing with two populations having both unequal size and unequal variances, to test the null hypothesis that the two population means are equal. Welch's t-test is intended for small-sized data samples. Once we have computed the test statistic t and the number of degrees of freedom ν, we can use Student's t-distribution with ν degrees of freedom to obtain a p-value, which is the probability of getting a test statistic larger than the one that was actually observed. In other words, the p-value

is the probability that the null hypothesis is true – that is, the probability that the two population means are equal.

The test statistic t is calculated as follows:

$$t = \frac{\overline{X}_1 - \overline{X}_2}{\sqrt{\frac{s_1^2}{N_1} + \frac{s_2^2}{N_2}}} \tag{2.6}$$

where $\overline{X}_i$, s_i^2 and N_i are the i^{th} sample mean, variance and size, respectively ($i = 1, 2$). The number of degrees of freedom ν is estimated from the *Welch-Satterthwaite equation*:

$$\nu \sim \frac{\left(\frac{s_1^2}{N_1} + \frac{s_2^2}{N_2}\right)^2}{\frac{s_1^4}{N_1^2 \nu_1} + \frac{s_2^4}{N_2^2 \nu_2}} \tag{2.7}$$

where $\nu_i = N_i - 1$, the degrees of freedom associated with the i^{th} variance estimate.

The t and p-values of each test we conducted are also displayed in table 2.1. The fact that all p-values are much smaller than 0.01 (1%) is a significant statistical confirmation that BW episodes and flow-over ones feature different average NMH.

All events are displayed in a scatter plot in figure 2.13, to better visualize their distribution in terms of NMH and upstream wind speed. As we can see, most of the rainless events are BW ones, while rainy events are almost equally divided between the two cases. It is evident that BW events tend to feature a larger NMH and a smaller upstream wind speed with respect to flow-over events, as already noted. Nonetheless, the upstream wind speed U is used to calculate the NMH, meaning that for every point in the scatter plot, its ordinate depends on its abscissa. This can be deceptive when it comes to interpret the events distribution.

A better visualization is achieved in figure 2.14, where the events are grouped in a histogram. It is evident the separation between light-coloured rectangles, representing flow-over events, most of which are situated to the left of the NMH $= 1$ threshold, and dark-coloured rectangles, representing BW events, most of which are situated in the NMH > 1 region of the graph. A remarkable exception is constituted by the light-green rectangle representing the Alpine flow-over events, all featuring a NMH between 1.3 and 1.6. The reason of this unexpected position has been discussed before.

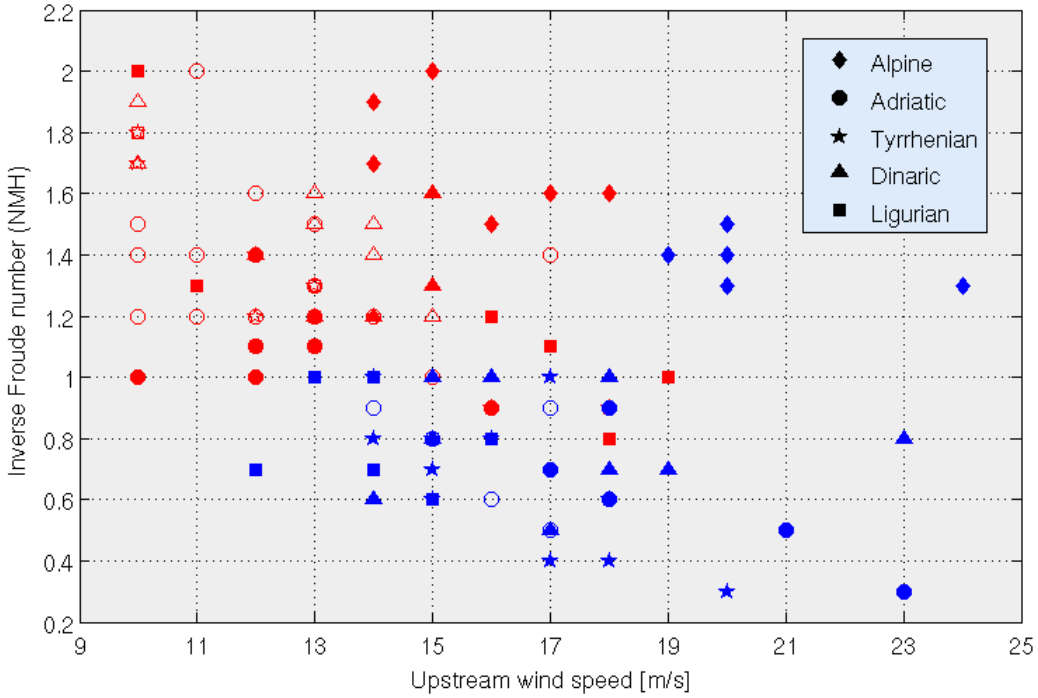

Figure 2.13: Scatter plot including both BW (red) and flow-over events (blue). Blank markers are rainless events, full ones are rainy events.

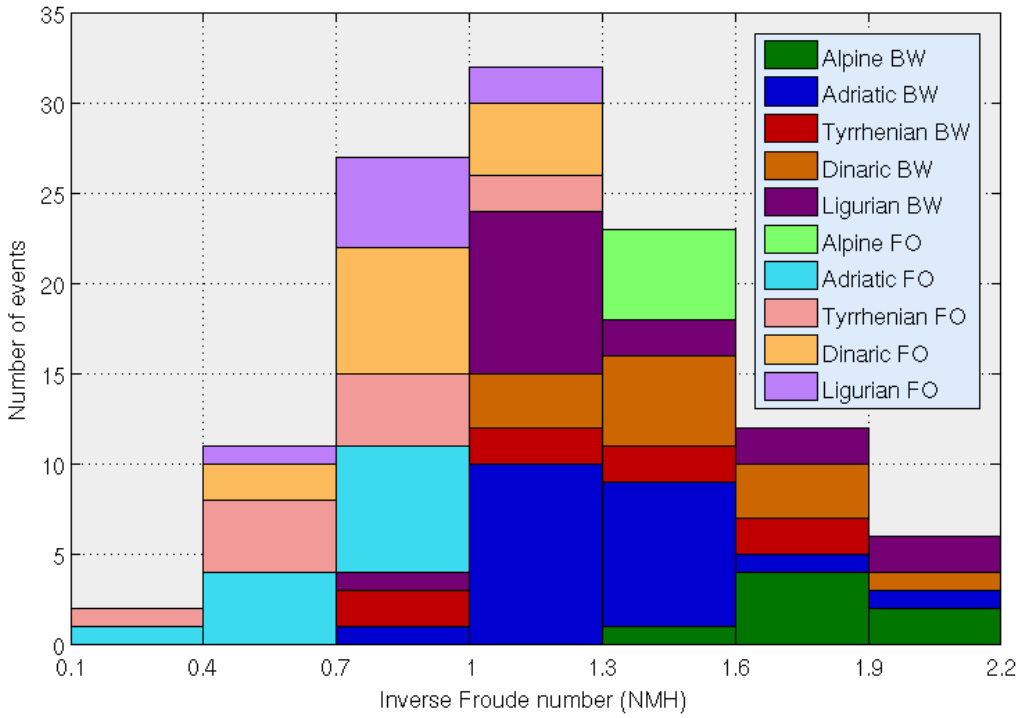

Figure 2.14: Histogram classifying the events by their NMH. Dark-coloured rectangles represent the BW events, light-coloured ones are flow-over events.

Chapter 3

The BOLAM and MOLOCH meteorological models

In this chapter we are going to describe the BOLAM and MOLOCH meteorological models, which we have used to carry out the climatology and to perform dedicated simulations of selected events.

3.1 The BOLAM model

The BOLAM model is the first meteorological model to have been entirely developed in Italy. It was first created at the CNR–ISAC institute in Bologna in 1992 and it has been continuously enhanced hitherto (Buzzi et al., 1994; Malguzzi and Tartaglione, 1999; Buzzi and Foschini, 2000; Malguzzi et al., 2006; Orlandi et al., 2010).

BOLAM has been employed for numerous research works, including case studies of heavy precipitation (see e.g. Buzzi et al., 1998, 2003; Davolio et al., 2009c), marine forecasting (Cavaleri et al., 2010) and idealized studies, using a channel version of the model grid (Miglietta and Buzzi, 2004). It has been tested and compared with other mesoscale limited-area models several times and has always exhibited favourable results. It was first tested for the COMPARE (Comparison of Mesoscale Prediction and Research Experiments) project organized by the World Meteorological Organization. Model intercomparison was carried out on a mid-latitude explosive cyclogenesis episode (Compare I: Gyakum et al., 1996), on a well documented event of flow over orography in the presence of lee waves and wakes (Compare II: Georgelin et al., 2000) and on a case of explosive development of a tropical cyclone over the Pacific Ocean (Compare III: Nagata et al., 2001). BOLAM turned out to be the second best model in the first case and the best one in the other cases. Further tests confirmed its satisfactory performance.

The BOLAM model is currently being employed for daily weather forecasting at several

Italian national agencies and regional meteorological offices (see e.g. Corazza et al., 2003 and Chessa et al., 2004), by the National Observatory of Athens in Greece (Lagouvardos et al., 2003) and by the National Center for Hydrological and Meteorological Forecasting (NCHMF) of Vietnam. Furthermore, it is being used for real-time weather forecasting at the CNR–ISAC institute in Bologna on behalf of the National Civil Protection Department – we used its output maps to develop our climatology in Chapter 2.

3.1.1 BOLAM main features and dynamics

BOLAM is a hydrostatic LAM (Limited Area Model) based on primitive equations; convection is parameterized. The prognostic variables are wind components u and v, absolute temperature T, surface pressure p_s, specific humidity q and turbulent kinetic energy TKE. The water cycle for stratiform precipitation is described by means of five additional prognostic variables: cloud ice, cloud water, rain, snow and graupel.

The model prognostic variables are distributed in the vertical on a non-regular Lorenz grid, with higher resolution in the atmospheric boundary layer near the ground.

The vertical discretization is based on a hybrid vertical coordinate system, where the terrain-following coordinate $\sigma = p/p_s$ gradually tends to a pure pressure coordinate with increasing height above the ground. The relaxing factor from σ to p, named α, is prescribed as a function of the maximum orography height in the domain:

$$\alpha \leq \frac{p_0}{p_0 - \min(p_s)} \tag{3.1}$$

while the pressure at some level σ is calculated:

$$p = p_0\sigma - (p_0 - p_s)\,\sigma^{\alpha}, \qquad 0 \leq \sigma \leq 1 \tag{3.2}$$

where p_s designates surface pressure and p_0 is a reference pressure, usually 1000 hPa. The α parameter is typically greater than 2, though smaller values have to be taken if some very high mountain is in the integration domain. The greater α is, the more quickly the σ-surfaces tend to p-surfaces with increasing height.

The horizontal discretization is based on a staggered Arakawa C-grid (Arakawa and Lamb, 1977) in (optionally) rotated geographical coordinates (latitude-longitude). In the rotated system the equator is located at the center of the integration domain, which has rectangular shape; this stratagem minimizes grid anisotropy caused by the convergence of meridians toward the pole. Using rotated coordinates is not straightforward, as meteorological fields and topography have to be interpolated when passing from one reference system to another during the pre- and post-processing stages; wind components also have to be transformed, as their orientation is different in the two systems. The

advection scheme implemented is the Eulerian Weighted Average Flux (WAF) scheme (Billett and Toro, 1997) which has second-order accuracy.

An explicit *time-split* temporal integration scheme is employed, except for sound waves which are vertically propagated via an implicit scheme; a forward-backward one is used for gravity modes. By using a time-split scheme, motions of different time scales are treated separately. The horizontal diffusion scheme is of the second order for all the prognostic variables, except for surface pressure. Local and vertically integrated divergence is slightly diffused to control internal and external gravity wave modes and prevent energy accumulation to small spatial scales.

The lateral boundary conditions are imposed on a number of grid point rows (typically 8) at the end of every time step, using a relaxation scheme (Lehmann, 1993) that absorbs wave energy, helping in reducing spurious reflection by the lateral boundaries. This scheme is particularly convenient as its relaxation coefficients depend on grid spacing, so that they automatically adjust as resolution changes.

3.1.2 BOLAM physics: water cycle

The set of parameterizations needed to account for small-scale phenomena is named "model physics". Their task is to represent all those physical processes that happen at a spatial scale smaller than grid spacing, hence they cannot be explicitly described. BOLAM physics includes atmospheric water cycle, turbulence and orographic drag, surface and soil processes, and radiation.

The atmospheric water cycle scheme is based on explicit assumptions of spectral distributions of clouds (droplets and ice crystals) and of liquid and solid hydrometeors. The spectral properties of hydrometeors are simulated assuming a generalized gamma function distribution. The main processes described by the microphysical scheme are:

- nucleation of cloud water (*cw*) and of cloud ice (*ci*);
- condensation and evaporation of *cw*;
- freezing of *cw*;
- nucleation sublimation and melting of *ci*;
- auto-conversion of *cw* and *ci*;
- sublimation of snow and graupel in both directions;
- collection–accretion–riming: 13 different hydrometeor interaction processes involving rain (freezing or not), snow and graupel (dry or melting), *cw* and *ci*;

- melting and evaporation of hydrometeors;
- terminal fall speeds computation and fall process, using a conservative-diffusive backward-upstream integration scheme;
- thermodynamic feedback based on enthalpy conservation.

Although this scheme has been devised to represent mainly stratiform precipitation processes – convection is parameterized – it has been formulated as coherent as possible with MOLOCH microphysical scheme, in order to attain the maximum consistency between the two models (MOLOCH is usually nested into BOLAM).

The effects of deep moist convection development are parameterized using the Kain–Fritsch convective scheme (Kain and Fritsch, 1990), updated to its latest revision (Kain and Fritsch, 2004). Parameterization of shallow moist convection is also implemented as comprised in that scheme, with some modifications.

3.1.3 BOLAM physics: turbulence and surface processes

The surface layer and the planetary boundary layer are modelled accordingly to the similarity theory (Monin and Obukhov, 1954). The mixing-length based turbulence closure model, widely used to compute the ABL (Atmospheric Boundary Layer) fluxes for atmospheric modelling, is applied to parameterize the turbulent vertical diffusion of momentum, heat and moisture. The turbulence closure is of order 1.5 (*E-l* scheme, Zampieri et al., 2005), in which the TKE is predicted.

In order to account for buoyancy effects in a stratified ABL, the Blackadar mixing length (Blackadar, 1962) is used together with stability functions depending on the Richardson number. For the unstable ABL case, a modified version of the non-local mixing length of Bougeault and Lacarrere (Bougeault and Lacarrere, 1989) is applied. The roughness length is computed as a function of vegetation and of sub-grid orography variance. Over the sea, a Charnock roughness (Charnock, 1955) is employed, accounting for the wave height as a function of the surface wind speed. The sea surface temperature (SST) is computed, depending on latent and sensible heat fluxes and radiative fluxes, using a simple slab ocean model.

A parameterization of the orographic wave drag, associated with the deceleration of the mean flow passing over orography, is applied.

A soil model using 4 to 6 layers is also employed. The layer thickness increases with depth, from a few cm to more than 1 m. The model calculates surface energy, momentum, water and snow balances, heat and water vertical transfer, vegetation effects at the surface (evapotranspiration, precipitation interception, wilting effects etc.) and within the soil (extraction of water by roots). The geographical distribution of different soil

types and physical features is also accounted for, as well as water freezing and melting effects.

3.1.4 BOLAM physics: radiation

The atmospheric radiation is computed with a combined application of the RG scheme (Ritter and Geleyn, 1992) and the ECMWF scheme (Morcrette, 1991; Mlawer et al., 1997). Since the ECMWF scheme is much more computationally expensive than the RG scheme, it cannot be applied at each time step and each grid column; therefore, the RG scheme is preferentially employed, being applied extensively at all grid points and in rapid update mode, whereas the ECMWF scheme is applied at alternate points and at long intervals to compute corrections to the RG scheme. The ECMWF radiation library includes definitions of the "climatology" (seasonal and geographical distribution) of different types of aerosol and of atmospheric composition. The model has been recently upgraded so that all inputs (astronomical functions, aerosol, ozone, greenhouse gases, albedo, emissivity and clouds) are now fully consistent between the two (GR and ECMWF) schemes.

3.1.5 BOLAM software features

The entire BOLAM code is written in Fortran 90 language. The model is fully parallelized through the domain splitting technique and is compatible with the MPICH2 and OpenMP parallel computing environments.

The domain splitting technique consists of dividing the integration domain into multiple subdomains, each of which is assigned to a single processor; the whole simulation is then split into multiple subprocesses that are executed at the same time. The number of subdomains – and of subprocesses as well – equals that of available processors.

BOLAM highest suitable resolution is limited by the hydrostatic approximation and the parameterization of convection, being typically 6 to 8 km. For accurately simulating smaller space scales, one-way nested simulations may be performed, typically by nesting the MOLOCH model into BOLAM. A direct employment of higher-resolution models such as MOLOCH is usually avoided for two reasons: it would be computationally too expensive, requiring both long integration time and extremely powerful computers; and it would necessitate quite an inaccurate interpolation to retrieve initial and boundary conditions. BOLAM thus acts as a means to conveniently proceed from larger to smaller scales, thereby reducing integration time and enhancing accuracy.

3.2 The MOLOCH model

The non-hydrostatic MOLOCH model was initially created at the CNR–ISAC institute in Bologna in 2000 (Tettamanti et al., 2002). It has been developed as a scientific tool in dynamic meteorology for high-resolution atmospheric simulations and mesoscale weather forecasting, allowing the explicit treatment of atmospheric convection.

Although specific research stand-alone versions of MOLOCH have been devised for scientific use (see e.g. Fantini and Malguzzi, 2008; Malguzzi et al., 2010; Fantini et al., 2012), the model has been mainly employed nested in BOLAM, as part of a model chain for simulating and studying meteorological events and for real-time weather forecasting. For instance, MOLOCH was used to study episodes of heavy precipitation (Davolio et al., 2006; Malguzzi et al., 2006; Davolio et al., 2007, 2009c) and of strong winds (Tettamanti et al., 2002; Davolio et al., 2009b; Buzzi et al., 2011).

MOLOCH has been tested several times and compared to numerous other models. For instance, it was tested for the MAP–DPHASE international forecasting demonstration project (Rotach et al., 2009), in which many mesoscale high-resolution NWP models were compared in real time, especially with regard to QPF (Quantitative Precipitation Forecasting, see Davolio et al., 2009a); it was tested for the European project RISKMED as well. MOLOCH performance was generally quite satisfactory in all cases (Richard et al., 2007; Diomede et al., 2008; Davolio et al., 2009a).

The MOLOCH model is currently being employed in real-time forecasting by several Italian agencies (for instance, Regione Liguria[1] uses it for public weather forecasting). Furthermore, it is being used for real-time weather forecasting at the CNR–ISAC institute in Bologna on behalf of the National Civil Protection Department – we used its output maps to develop our climatology in Chapter 2.

3.2.1 MOLOCH main features and dynamics

MOLOCH is a non-hydrostatic, fully compressible model which explicitly resolves convection, integrating the set of atmospheric equations. Its prognostic variables are pressure p, absolute temperature T, specific humidity q, horizontal (u, v) and vertical (w) wind components, turbulent kinetic energy TKE and five water species: cloud water, cloud ice, rain, snow and graupel. They are represented on the latitude-longitude, optionally rotated Arakawa C-grid (Arakawa and Lamb, 1977). MOLOCH shares several features with BOLAM, which we will not describe here again.

A hybrid terrain-following coordinate ζ, smoothly relaxing to horizontal surfaces with increasing height, is employed. Unlike BOLAM σ coordinate which is associated to

[1] `http://www.arpal.gov.it/`

pressure, MOLOCH ζ coordinate is associated to height:

$$\zeta = H\left(1 - \exp\left(-\frac{z - h(1-\zeta/H)}{H}\right)\right) \tag{3.3}$$

where h is the height of the orography ($h < z < \infty$), $H = R_d T_0/g$ is troposphere scale height and T_0 a reference temperature.

Model dynamics are integrated in time with an implicit scheme for sound waves vertical propagation, while explicit, time-split schemes are implemented for the remaining terms of the equations of motion. Three-dimensional advection is computed using the Eulerian Weighted Average Flux scheme (Billett and Toro, 1997) just like in BOLAM. Horizontal second-order diffusion and a small divergence damping are included to prevent energy accumulation to small spatial scales.

3.2.2 MOLOCH physics

MOLOCH microphysical scheme was initially based on the parameterization proposed by Drofa and Malguzzi (Drofa and Malguzzi, 2004); it has been later reviewed and upgraded. The scheme is essentially akin to the BOLAM one and the processes it includes are just the same. However, specific differences have been introduced in the MOLOCH scheme in order to deal with convective systems. In particular, it has the capability of implementing the so-called two-moment microphysics, by integrating in time *cw* and *ci* spatial distributions, thus accounting for cloud spectra evolution.

The MOLOCH radiation, turbulence and soil–surface schemes are essentially similar to the BOLAM ones which we have described in detail in sections 3.1.3 and 3.1.4.

3.2.3 MOLOCH software features

MOLOCH is entirely written in Fortran 90 language, just like BOLAM. The model is fully parallelized as well and is compatible with the MPICH2 and OpenMP environments. MOLOCH runs are usually nested into BOLAM ones, which are performed at a smaller resolution.

The model is optimized to operate as short-range (12-48 hours) weather forecasting model, with 1 to 4 km horizontal resolution and 40 to 80 vertical levels. For research purposes, it has been tested with horizontal resolution up to 500 m and more than 100 levels.

3.3 BOLAM and MOLOCH execution process

Both BOLAM and MOLOCH need initial and boundary conditions in order to integrate the equations of motion within a selected domain. Either the ECMWF or the GFS analyses and subsequent forecasts may be employed as such fields for BOLAM, whereas MOLOCH requires BOLAM output fields, being nested into it.

The pre-processing stage of the model run sets the stage for the simulation. It includes several interpolations operating on the initial and boundary conditions, on soil and vegetation fields and on the orography field; all data fields are thus made compatible with the resolution that has been selected for model run. The integration domain, the rotated coordinate system and further parameters are also set at this time. Several output files (Model History Files, `.mhf` format) are eventually generated, which will be subsequently used as initial and boundary conditions during the actual simulation.

Before launching the model run, several parameters may be set up, including time step, simulation duration, number of processors to be employed etc. The simulation eventually outputs a `.mhf` file.

The model output file is finally post-processed and a `.ppf` file (ASCII format), containing all output fields in readable format, is generated. This is compatible with graphics software such as NCAR Graphics, which can plot the requested meteorological fields using either the model levels or, alternatively, user-selected levels after calculating the proper values through interpolation.

Chapter 4

The 2013 Alpine case study

In order to attain a deeper knowledge of barrier winds in the Italian region, we chose three representative events from our climatology and performed dedicated simulations on them with BOLAM and MOLOCH models.

This focused approach is motivated by the following reasons and targets:

- By restricting our attention on few selected case studies, we are able to isolate the most significant ones and focus on their crucial features.
- Dedicated simulations allow us to fully characterize an event in terms of whatever aspects we deem to be necessary: we can retrieve (nearly) any piece of information, such as fields at arbitrary height and time, computed quantities like averages, maxima and minima etc.
- Model performances can be compared with each other and their results can be contrasted with observational data: in this way we can both evaluate their forecasting accuracy and try to grasp the role of model resolution in this type of simulations.
- Finally, the model orography can be altered in order to conduct *sensitivity tests*. By reducing the height of the mountains the incoming flow impinges on, we are actually reducing the NMH as well; we can then perform a simulation with the lowered mountains and analyze the modifications in BWs speed, temperature and rainfall patterns etc., thus analyzing the influence of the Froude number on BWs occurrence and characteristics.

We have to keep in mind that the Froude number theory was devised for idealized flows over simply shaped orography. Therefore, we cannot expect it to satisfactorily account for the complexity and variability of realistic conditions. Nonetheless, we can try to identify the impact of upstream flow alteration on the BWs development and features, and then explain the results through a cautious use of the theory.

The first case study we selected is an Alpine one which occurred on February 11, 2013. It lasts over 15 hours and features intense low-level winds, both incoming and barrier ones; it also features abundant precipitation and a cold pool. In the following section we are going to discuss the event features, as well as illustrate the results of the simulations we performed with BOLAM and MOLOCH.

4.1 Event simulations

4.1.1 BOLAM simulation

The first simulation we performed is a 36-hours BOLAM run, from February 11, 2013, 00 UTC to February 12, 2013, 12 UTC. We choose the initialization time so as to prevent the initial condition adjustment following the beginning of the run from affecting the accuracy of the simulation. Since the core of the event begins around 08 UTC on February 11 and the adjustment duration can be estimated at 3 to 6 hours at most, a sufficiently long time has passed from the initialization. The integration domain is displayed in figure 4.1.

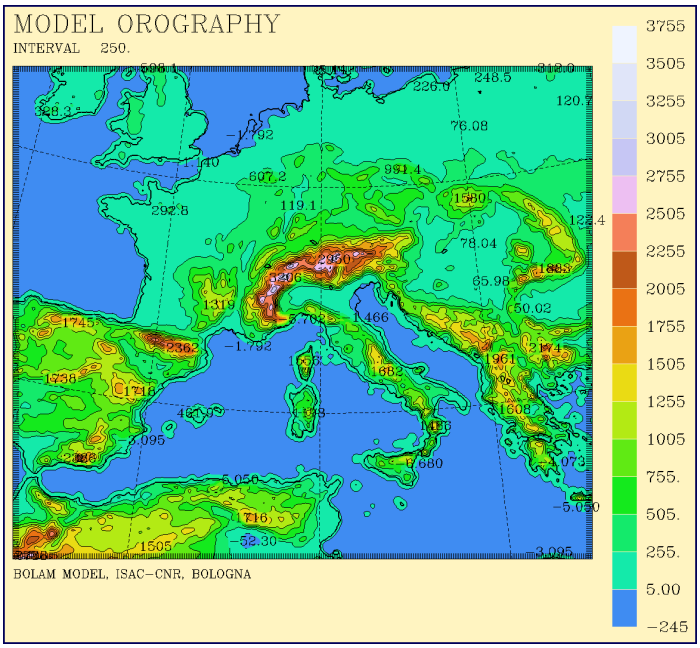

Figure 4.1: BOLAM main run integration domain.

The initial and boundary conditions have been retrieved from the 00 UTC analysis and subsequent forecasts of the GFS model of NOAA–NCEP (USA). Grid spacing has been set at 0.08 degrees (approximately 9 km) both in longitude and latitude; the domain size is 322 points in longitude and 274 in latitude. 50 hybrid-coordinate vertical levels and 7 soil levels have been employed. Time step has been set at 80 seconds and the combined

radiation scheme (RG + ECMWF, see subsection 3.1.4) has been used. These settings have been also employed for all of the other BOLAM simulations performed on this case study.

The synoptic situation that brings about the Alpine event is displayed in figure 4.2, concerning the central part of the event. A deep trough moves quickly through western Europe until its minimum is located over the Ligurian Sea (figure 4.2a. This generates a deep cyclone over northern Italy (figure 4.2b), as regularly happens in this region (cyclone reinforcement caused by the presence of the Alps was analyzed, for instance, by Buzzi and Tibaldi, 1978 and by Orlanski and Gross, 1994 who also mentions the possibility of BWs occurrences in these cases).

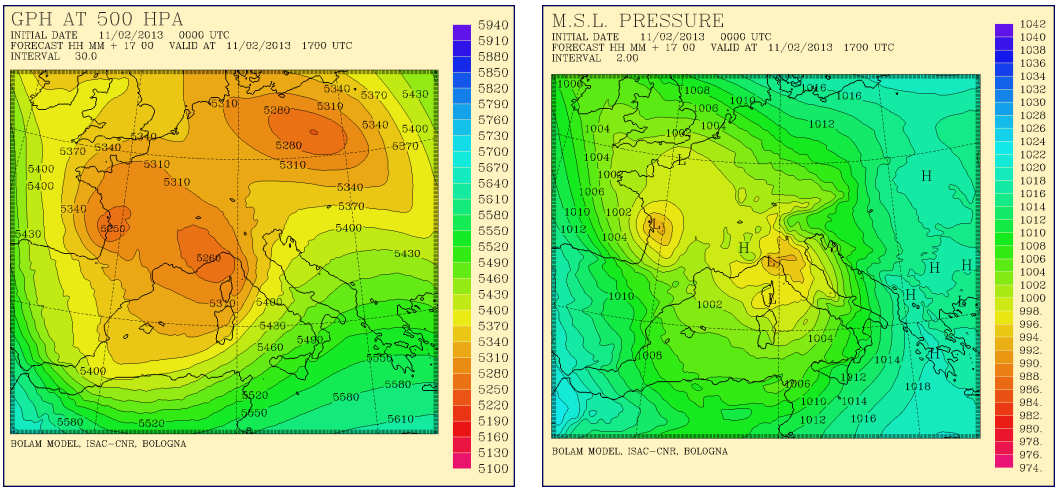

(a) 500 hPa geopotential height (dam). **(b)** M.s.l. pressure (hPa).

Figure 4.2: BOLAM run, 500 hPa geopotential height and m.s.l. pressure at 17 UTC.

Intense winds are generated over the entire Italian region and especially over the Adriatic Sea, where a strong and wide band (about 200 km) is gradually formed, as shown in figures 4.3 and 4.4. These winds peak at 20 m/s speed near the surface and exceed 25 m/s at the 950 hPa level during the central part of the event; the incoming flow stretches up to 1500 m altitude, where there is strong vertical shear as winds veer and reduce in intensity. An intense and extensive barrier wind is established on the southern side of the Alps, reaching over 15 m/s near the surface (see figure 4.4a) and 32 m/s at 950 hPa; the BW width exceeds 50 km width for several hours (see the second chart in figure 4.3). As the BW extends all the way in front of the incoming flow, which consists of a quite wide band, this is clearly a *first-type* event.

As we can observe from figure 4.4b, there is no BW at 900 hPa, although a slight turn of the incoming flow is evident in the immediate vicinity of the mountain. In this case the presence of the cyclone over northwestern Italy – clearly highlighted by the

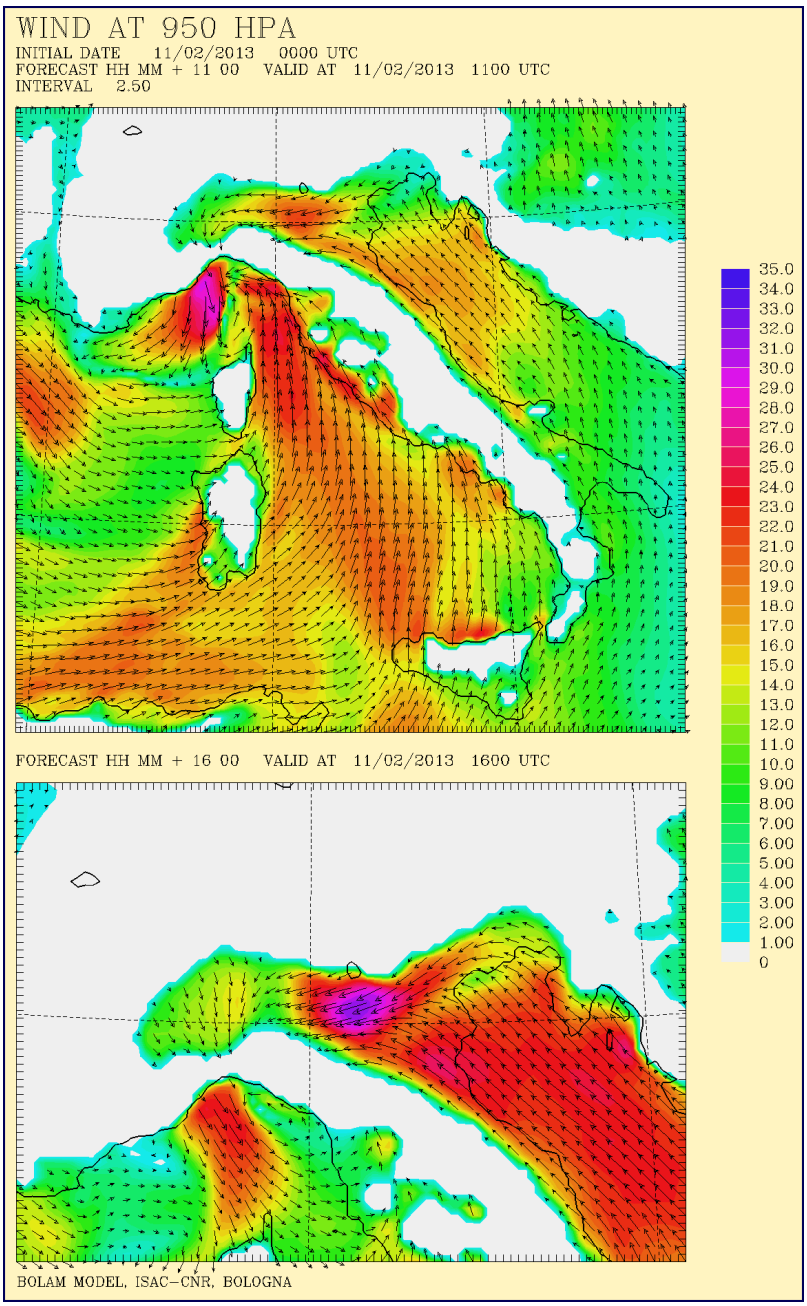

Figure 4.3: BOLAM run, wind at 950 hPa (m/s) at 11 UTC (top chart) and at 16 UTC (bottom chart, zoom over northern Italy).

counter-clockwise rotating winds in the left part of the chart – may be confusing, as it causes winds to turn left approximately where they would because of the barrier effect (it is often problematic to separate the synoptic influence from the barrier effect, as pointed out by Chen and Smith, 1987). Nonetheless it is clear, by comparing figures 4.4b and 4.3 and remembering the criteria discussed in section 2.1, that the BW does not extend to the 900 hPa level.

The cyclone sweeps quickly through northern Italy and a cold front eventually inter-

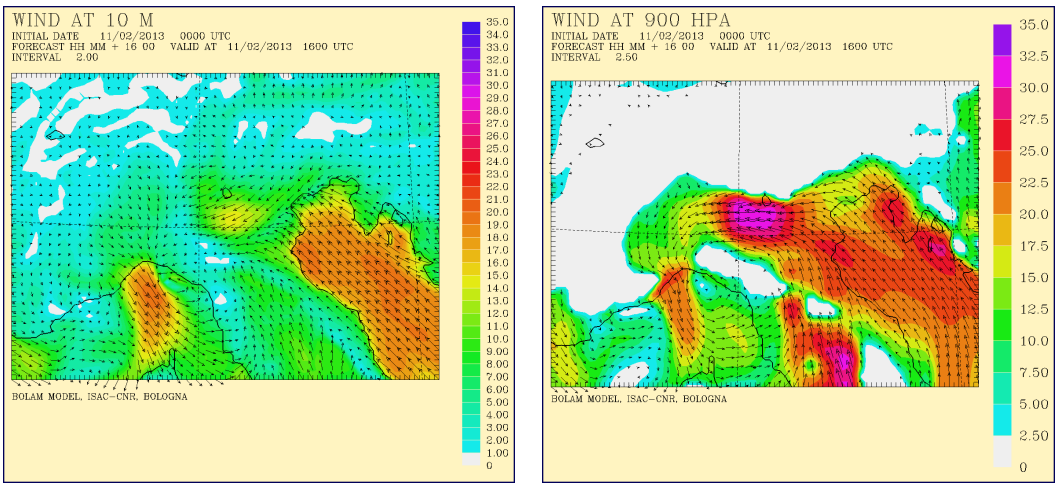

(a) Wind at 10 meters (m/s). **(b)** Wind at 900 hPa (m/s).

Figure 4.4: Wind at 10 meters and at 900 hPa, BOLAM forecast for 16 UTC (zoom over northern Italy).

rupts the incoming flow: strong southerly winds are substituted by lighter westerly ones, as we can observe in figure 4.5. The front, highlighted by strong horizontal shear with light southwesterly winds to the west and intense southeasterly ones to the east, is visible few kilometers south of the central part of the BW in figure 4.5a; two hours later, it has moved about a hundred kilometers eastward and is visible south of the eastern half of the BW (figure 4.5b). As soon as the incoming flow stops impinging against the Alps, the BW also disappears. The event is essentially over at 00 UTC on February 12.

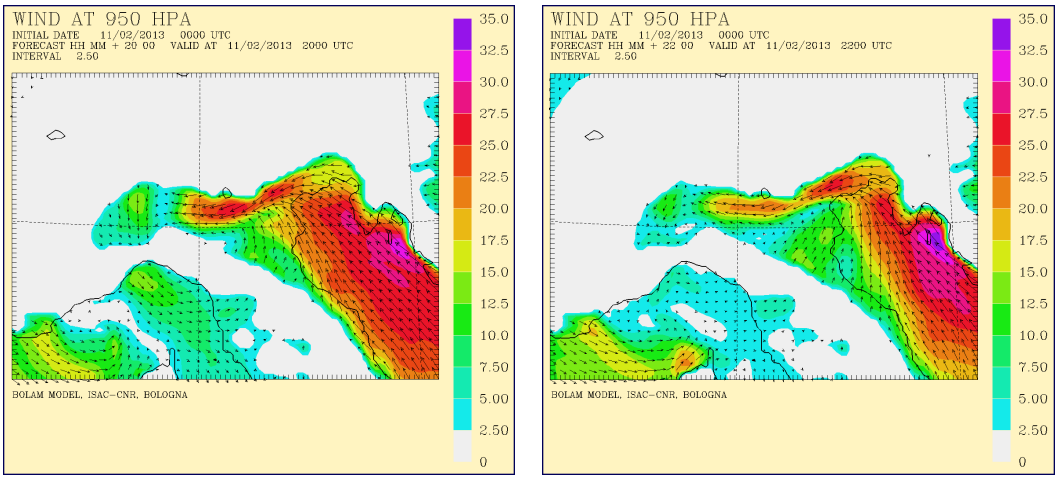

(a) Wind at 950 hPa (m/s) at 20 UTC. **(b)** Wind at 950 hPa (m/s) at 22 UTC.

Figure 4.5: Wind at 950 hPa, BOLAM forecast for 20 and 22 UTC (zoom over northern Italy).

A considerable amount of precipitation is associated with this event throughout northern Italy and especially in Veneto and Friuli regions: see figure 4.6 where the total cumulated precipitation at the end of the simulation is displayed (see also section 4.2 where model forecasts are contrasted with observational data). Snowfall predominates above a few hundred meters altitude, although some cities in the Veneto plains, such as Padua and Treviso, also received mostly snowfall (see section 4.2 for a comparison between model forecasts and observational data). The presence of the very BW and of a cold pool near the surface (see later) prevented the incoming flow from warming up the lowest layers which remained around freezing throughout the event, with a moderate temperature inversion in the first few hundred meters.

As we can see in figure 4.6, there are two maxima, the first one near the Adriatic coast while the second one is located farther downstream over the Alps, albeit being closer to the mountain foot than to the mountain top. This precipitation pattern is typical of BWs events, as we remarked in section 1.3, due to the fact that the incoming winds are forced to ascend more upstream than they would otherwise (the presence of a cold pool enhances this effect). It is apparent, by comparing figure 4.6 with the bottom chart in figure 4.3, that the first maximum is situated exactly where there is the confluence of the incoming flow and the BW.

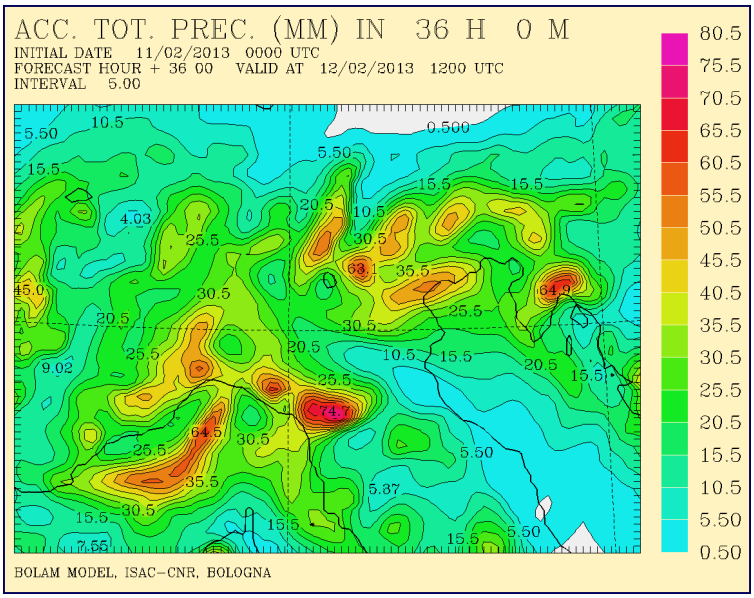

Figure 4.6: BOLAM run, total accumulated precipitation (mm) at the end of the simulation (zoom over northern Italy).

This is also visible in figure 4.7, where the hourly precipitation is shown at four instants. At 16 UTC (figure 4.7a), during the central part of the event, the confluence is situated immediately off the Adriatic northern coast (compare this chart with the bottom one in figure 4.3) and precipitation maximum coincides with it. At 20 UTC (figure 4.7b), when the cold front has just begun to sweep the northern Adriatic Sea, the confluence is

enhanced and the principal maximum is more intense and situated further downstream than before; there is also a secondary maximum caused by the very BW ascending over the small spur of the Alps situated to the east of the Garda Lake. At 22 UTC (figure 4.7c) there is a second maximum over the Alps, as the BW is being gradually eroded. At 00 UTC on February 12 (figure 4.7d), when the BW has almost disappeared, only the maximum over the Alps is left and located further to the east than before, due to the westerly winds following the cold front.

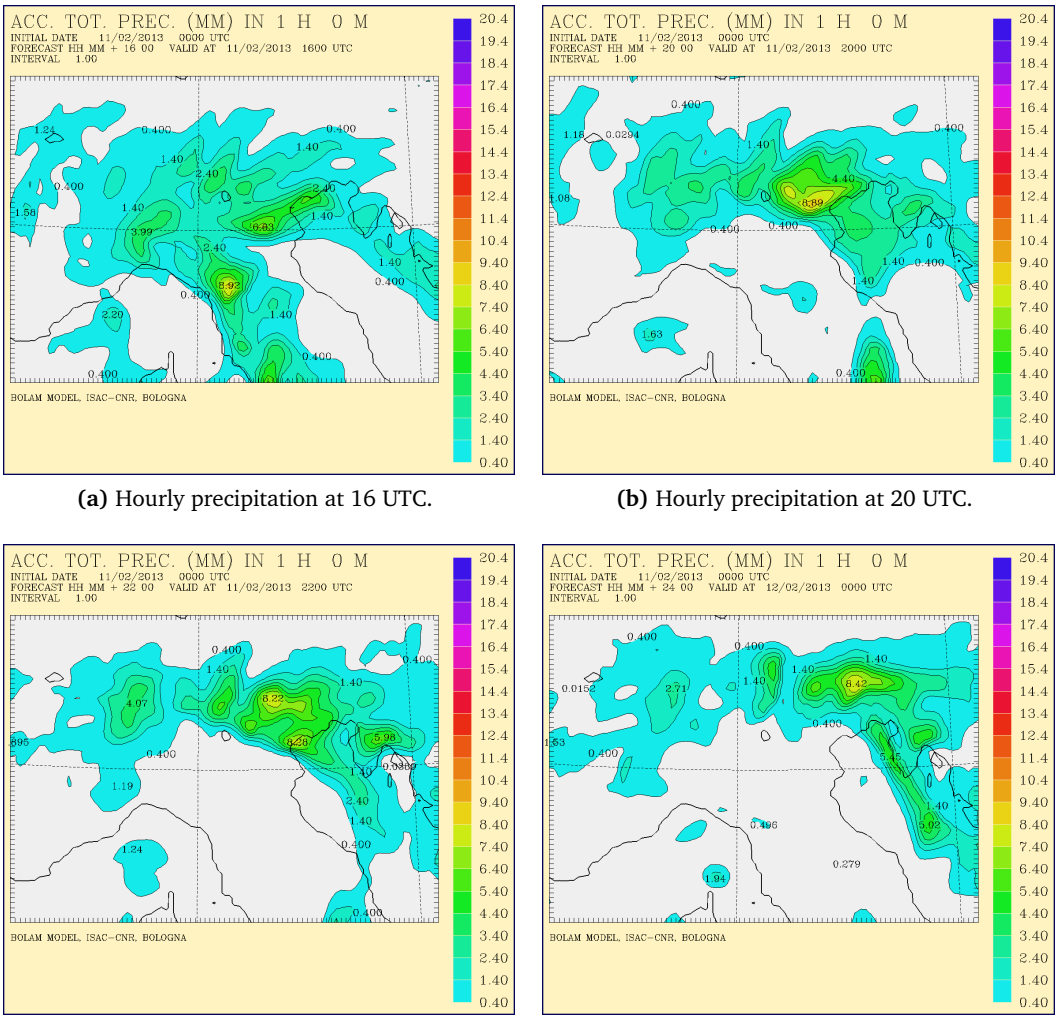

(a) Hourly precipitation at 16 UTC.

(b) Hourly precipitation at 20 UTC.

(c) Hourly precipitation at 22 UTC.

(d) Hourly precipitation at 24 UTC.

Figure 4.7: BOLAM run, hourly precipitation (mm) at 16, 20, 22 and 24 UTC (zoom over northern Italy).

As the incoming flow is quite intense near the surface and travels a long path over the Adriatic Sea, it collects a large amount of moisture: this may have contributed to enhance precipitation. This reasoning is supported by the fact that the relative humidity of the

flow increase considerably between the beginning and the core of the event; however, that can be also due to the cyclone advecting humidity northwards.

This event also features a cold pool on the southern flank of the eastern Alps, as we can see in the meridional cross section of θ_e and w shown in figure 4.8a; the cross section has been computed at the longitude shown in figure 4.8b. The cold pool is detectable as the violet "bubble" of colder equivalent potential temperature on the southern side of the Alps in figure 4.8a. The incoming airflow, being several degrees warmer than the cold pool air, is forced to ascend over it, thus being unable to displace it for several hours: although the cyclone transports warmer air towards the Alps, temperature varies very little throughout the day over the Veneto and Friuli plains. A strong gradient progressively develops near the Adriatic coast, with temperatures just above freezing few kilometers inland and well over 5 °C few kilometers off the coast: see figure 4.9 which compares 2 meters temperature at 11 UTC (the beginning of the event) and 19 UTC (the last part).

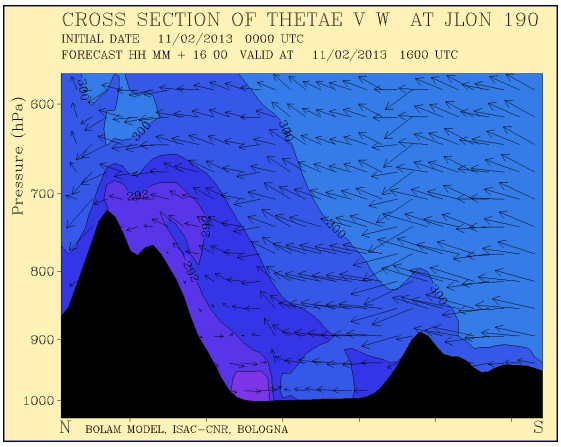

(a) Cross section of θ_e (K) and w at 16 UTC (zoom over northern Italy).

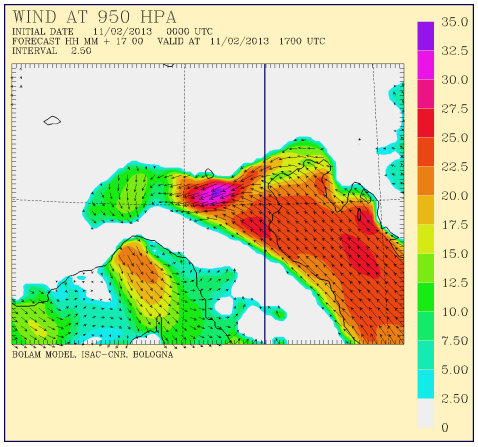

(b) Location where the cross section has been computed.

Figure 4.8: BOLAM run, longitudinal cross section of equivalent potential temperature θ_e and vertical velocity w at 16 UTC, and cross section location.

In this case the cold pool has no evaporative origin – most of the precipitation falls during the second half of the event – but it simply consists of a layer of pre-existing air which is much colder than the incoming flow. Such temperature pattern is typical in winter over the Po Valley, as strong nocturnal inversions are favoured by the flat terrain and the light winds which usually blow in this region. Nonetheless, evaporative cooling most likely plays a significant role in maintaining the cold pool also during the second part of the event.

The "pressure nose" typical of BWs episodes can be seen in figure 4.10: pressure in Veneto and Friuli plains is over 2 hPa higher than that a hundred kilometers off the

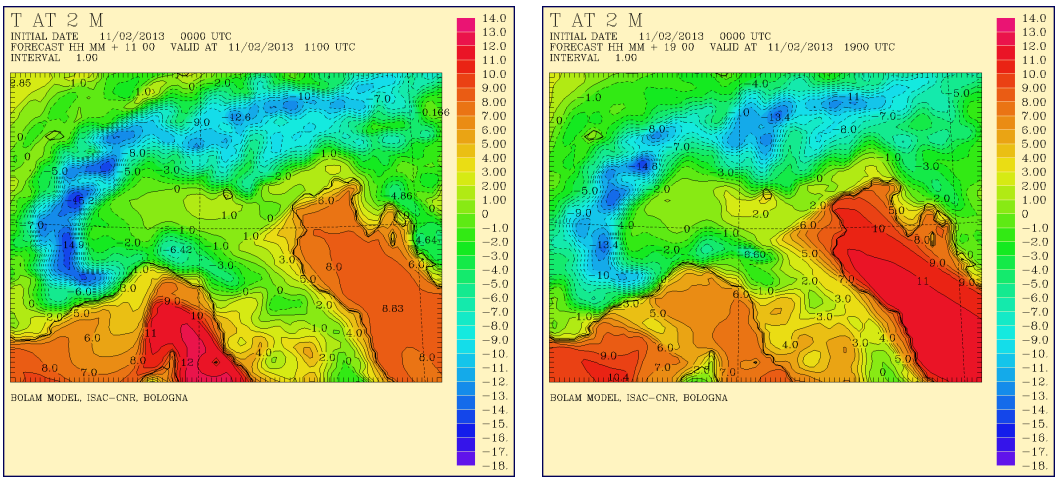

(a) 2 m temperature (°C) at 11 UTC. **(b)** 2 m temperature (°C) at 19 UTC.

Figure 4.9: BOLAM run, temperature at 2 m (°C) at 11 and 19 UTC (zoom over northern Italy).

Adriatic coast. Naturally part of this difference could be due to the cyclone, though most of it is caused by the barrier effect: as we will see in subsection 4.3 when discussing the sensitivity tests, if we lower the orography so much as to make the BW disappear the pressure "nose" strongly reduces as well.

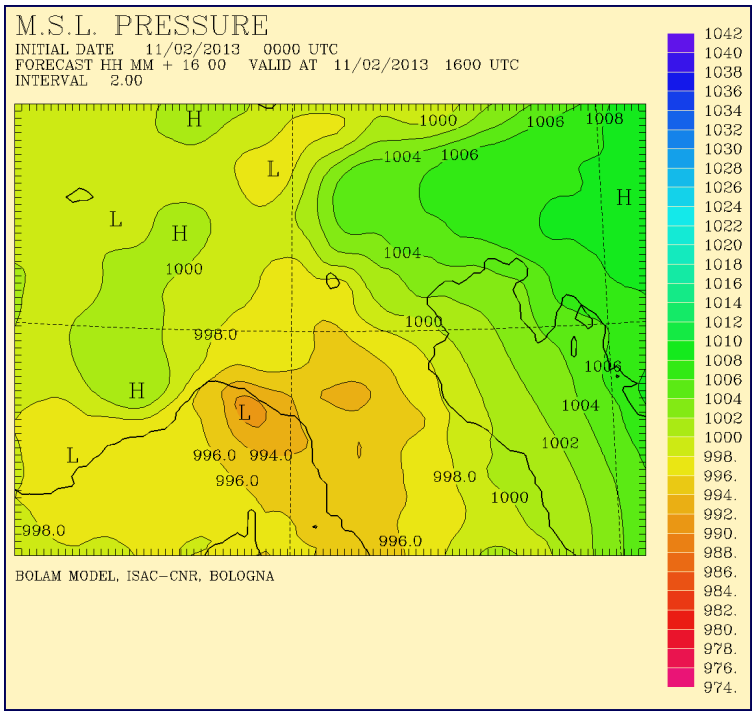

Figure 4.10: BOLAM run, m.s.l. pressure (hPa) at 16 UTC (zoom over northern Italy).

4.1.2 MOLOCH simulation

In order to analyze the event in detail and to investigate the role of model resolution in providing an accurate forecast, a 20-hours simulation with MOLOCH has been performed, from 04 UTC on February 11 until 00 UTC on February 12. The model has been nested into the BOLAM run, whose output data has been used for initial and boundary conditions. The initialization time has been chosen so as to minimize the impact on the simulation reliability of both models initial condition adjustment.[1] The integration domain is displayed in figure 4.11.

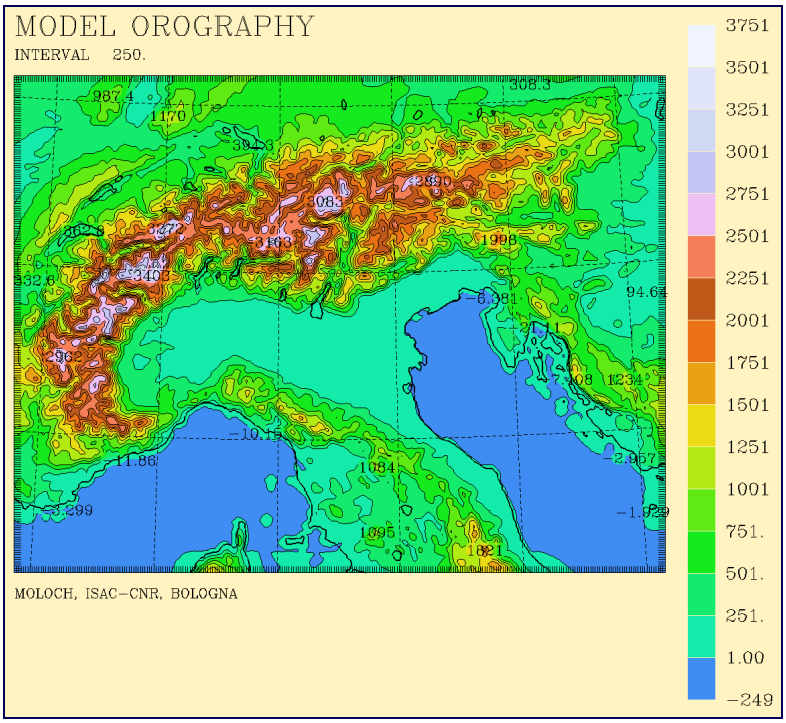

Figure 4.11: MOLOCH main run integration domain.

Grid spacing was set at 0.027 degrees (approximately 3 km) both in longitude and latitude; the domain size is 290 points in longitude and 222 in latitude. 50 vertical levels and 7 soil levels were employed. Time step was set at 50 seconds and the combined radiation scheme (RG + ECMWF, see subsection 3.1.4) was used. These settings have been also employed for all of the other MOLOCH simulations performed on this case study.

As for low-level winds, BOLAM and MOLOCH results are very similar, only differing in small areas and at some instants, the difference hardly exceeding 2 m/s (a comparison is drawn between the two models' forecasts for low-level wind at 16 UTC in figures 4.12

[1] That is, the initialization time is not too close to 00 UTC so that BOLAM output can be trusted for providing accurate initial conditions to the MOLOCH run, while it is not too close to the core of the event in order to account for the initial condition adjustment of MOLOCH itself.

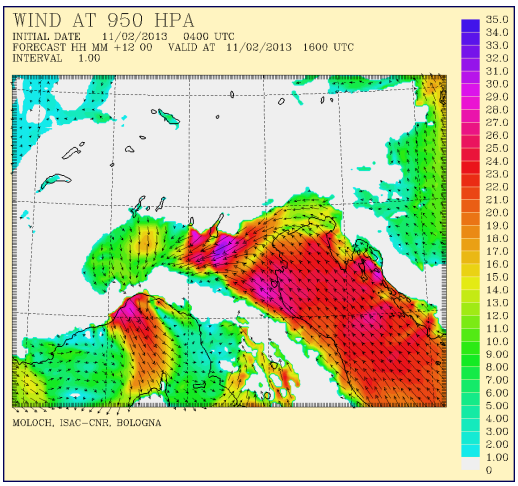

(a) MOLOCH forecast for wind at 950 hPa (m/s) at 16 UTC.

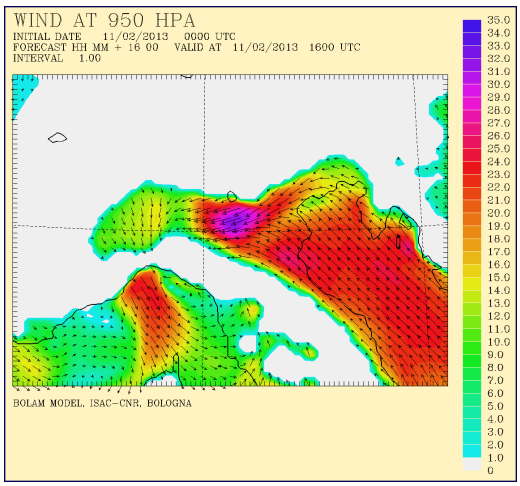

(b) BOLAM forecast for wind at 950 hPa (m/s) at 16 UTC.

Figure 4.12: Comparison between MOLOCH and BOLAM forecasts for wind at 950 hPa.

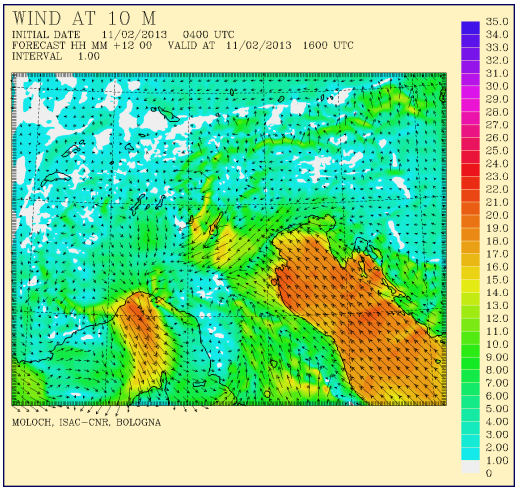

(a) MOLOCH forecast for wind at 10 meters (m/s) at 16 UTC.

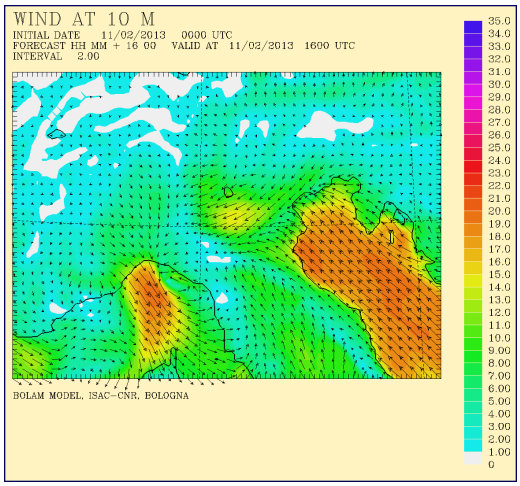

(b) BOLAM forecast for wind at 10 meters (m/s) at 16 UTC.

Figure 4.13: Comparison between MOLOCH and BOLAM forecasts for wind at 10 meters.

and 4.13). Small dissimilarities in wind fields are normal, as MOLOCH more effectively resolves small-scale features such as (local) katabatic winds on the lee of mountains, due to its higher resolution; these features are visible in both figures 4.12a and 4.13a as small spots of stronger winds in the vicinity of the orography.

However, it is noteworthy that the most evident dissimilarity between the two forecasts relates to the BW maximum: MOLOCH predicts it to be located more upstream (with respect to the very BW) and to be more elongated and meridionally-oriented than

BOLAM – compare figure 4.12a with figure 4.12b and figure 4.13a with figure 4.13b). This difference might be explained by the fact that the BW maximum is located on the lee of the small spur of the Alps that is few kilometers east of Garda Lake: MOLOCH might better account for this small-scale orographic variability due to its greater resolution; on the other hand, it is possible that MOLOCH overestimate wind speed in some areas, thus misplacing the BW maximum.

Moreover, MOLOCH overestimates the incoming wind speed at the southern boundary of the BW (off the Adriatic coast) with respect to BOLAM (contrast figure 4.12a with figure 4.12b and figure 4.13a with figure 4.13b). On the other hand, the wind speed minimum visible in the eastern Po Valley in figure 4.12a is less pronounced in figure 4.12b.

There differences in forecasts are normal in the vicinity of mountains and at locations where strong gradients are found, especially between a hydrostatic model like BOLAM and a non-hydrostatic, convection-resolving model like MOLOCH. We will further discuss these dissimilarities in section 4.2 while contrasting model forecasts with observational data.

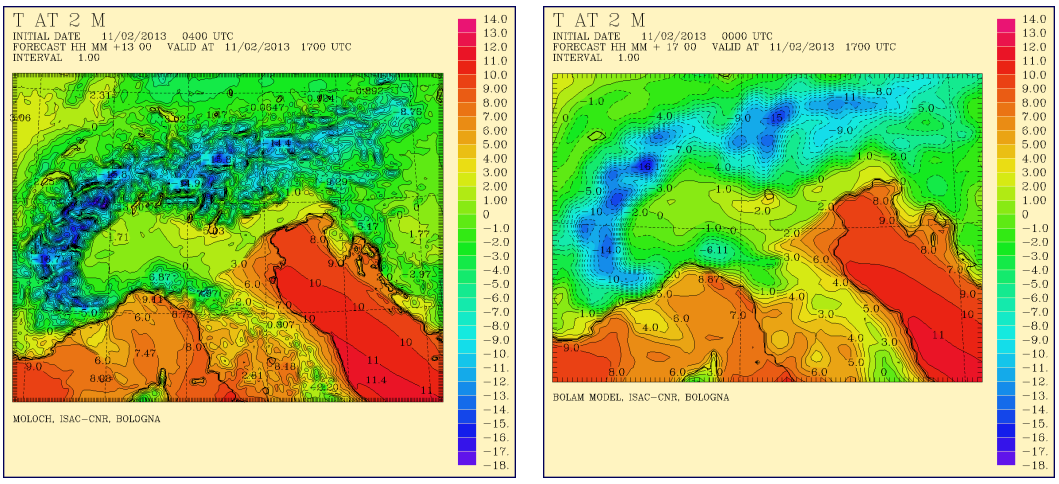

(a) MOLOCH forecast for temperature at 2 meters (°C) at 16 UTC.

(b) BOLAM forecast for temperature at 2 meters (°C) at 16 UTC.

Figure 4.14: Comparison between MOLOCH and BOLAM forecasts for temperature at 2 meters.

Apart from the above-mentioned differences, wind patterns and distributions are essentially the same between BOLAM and MOLOCH forecasts. Surface pressure and temperature and humidity at various levels are also very similar between the two forecasts: see, for instance, figures 4.14 and 4.15 where a comparison is drawn between the two forecasts for temperature at 2 meters and relative humidity at 950 hPa. MOLOCH slightly overestimates temperature in small areas with respect to BOLAM (compare figure 4.14a

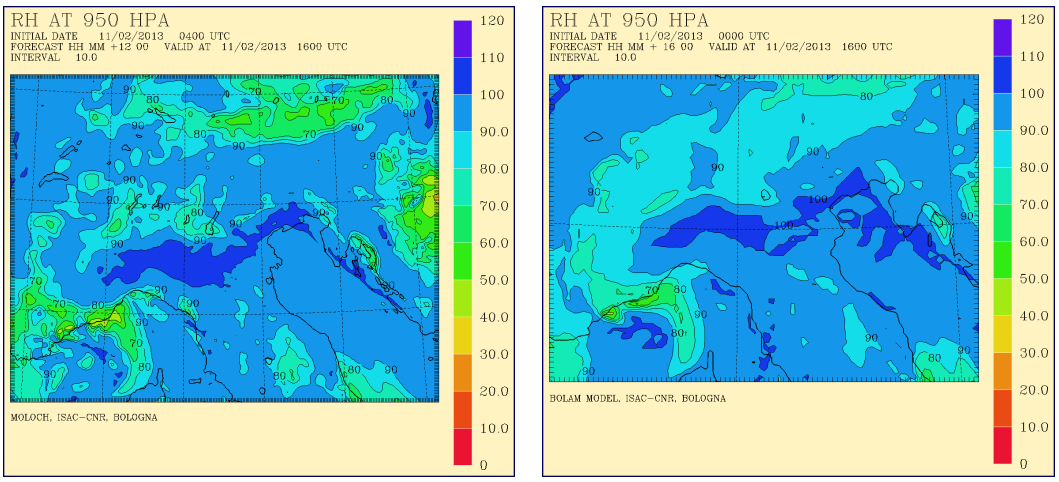

(a) MOLOCH forecast for relative humidity (%) at 950 hPa at 16 UTC.

(b) BOLAM forecast for relative humidity (%) at 950 hPa at 16 UTC.

Figure 4.15: Comparison between MOLOCH and BOLAM forecasts for relative humidity at 950 hPa.

with figure 4.14b); again, this difference may be due to MOLOCH better resolving small-scale features such as adiabatic warming produced by katabatic winds on the lee of mountains, and we cannot, in principle, state whether it is an overestimation or just a better performance. The same reasoning is valid for relative humidity, which is also overestimated by MOLOCH with respect to BOLAM, especially over the Alps.

MOLOCH predicted precipitation is slightly higher than the BOLAM one: see the comparison in figure 4.16. The difference between the two forecasts is not found everywhere and hardly exceeds 10%, except for the maxima which MOLOCH heavily overestimates with respect to BOLAM, with differences up to 60% for the principal maximum, the one located near the Adriatic coast (compare figure 4.16a with figure 4.16b); these differences are restricted to small areas, while on the whole MOLOCH predicted maxima are sharper and smaller than BOLAM ones.

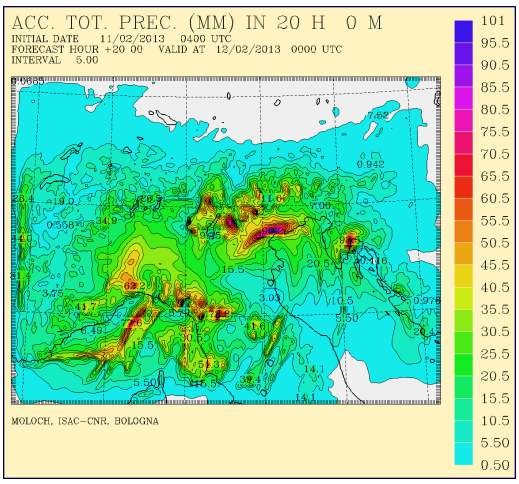

(a) MOLOCH forecast for cumulated precipitation (mm) at 00 UTC on February 12.

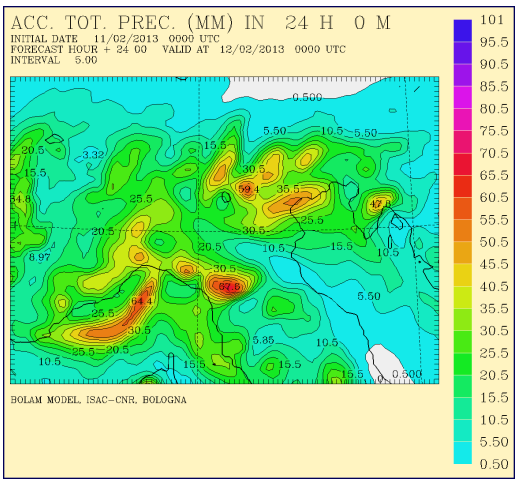

(b) BOLAM forecast for cumulated precipitation (mm) at 00 UTC on February 12.

Figure 4.16: Comparison between MOLOCH and BOLAM forecasts for total cumulated precipitation (note that even though the MOLOCH run is initiated at 04 UTC, the total precipitation is actually the same as no precipitation occurs from 00 UTC to 04 UTC.

4.2 Model forecasts vs observational data: a comparison

BOLAM and MOLOCH results have been compared with observational data obtained from Veneto agency ARPAV[2] (*Agenzia Regionale per la Prevenzione e Protezione Ambientale del Veneto*, Veneto Environmental Preservation and Protection Regional Agency).

Three types of data have been employed: ground station data, including pressure, temperature at 2 meters and wind at 10 meters; SODAR[3] (SOnic Detection And Ranging) wind data; microwave radiometer[4] temperature data. Sensitivities are: 0.1 hPa for pressure data; 0.1 °C and 0.5 °C, respectively, for ground station and radiometer temperature data; 0.1 m/s and 1° for ground stations wind speed and direction; 0.1 to 0.3 m/s and 1° to 5° for SODAR wind speed and direction (however, errors may be much larger than sensitivities, up to few m/s for SODAR in bad weather conditions). Measurements were taken at various locations shown in figure 4.17.

Wind measurements are displayed in figures 4.18 (ground data for Veneto provinces capital cities), 4.19 and 4.20 (Legnago and Loncon SODAR data, respectively). Ground

[2] `http://www.arpa.veneto.it/`.

[3] SODAR is a wind profiler, that is a remote-sensing meteorological instrument which measures wind intensity and direction at several heights above the ground. It is an active instrument, in that it emits sound waves impulses and measures their scattering by atmospheric turbulence; Doppler effect equations are then employed to reconstruct the wind vector value at every level.

[4] A radiometer is a passive instrument, measuring the amount of electromagnetic radiation received by some source. Radiative transfer equations are then used to reconstruct the distribution of the required quantity, such as temperature.

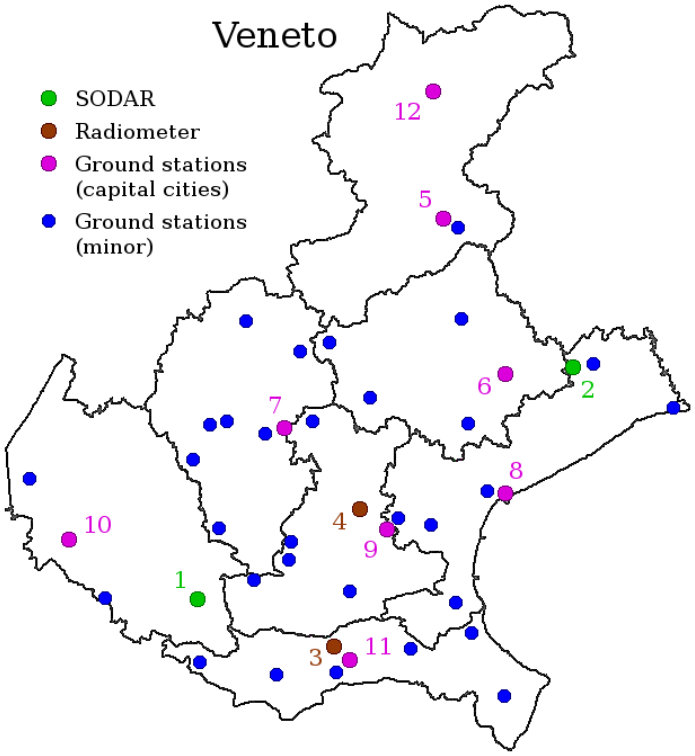

Figure 4.17: Locations in Veneto where ARPAV data were collected (see figure 2.2 for larger-scale perspective and topography). SODAR: 1. Legnago, 2. Loncon; radiometer: 3. Rovigo, 4. Padua; ground stations: 5. Belluno, 6. Ponte di Piave, 7. Quinto Vicentino, 8. Cavallino (Treporti), 9. Legnaro, 10. Villafranca Veronese, 11. Sant'Apollinare, 12. Villanova (Borca di Cadore).

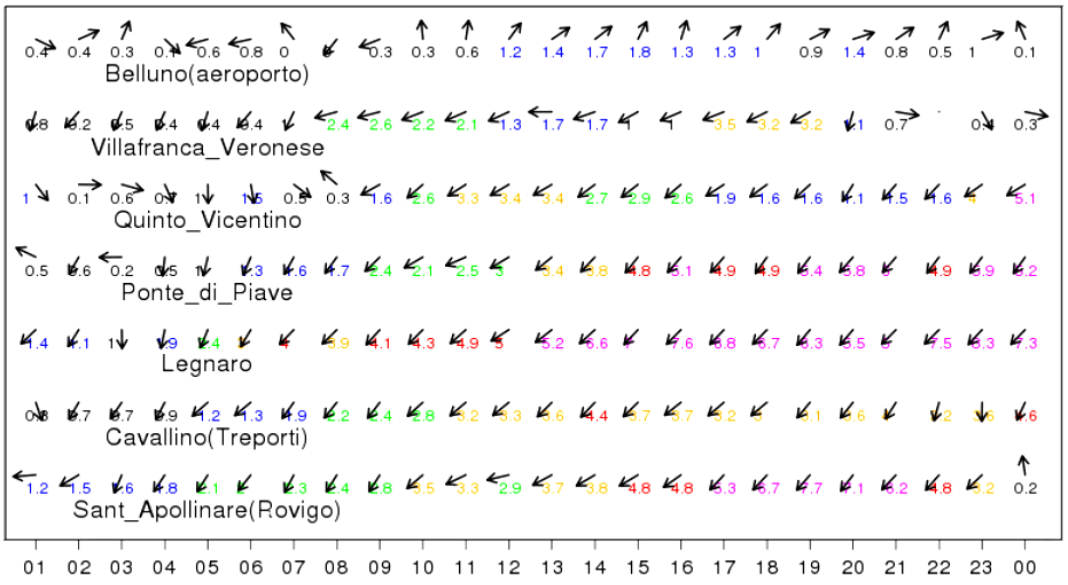

Figure 4.18: Hourly wind (m/s) at 10 m for Veneto provinces capital cities (measurements were taken at nearby locations, see figure 4.17). Day is February 11, time is CET or UTC+1.

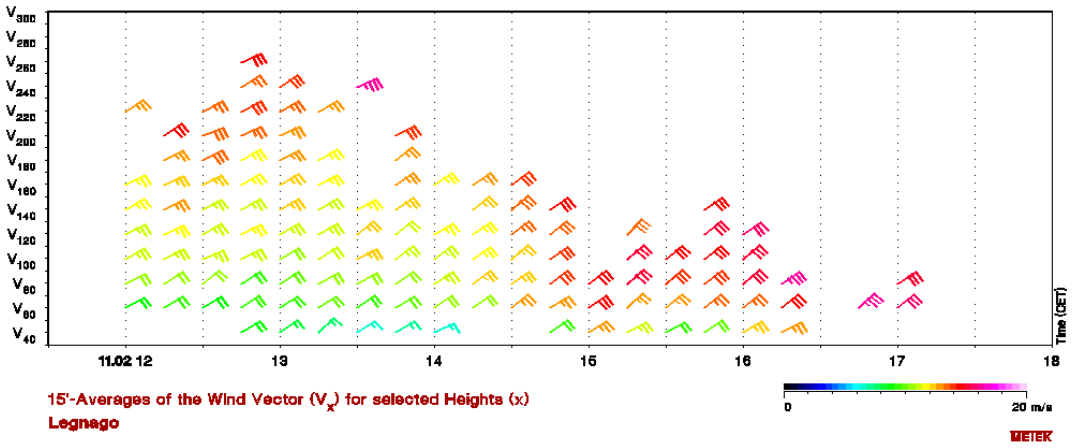

Figure 4.19: SODAR wind profile in Legnago (see figure 4.17). Day is February 11, time is CET or UTC+1.

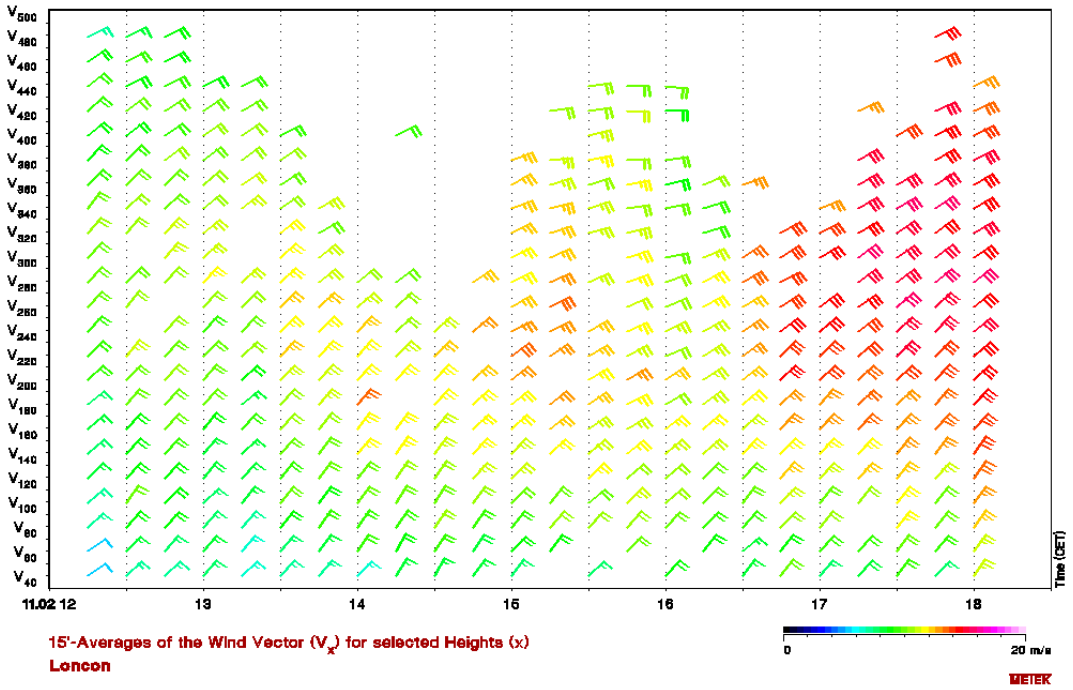

Figure 4.20: SODAR wind profile in Loncon (see figure 4.17). Day is February 11, time is CET or UTC+1.

data can be contrasted with figure 4.21, where MOLOCH surface wind maps for four instants (10, 14, 18, 22 UTC) are shown; SODAR data is to be contrasted with figures 4.3, 4.5 and 4.12.

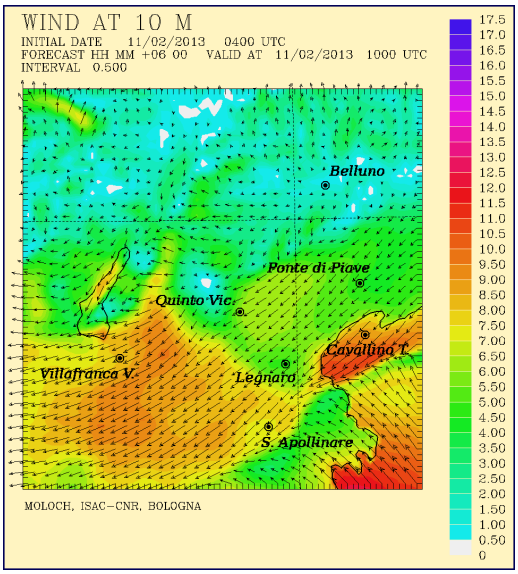

(a) 10 m wind (m/s) at 10 UTC.

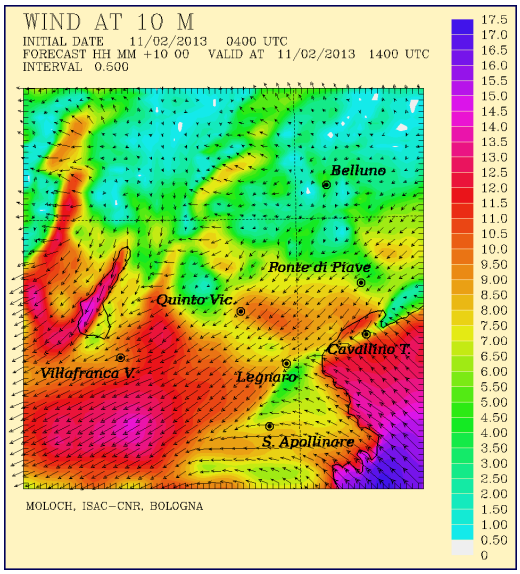

(b) 10 m wind (m/s) at 14 UTC.

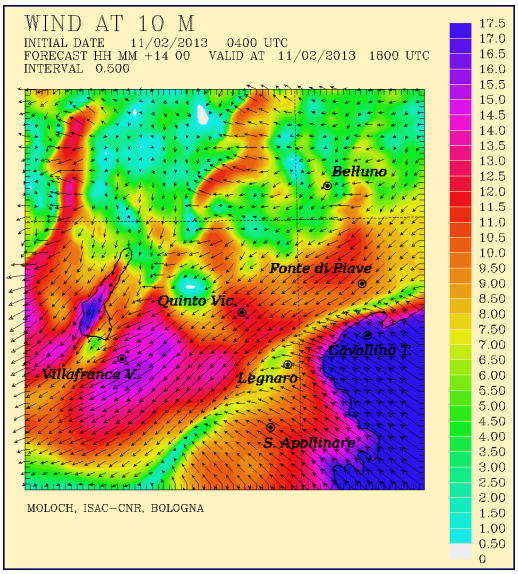

(c) 10 m wind (m/s) at 18 UTC.

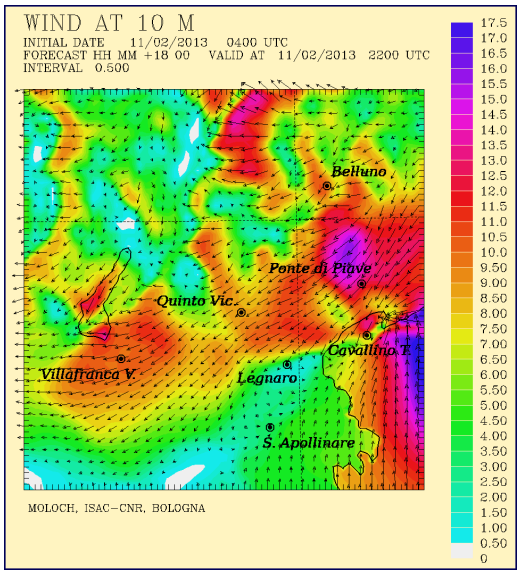

(d) 10 m wind (m/s) at 22 UTC.

Figure 4.21: MOLOCH forecasts for wind at 10 meters at 10, 14, 18 and 22 UTC (zoom over Veneto); the cities where observational data was collected (figure 4.18) are indicated.

There is quite a good agreement between model forecasts and SODAR data at every instant (the 950 hPa level height is between 420 m and 450 m throughout the event, wind at lower levels has been obtained through dedicated routines and interpolation):

differences in wind speed do not exceed 2 m/s while differences in wind direction are generally smaller than 10°.

Consistency is worse for ground data. Contrasting figure 4.18 with figure 4.21, we can firstly observe that MOLOCH appears to generally overestimate wind at 10 meters by at least 2 m/s. Secondly, wind forecast is better at locations like Ponte di Piave, Quinto Vicentino, Belluno and Legnaro, whereas it is worse for Villafranca, Cavallino T. and Sant'Apollinare, which are situated in the vicinity of areas with strong horizontal shear. Naturally, in such a case it is quite difficult to draw a comparison between observational data and forecasts, as ground stations provide *punctual* data whereas the model provides *discrete* data at grid points which have to be interpolated: whenever a strong gradient is present, a small difference in the interpolation can produce a large difference with respect to the observed value. As a result, strong northeasterly winds are predicted for the Villafranca area (see figure 4.21) whereas observed winds are light and even change direction from 19 UTC on (figure 4.18); the opposite happens for Sant'Apollinare, where observed winds blow from northeast throughout the day whereas southeasterly winds are predicted during the last part of the event.

Overall, MOLOCH appears to have underestimated the BW width – at least at 10 meters – by 10% to 15%, which is equivalent to roughly 2-3 grid points or 8-10 km.

A comparison between observational data and MOLOCH forecasts has been drawn in figures 4.22 and 4.23 for precipitation and temperature at 2 meters, respectively. Figure 4.22 shows precipitation data for four Veneto capital cities and MOLOCH forecasts for the same locations. As we can see, there is good agreement between forecasts and observational data, at least as concerns total precipitation, which MOLOCH correctly predicts in 2 cases out of 4, overestimates (by roughly 20%) in one case and underestimates (by roughly 20% again) in the fourth case. The model appears to generally distribute the precipitation over a shorter time, possibly due to the underestimation of the BW width, which enhances convergence where it is not present (given the sharp gradients of both wind and temperature which are associated with this BWs event, a slight error in forecasts can produce a dramatic difference with respect to the observational data, as already noted). Figure 4.23 shows temperature data for four Veneto capital cities and MOLOCH forecasts for the same locations. The model seems to have generally overestimated temperature at 2 meters especially during morning hours, possibly due to an underestimation of the cold pool extent. The largest difference, over 2 °C, is found at Villafranca from 10 to 13 UTC.

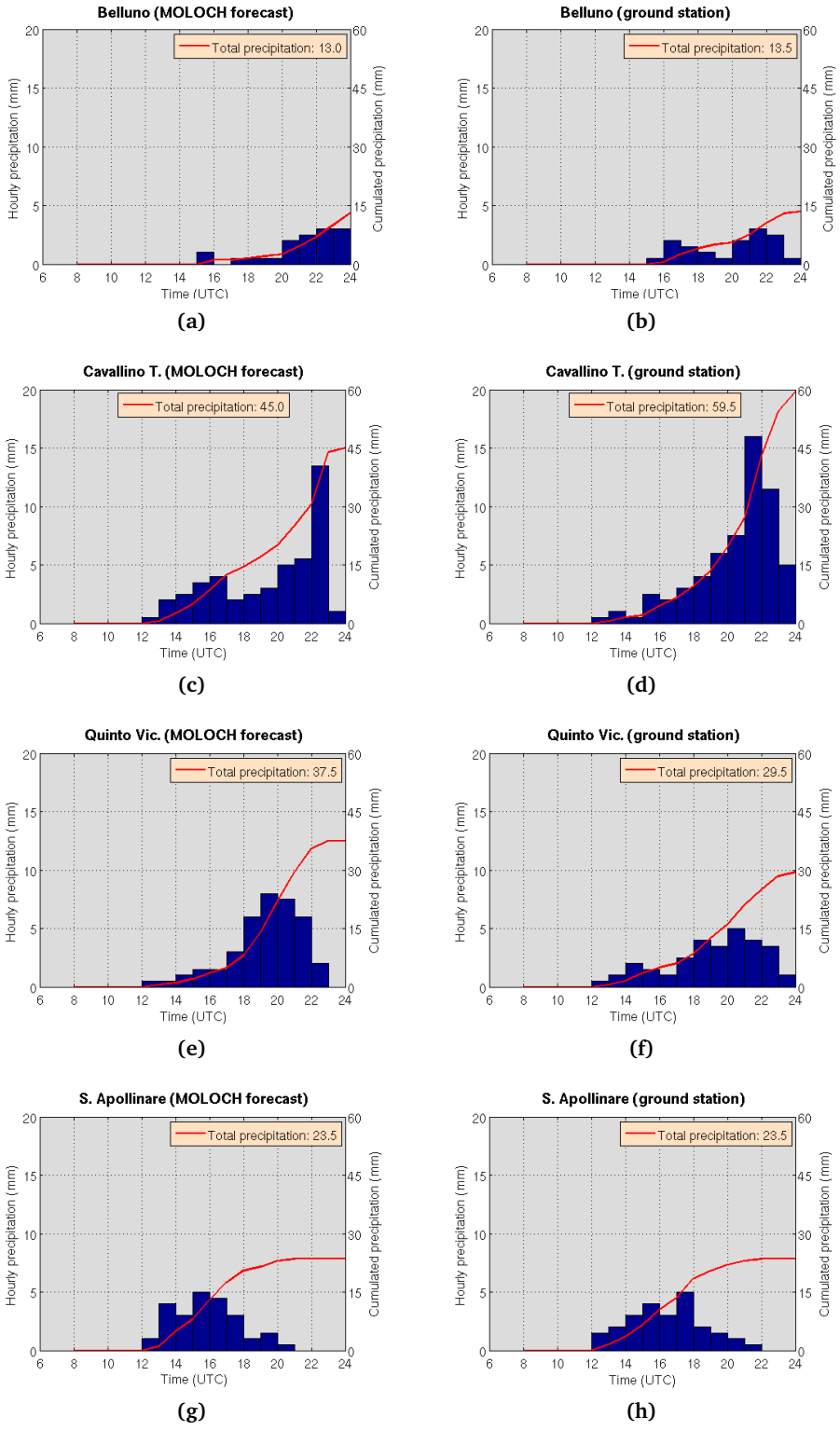

Figure 4.22: Hourly and cumulated precipitation at four locations in Veneto, comparison between MOLOCH forecast and observational data from ground stations; day is February 11.

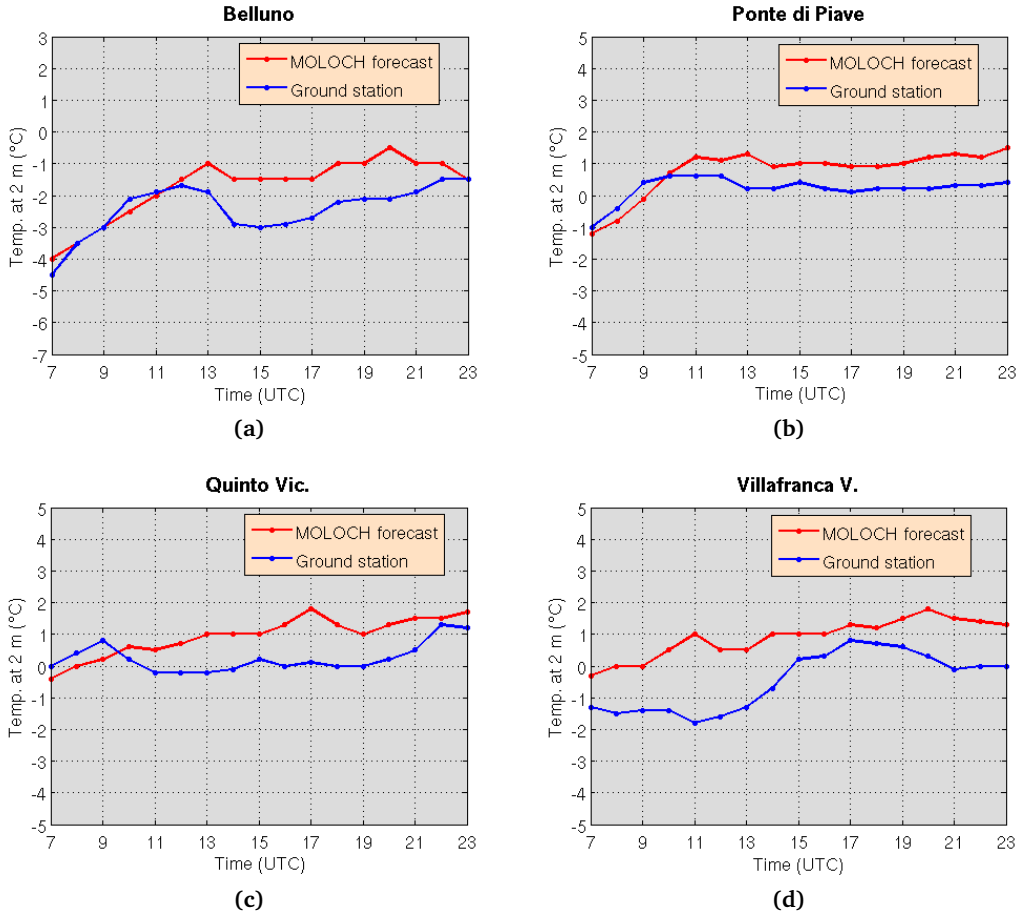

Figure 4.23: Temperature at four locations in Veneto, comparison between MOLOCH forecast and observational data from ground stations; day is February 11.

Temperature profiles and inversion height measurements for Padua and Rovigo are displayed respectively in figures 4.24 and 4.25. These data are fairly consistent with forecasts and clearly show the presence of the cold pool: the sudden increase of the inversion layer height[5] is representative of the warmer incoming flow ascending over the colder layer where BWs occurred.

Overall, there is good consistency between MOLOCH forecasts and observational data. There are some dissimilarities especially in the surface wind field due to a general underestimation of the BW width by the model. Nonetheless, since an adequate number of wind measurements at various heights is lacking, we cannot ascertain whether these differences are also found for higher levels or not. MOLOCH also appears to have

[5]The inversion height is computed via an interpolation by the radiometer: as few measurements are actually collected for higher levels, the interpolation is not as accurate for them as it is for the lower levels. Therefore, the fact that the inversion height is almost always found to be 700 m in the second half of the day is an artifice and this value has to be regarded as just an estimate.

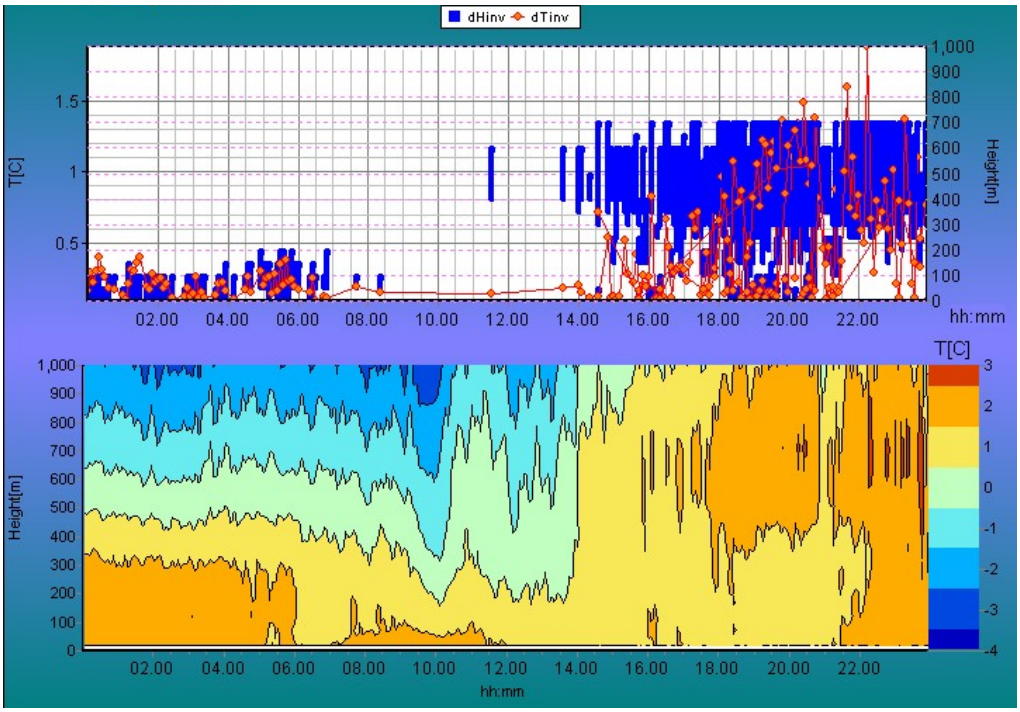

Figure 4.24: Padua radiometer: BL temperature profile and inversion height. Day is February 11, time is CET or UTC+1.

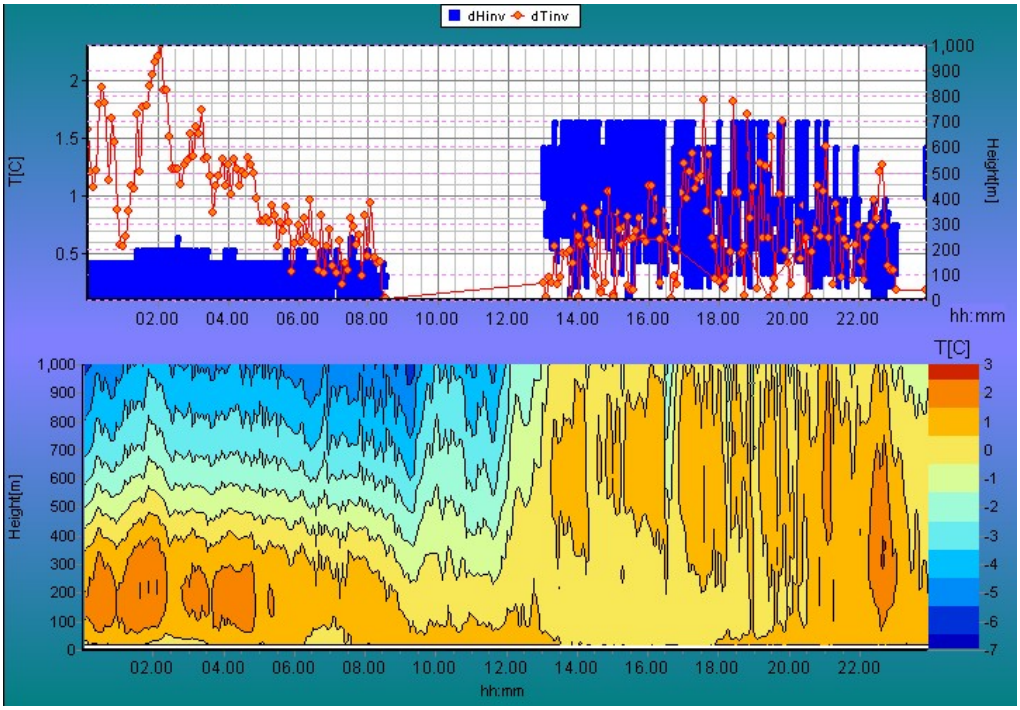

Figure 4.25: Rovigo radiometer: BL temperature profile and inversion height. Day is February 11, time is CET or UTC+1.

overestimated both temperature and precipitation over the Veneto plains, though not at all locations and at every instant. A comparison between observational data and BOLAM output has not been drawn, due to its low resolution (9 km): such a comparison would be too inaccurate especially in a case like the present one, featuring strong gradients.

4.3 Sensitivity tests: reduced-orography simulations

Sensitivity tests have been conducted on this case study in order to investigate how and to what extent the upstream Froude number modulates the occurrence and features of BWs.

Our objective was to simulate a BWs event and subsequently alter conditions gradually so as to induce an increasing modification of the upstream Froude number, up to the point that BWs no longer occur. In doing that, we sought to avoid in-progress modifications to any of the models' parameters and quantities, as it is quite difficult to introduce a *stable* modification of the Brunt-Väisälä frequency N or the incoming wind U during model run without losing physical sense. Therefore, we focused on altering the orography, which is the only way to permanently change the upstream Froude number:[6] multiplying the mountain height H by some *scaling factor* m before model run, the NMH will be scaled by m as well at every instant.

Since the incoming flow impinges directly on the eastern Alps, we chose not to lower the entire topographic barrier, opting to employ a scaling function which mainly lowered the eastern Alps and the surrounding orography, leaving the western Alps and the other Italian as well as European mountains unaltered. The scaling function has been devised as follows, starting from the Gaussian functions:

$$G_x(i) = \exp\left(-\left(\frac{i-i_0}{\sigma_x}\right)^2\right), \qquad G_y(j) = \exp\left(-\left(\frac{j-j_0}{\sigma_y}\right)^2\right) \tag{4.1}$$

where $i = 1, \ldots$ nlon, $j = 1, \ldots$ nlat, and nlon, nlat are the number of grid points in longitude and latitude, respectively. Then:

$$r_0(i,j) = 0.5\, G_x(i)\, G_y(j), \qquad s_1(i,j) = 1 - r_0(i,j); \tag{4.2a}$$

$$r_n(i,j) = 2\, r_{n-1}(i,j) s_n(i,j), \qquad s_{n+1}(i,j) = 1 - r_n(i,j). \tag{4.2b}$$

This recursive formula generates a scaling function $s_n(i,j)$ which has roughly the shape of an upside-down hat: see figure 4.26 for an example. Such function equals 0.5 – the scaling factor – in its midpoint (i_0, j_0), smoothly increases in the nearby interval and

[6] at least in a real case simulation.

finally soars sharply to 1. Horizontal cross sections of the resulting 3D function are elliptical.

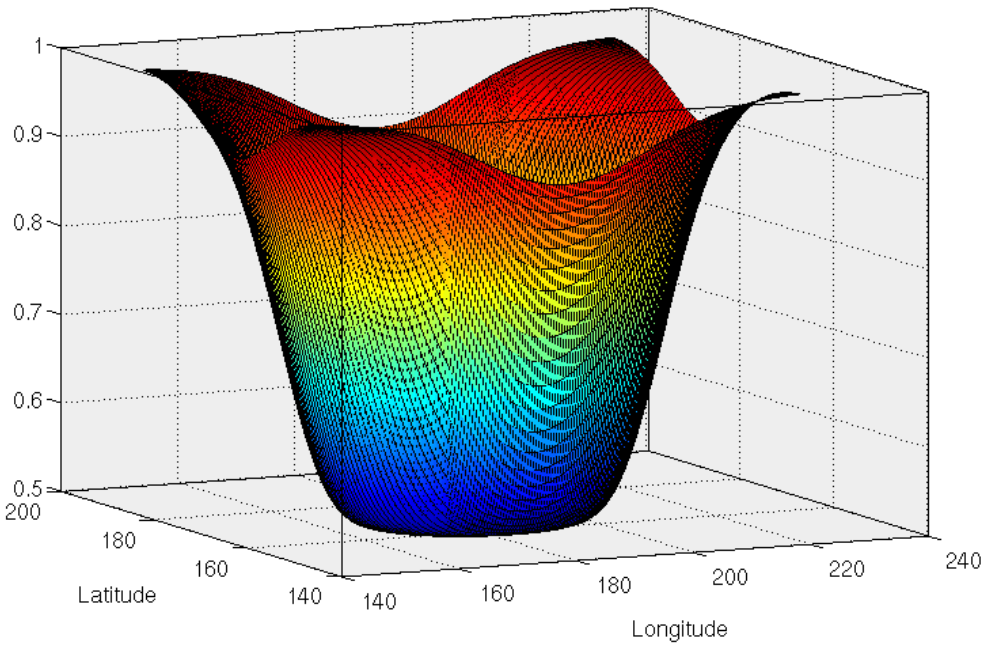

Figure 4.26: Scaling function $s_4(i,j)$, one of those used to lower the eastern Alps (the latitude and longitude points are the actual ones in BOLAM domain).

We reputed this scaling function, which originates from Gaussian function, to be the most appropriate one for lowering the orography while maintaining its shape. A simple Gaussian would not be adequate in this case, being too smooth: using a narrow Gaussian would excessively alter the mountain profile, up to the point that it becomes a double-peaked one; while using a wide Gaussian would also lower far portions of the orography, which we sought to avoid. On the other hand, by employing the scaling function $s_n(i,j)$ we can select the portion of topography that is required to be lowered and adjust the function gradient to the desired value by modifying σ_x, σ_y and the number of recursions n. This way, we have total control of the extent to which the orography is lowered at any grid point. When a different scaling factor m_{NEW} is needed, the second equation in (4.2b) is substituted by: $s_{n+1}(i,j) = 1 - 2\,m_{\mathrm{NEW}} r_n(i,j)$.

For our sensitivity tests, we used function $s_4(i,j)$ for both BOLAM and MOLOCH simulations. The lowered orography $h_L(i,j)$ is obtained by multiplying the real orography $h_R(i,j)$ by the scaling function, yielding: $h_L(i,j) = h_R(i,j)\,s_4(i,j)$. An example of scaled orography, relative to the simulation with scale factor 0.4, is displayed in figure 4.27 that is to be compared with figure 4.1.

Six simulations have been performed with BOLAM, with scaling factors of 0.1 to 0.6

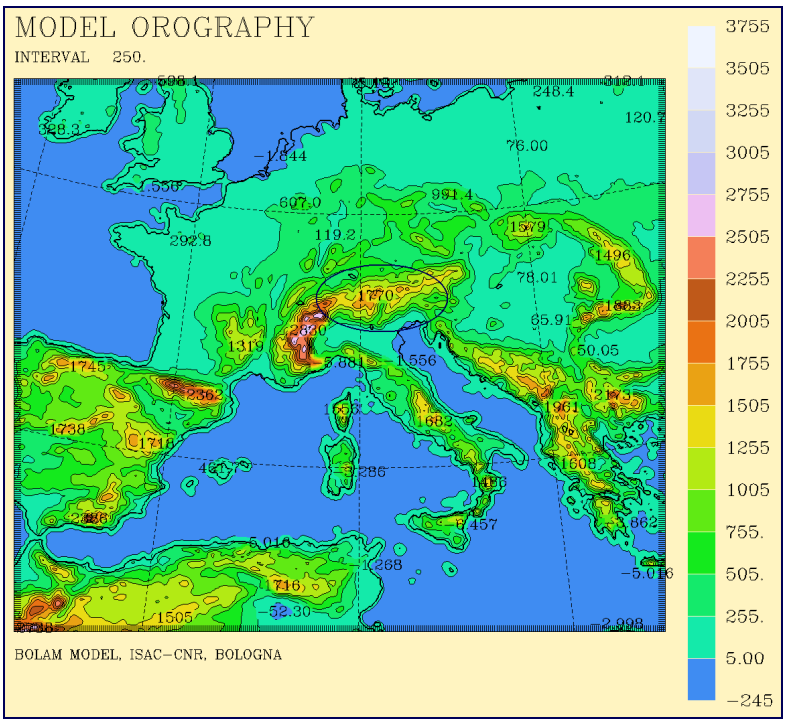

Figure 4.27: BOLAM simulation with scale factor 0.4, integration domain; the portion of the orography that has been reduced by more than 20% (half the scale factor) is that within the blue ellipse.

(mountains lowered by 10% to 60%). A MOLOCH simulation has been nested into each of the BOLAM ones, with equally lowered orography. Two further simulations have been conducted nesting MOLOCH with lowered orography – by 20% and 40%, respectively – into the main BOLAM run: this way MOLOCH initial and boundary conditions are those determined by the real orography, hence we could analyze their influence on the wind and thermodynamic patterns of the event and ultimately try to evaluate the extent of the blocking upstream influence. For the sake of conciseness, these MOLOCH simulations will be henceforth referred to as *hybrid* ones.

The barrier wind width, height, maximum and average speed, and duration all decrease noticeably as the orography reduces, up to the point that no more BW is found for 60% reduction: flow over the orography occurs in this case. An example of 950 hPa wind map for the simulation with 40% reduced orography is displayed in figure 4.28b, together with the analogous map for the simulation with realistic-orography (figure 4.28a). As we can observe:

- the BW is less than half as wide as in the real case;
- the BW vertical extent (henceforth referred to as depth) is also about 30% less than that of the real case;
- the BW direction is slightly different from the real case as well, as they have veered;
- both the BW maximum and the average speeds have reduced by roughly 15%;

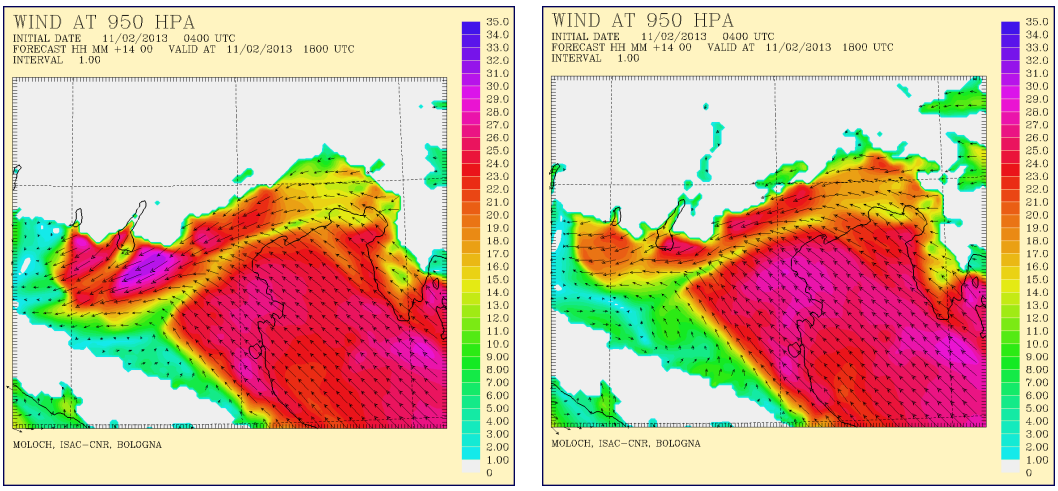

(a) Realistic-orography simulation. **(b)** Simulation with 40% reduced orography.

Figure 4.28: Comparison between the realistic-orography simulation and the one with 40% reduced orography, MOLOCH forecast for 950 hPa wind (m/s) at 18 UTC.

- "transitional" winds are found in front of the eastern part of the incoming flow, with a less sharp boundary between the incoming and the barrier flow than in the real case.[7]

Furthermore, the larger the reduction of the orography, the later the BW onset is. We considered the case of 50% reduction to still feature a BW, at least a shallow and narrow one which is established for just a few hours before the passage of the cold front.[8] Similar observations are valid for wind near the surface as well: reductions in BW extent, duration and speed are roughly the same as those for wind at 950 hPa (see figure 4.29). Wind at higher levels flows over the Alps even for small reductions of the orography.

The BW average speed v_b has been computed for each simulation by means of a dedicated routine, averaging winds over four distinct regions along the BW, over three instants (hours) during the core of the event and finally over the vertical up to the BW upper boundary, using a weighted average with density as a weighting function. The BW width and depth have been also computed by averaging over the same four regions and three instants (width has been averaged over the vertical as well). Variation in wind intensity and direction has been taken into account as a criterion to determine the BW upper and lateral boundaries: we set a threshold of 10° for variation in wind direction and one of 80% of the BW maximum speed for variation in wind speed; the BW boundary

[7] Hence, this is no longer a pure first-type event, being somewhat a hybrid of a first-type and a second-type event.

[8] The cold front, arriving at the same time (about 19 UTC) in all simulations, abruptly extinguishes the event so that we cannot state, in principle, how long it would otherwise last.

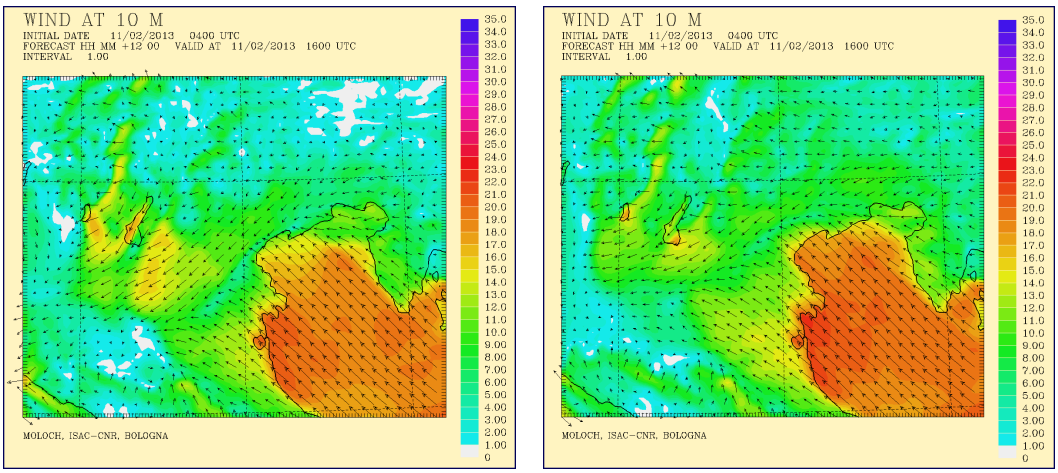

(a) Realistic-orography simulation. **(b)** Simulation with 40% reduced orography.

Figure 4.29: Comparison between the realistic-orography simulation and the one with 40% reduced orography, MOLOCH forecast for wind at 10 meters (m/s) at 16 UTC.

has been placed where at least one of the two thresholds is surpassed.[9] These features are displayed for each simulation in table 4.1.

As for pressure, in simulations with orography lowered by 20% or more the cyclone over northern Italy is larger in extent, albeit equally as deep, with respect to the real case. The pressure "nose" on the southern flank of the Alps becomes very small – practically indistinguishable from the effect of the cyclone – for 30% or greater reduction (see figure 4.30).

A marked difference is observed for temperature patterns and the cold pool. Temperatures in the plains just south of the Alps are roughly the same in all simulations. However, the cold pool narrows with decreasing orography so that the warmer incoming flow is less obstructed: as a result, the temperature gradient is displaced downstream (few kilometers inland) as visible in figure 4.31. Furthermore, in cases with little or no BW, there is no effective advection of cold air westwards: consequently the region downstream of the BW remains quite cold (temperatures around freezing) throughout the event in the real case, whereas it warms up over time due to the incoming winds in cases with orography reduced by at least 40% (contrast figure 4.31a with figure 4.31b).

Precipitation distribution is also totally different between the simulations: the greater the reduction of the orography, the further downstream maxima are displaced, as we can see in figure 4.32, where BOLAM forecast for total precipitation is shown for the simulation with realistic orography (figure 4.32a) and the one with 40% reduced orogra-

[9] It is not always straightforward to proceed in such a way, as wind intensity and direction often vary quite smoothly, so that there is no sharp boundary between the BW and the surrounding circulation. Luckily enough, in this case there is quite a pronounced boundary so we could employ tight thresholds.

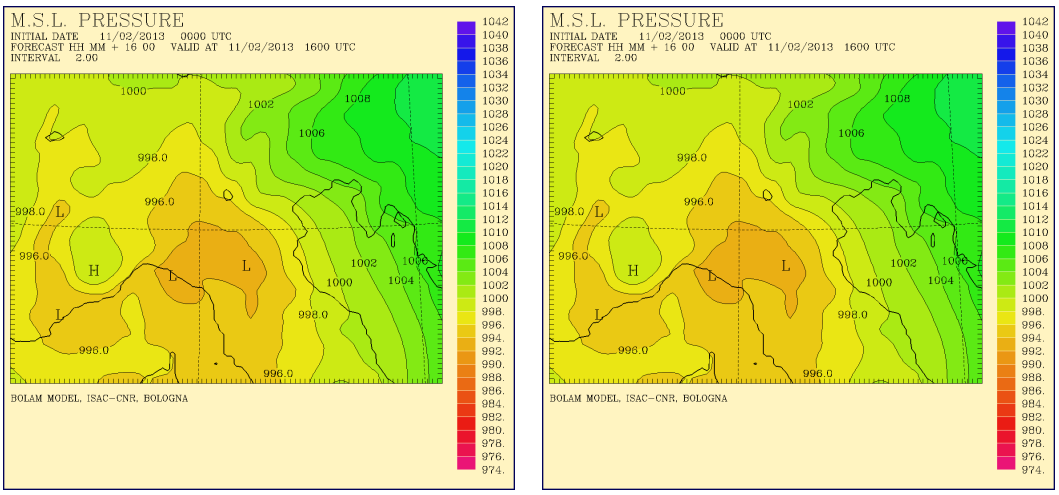

(a) Realistic-orography simulation. **(b)** Simulation with 40% reduced orography.

Figure 4.30: Comparison between the realistic-orography simulation and the one with 40% reduced orography, BOLAM forecast for m.s.l. pressure (hPa) at 16 UTC.

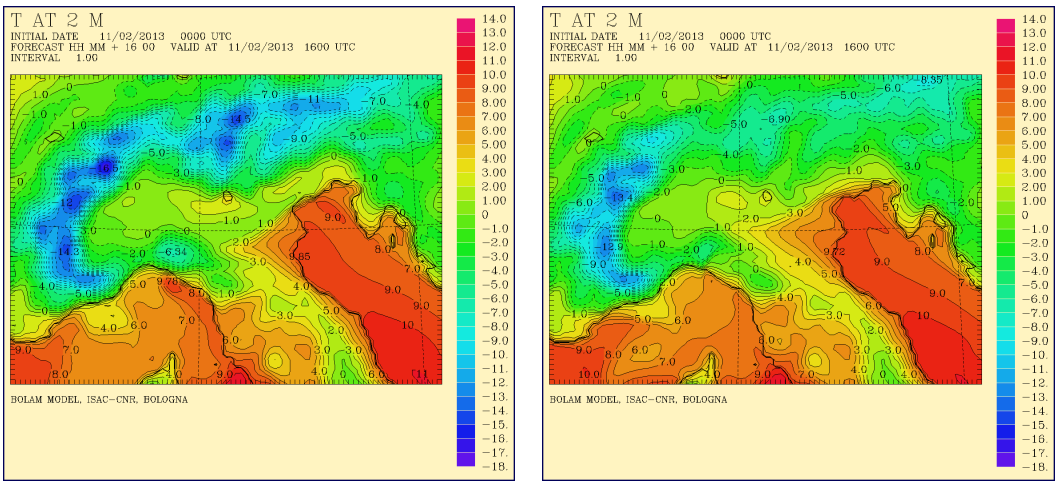

(a) Realistic-orography simulation. **(b)** Simulation with 40% reduced orography.

Figure 4.31: Comparison between the realistic-orography simulation and the one with 40% reduced orography, BOLAM forecast for temperature at 2 meters (°C) at 16 UTC.

phy (figure 4.32b). Since the cold pool is still found in the simulation with 60% reduced orography, the precipitation pattern does not become any similar to that of orographic precipitation produced by flow over the mountains – that is, with maxima situated more or less over the mountain top and total precipitation progressively decreasing moving upstream – even in the simulations with large reduction of the orography. The reason is probably that the incoming flow is in any case much warmer than the pre-existing low-level air present in the Po Valley, so that it is forced to ascend relatively far from the

mountains, behaving in a similar way to warm fronts.

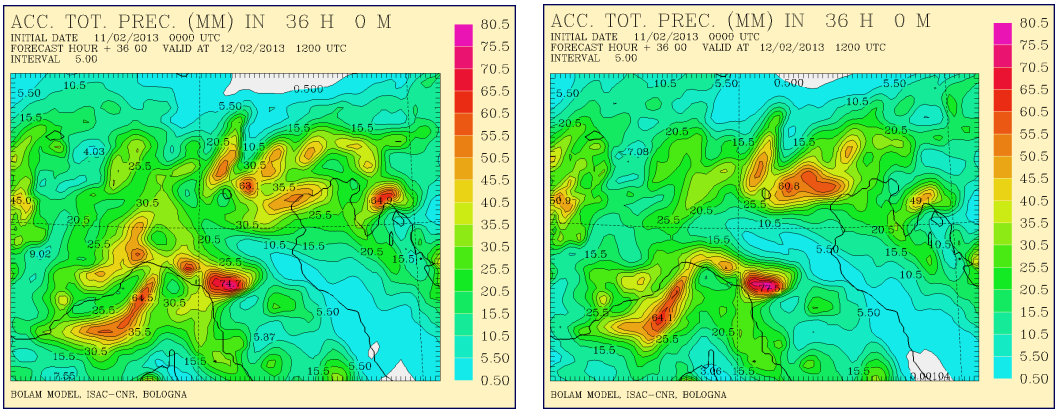

(a) Realistic-orography simulation. **(b)** Simulation with 40% reduced orography.

Figure 4.32: Comparison between the realistic-orography simulation and the one with 40% reduced orography, BOLAM forecast for total precipitation (mm).

The incoming winds become more and more intense with decreasing orography: see again figure 4.28. This is an example of upstream influence: a modification of the orography situated downstream of the incoming flow changes the very airflow, even far from the mountains.

The hybrid MOLOCH simulations showed little or no differences from the equivalent non-hybrid ones. The barrier wind is, on average, slightly wider and more intense in the hybrid simulations, possibly due to the fact that they have been initialized with weaker winds, as we just observed. All differences are barely visible in charts to the naked eye.

4.4 The Barrier Wind Index

The NMH has been computed for each simulation via a dedicated routine, operating within a square region of 25×25 grid points about 200 km upstream of the Alps (see figure 4.33). The lower 11 levels of MOLOCH model, up to a height of roughly 1700 m, have been employed for the calculation, except for the first (the lowest one) which has been excluded to avoid boundary layer effects, as the model erroneously forecasts a superadiabatic lapse rate for some instants.

The square region has been placed in an area where the wind field is quite uniform and multiple attempts have been made before choosing the suitable placement, in order to reduce the arbitrariness associated with this choice. Several attempts have also been made to decide the number of atmospheric levels to be used in the computation of N. Nonetheless, the upper boundary of the incoming flow has been relatively straightforward to identify, as both the intensity and the direction of the flow are nearly uniform

throughout the lower 11 levels, whereas a strong vertical wind shear is found above.[10] This pattern persists throughout the event.

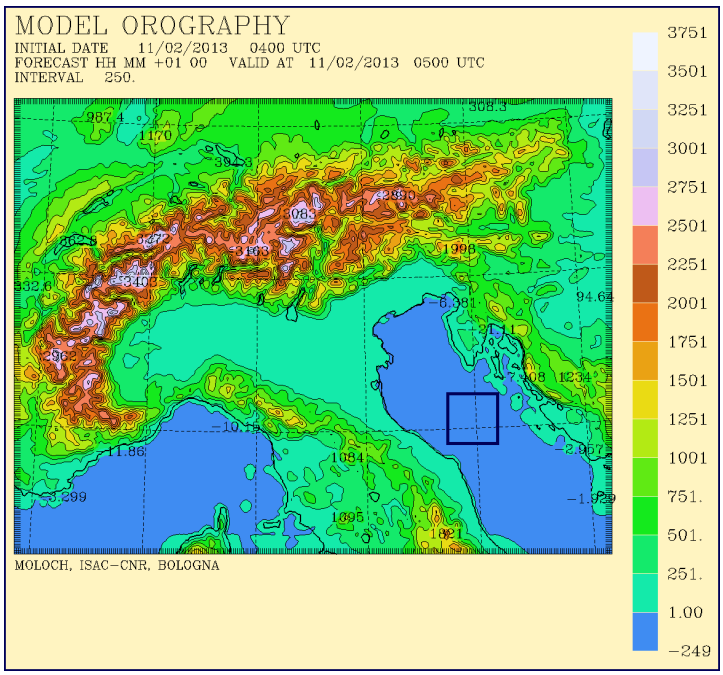

Figure 4.33: MOLOCH domain: U, N and the NMH have been computed within the region in the blue square.

The quantities in the NMH expression NH/U have been estimated as follows:

- The height of the mountain H has been estimated as the average over a sample of 40 longitudinal cross section of the maximum mountain height within each cross section. The total height has been subsequently rounded to 2500 m (so in the case of 10% reduction, it is 2250 m and so on).

- The Brunt-Väisälä frequency N has been averaged over the square region, over the selected levels of the model and finally over time (from the onset to the central part of the event, just before the cold front arrival). Virtual potential temperature θ_v has been employed for the calculation.

- The incoming wind speed U has been averaged over the square region and over time just as the Brunt-Väisälä frequency, while a weighted average has been preferred over the vertical, with density as a weighting function.

A comparison of the major features for all the simulations is displayed in table 4.1 (the one with 60% reduced orography has not been included as it features no BW).

[10] More precisely, the incoming flow is nearly normal to the Alps throughout the lower 11 levels whereas it sharply veers above, becoming much weaker as well.

Orography	v_u [m/s]	v_b [m/s]	W [km]	D [m]	NMH	BWI
Real	15.6	20.1	44	710	1.63	1.61
10% red.	15.8	19.4	37	620	1.45	1.12
20% red.	16.1	19.0	30	570	1.28	0.81
20% red. (H)	15.8	19.1	32	590	1.31	0.90
30% red.	16.3	18.7	22	510	1.11	0.52
40% red.	16.5	18.0	17	480	0.95	0.36
40% red. (H)	16.1	18.2	18	490	0.98	0.37
50% red.	16.6	15.8	14	440	0.79	0.23

Table 4.1: Principal features for all simulations (H designates MOLOCH hybrid simulations): v_u is the upstream wind average speed, v_b is the BW average speed, W is its average width and D is its average depth. The NMH is the Non-dimensional Mountain Height, the BWI is the Barrier Wind Index.

In order to characterize to what extent the BW occurs in each simulation, a non-dimensional Barrier Wind Index (BWI) has been devised as follows:

$$\mathrm{BWI} = \frac{w d v_b}{v_u} = \frac{W\,[\mathrm{km}]}{50\,[\mathrm{km}]}\,\frac{D\,[\mathrm{m}]}{500\,[\mathrm{m}]}\,\frac{v_b}{v_u} \tag{4.3}$$

where w and d are the *normalized* BW average width and depth, respectively. The BWI equals 1 when the BW has 50 km width, 500 m depth and an average speed equal to the average speed of the incoming low-level airflow during the steady-state stage of the event.

The BWI for each simulation is shown in table 4.1 and a plot of the BWI versus the NMH for the present case study is displayed in figure 4.34.

The blue crosses in figure 4.34 are not strictly error bars, nonetheless they are large in size to represent the somewhat large uncertainties associated with the Non-dimensional Mountain Height and the Barrier Wind Index: we consider a cautious estimate for them to be around 0.1, given the arbitrariness of both mountain height H and the extent and position of the region where average U and N are computed.

The nearly linear profile in figure 4.34 will be discussed in Chapter 7 together with plots related to the other case studies.

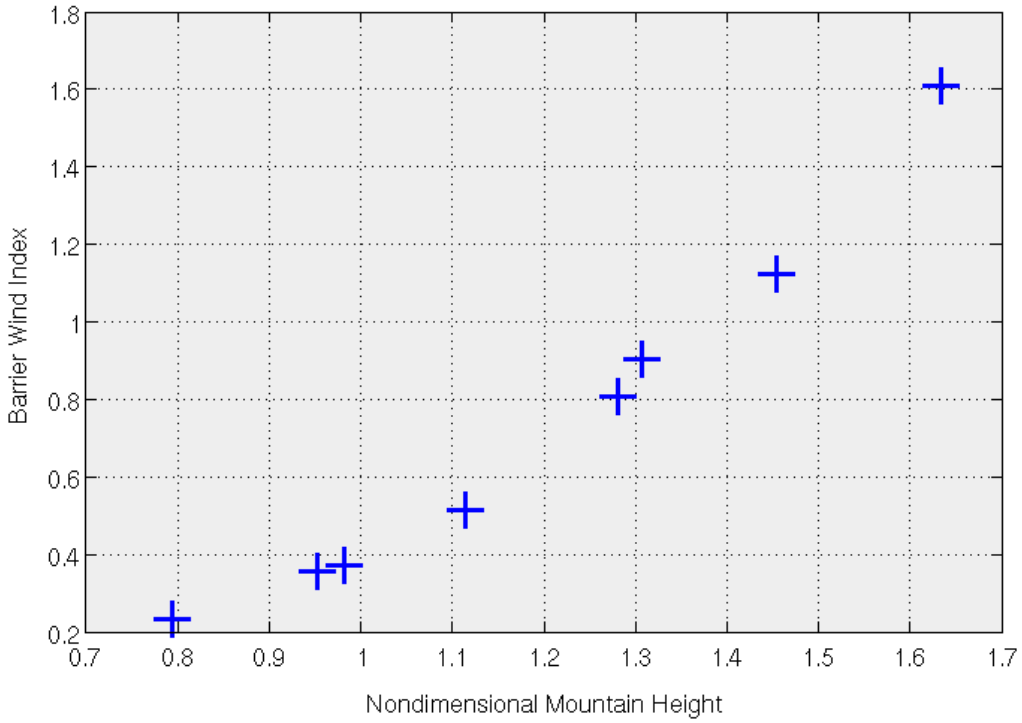

Figure 4.34: Plot of the BWI versus the NMH for the Alpine case study.

Chapter 5

The 2012 Dinaric case study

The second case study we selected is a Dinaric one which occurred on December 25 and 26, 2012. It lasts nearly 24 hours and features intense and extensive barrier winds, which stretch all the way from the southern Adriatic Sea to the Istrian peninsula and extend over 50 km in width. This event is rainless, at least during the BWs period: as they are eventually replaced by flow over the Dinaric Alps, rain started to fall over the mountains.

5.1 Event simulations

5.1.1 BOLAM simulation

The first simulation we performed is a 48-hours BOLAM run, from December 25, 2012, 00 UTC to December 27, 2012, 00 UTC. The integration domain is the same as shown in figure 4.1. The model settings – initial and boundary condition type, grid size and spacing, resolution, number of vertical and soil levels, time step and selected radiation scheme – are also the same as those employed for the previous case study (see subsection 4.1.1). The accuracy of the simulation was not affected by the initial condition adjustment period, as the core of the BWs event does not start before 09 UTC.

The synoptic situation that produces this Dinaric event is displayed in figure 5.1, concerning the central part of the event. A pronounced geopotential ridge is located over the southeastern Mediterranean Sea, with values well above the average for this period (figure 5.1a[1]). A high pressure system is located over the southern Mediterranean Sea, just as the corresponding geopotential ridge to which it is vertically well aligned (figure 5.1b). This synoptic situation usually produces southwesterly to southerly low-level

[1]This is an upper-level synoptic situation that is often associated with Dinaric BWs episodes: contrasting figure 5.1a with figure 2.10, we note that even though in the second there is a trough over northwestern Italy and the correspondent ridge is situated further southeast than in the first chart, the two patterns are similar in that geopotential isolines over Italy are roughly normal to the Adriatic coasts

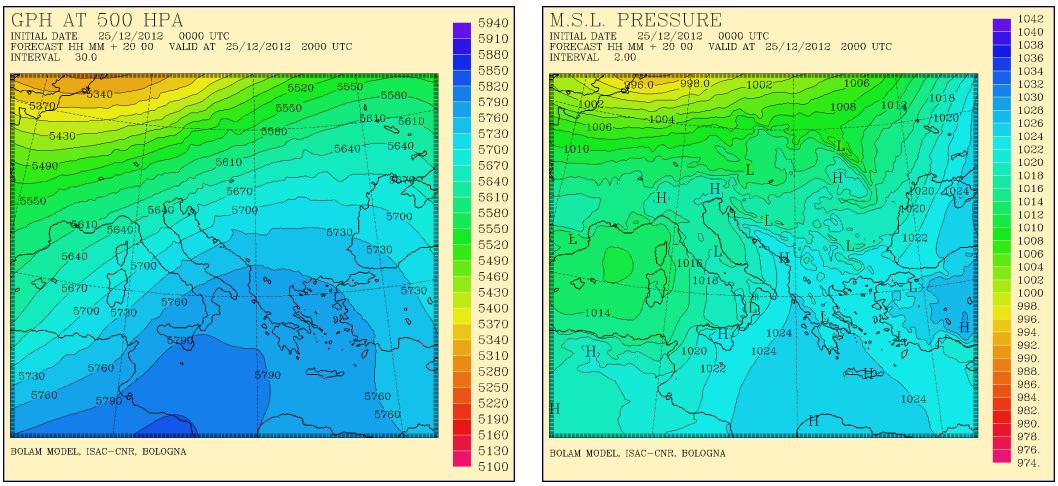

(a) 500 hPa geopotential height (dam). **(b)** M.s.l. pressure (hPa).

Figure 5.1: BOLAM run, 500 hPa geopotential height and m.s.l. pressure at 20 UTC on December 25.

winds which may be blocked by the Dinaric Alps, generating southeasterly BWs that blow parallel to the Balkan coast.

The BWs occurring during this event are displayed in figure 5.2, concerning the central part (figure 5.2a) and the end of the event (figure 5.2b). The barrier flow begins to develop around 00 UTC on December 25 and is established at 09 UTC, lasting until 14 UTC on the following day, when it is gradually replaced by flow passing over the Dinaric Alps.[2] Related wind speeds are extensively stronger than 15 m/s throughout the event, with maxima peaking at nearly 25 m/s – both these data relate to the 950 hPa level, while no BWs are predicted at higher levels. Winds near the surface are weaker, peaking slightly over 15 m/s just as for the Alpine case study: see figure 5.3. The BWs width remains around 60 km up until the last hours, when it is rapidly eroded by strong winds coming from the central Apennines.

The incoming flow consists of a wide band (over 100 km) of intense winds which are stronger than 10 m/s throughout the event, peaking at around 20 m/s (these values refer to the 950 hPa level). There is little vertical shear, as both wind direction and intensity are quite uniform up to 2000 m altitude. Wind at 900 hPa is slightly deflected by the mountains (roughly 30°) though it does not attain a BW pattern. No BWs are predicted in front of the incoming flow, which makes a gentle turn to the left and blends into the BWs: this is a second-type event.

No precipitation at all is predicted throughout the event: only when the pattern

[2] See the end of section 2.1 for thresholds and criteria for determining the event starting and ending times.

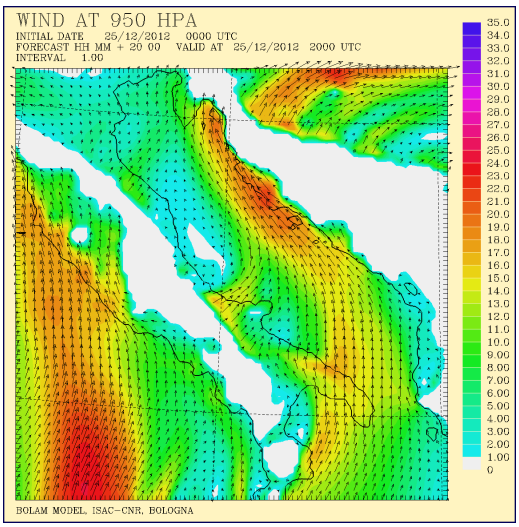

(a) 950 hPa wind (m/s) at 20 UTC on December 25 (zoom over the Ligurian Sea).

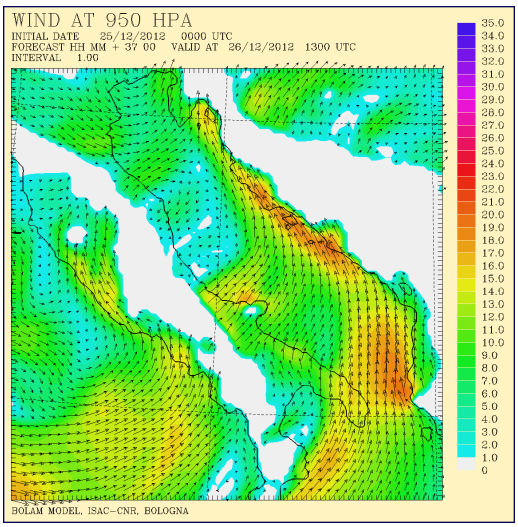

(b) 950 hPa wind (m/s) at 13 UTC on December 26 (zoom over the Ligurian Sea).

Figure 5.2: BOLAM run, wind at 950 hPa at two instants.

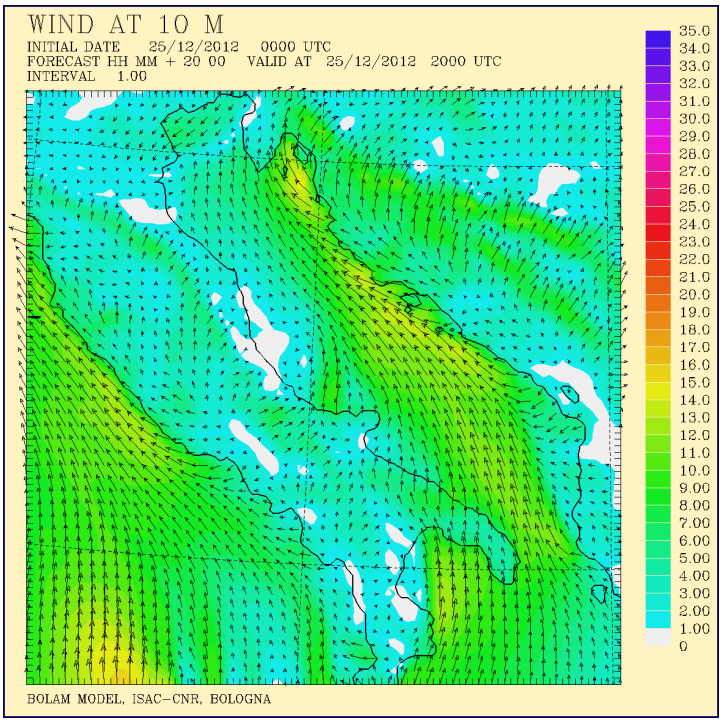

Figure 5.3: BOLAM run, wind at 10 meters (m/s) at 20 UTC on December 25 (zoom over the Adriatic Sea).

changes and the incoming winds start to flow over the mountains, around 13 UTC on December 26, little rainfall starts to fall in small areas over the southern Dinaric Alps. No cold pool is predicted as well, as there is no low-lying layer of colder air on the windward side of the mountains.

Surface pressure steadily decreases throughout the event, from 1024 hPa at 00 UTC on December 25 to 1018 hPa at 14 UTC on December 26. Nonetheless, this is an anticyclonic event in that there is no cyclone associated with the BWs – a weak cyclone is established over northern and central Italy during the second half of the event, but it is too distant and weak to influence the low-level circulation over the southern Adriatic Sea. A pressure "nose" is present, as displayed in figure 5.4, with pressure on the southern flank of the Dinaric Alps being roughly 2 hPa higher than that upstream.

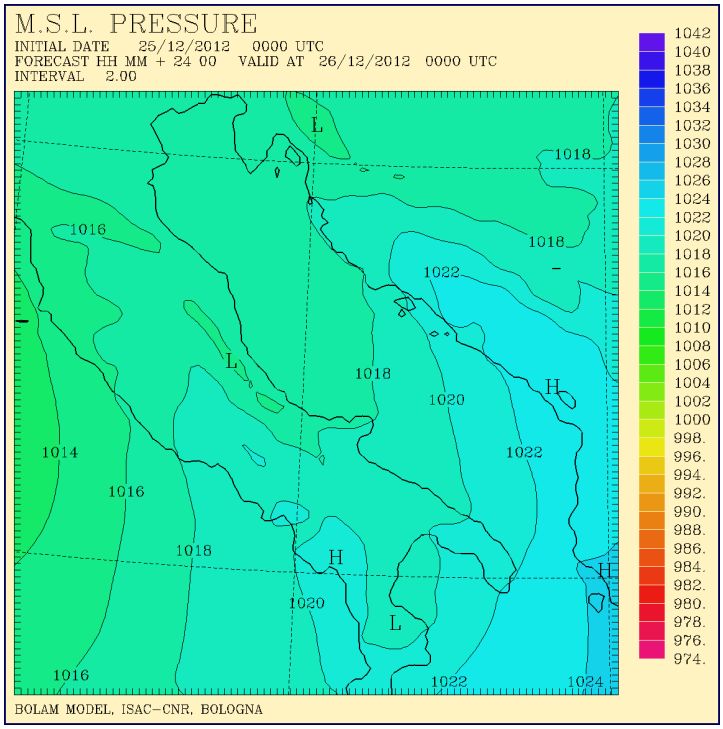

Figure 5.4: BOLAM run, m.s.l. pressure (hPa) at 00 UTC on December 26 (zoom over the Adriatic Sea).

The BW role in advecting air is evident in figure 5.5: the incoming flow brings warm, moist air towards the southern portion of the Dinaric Alps and the BWs advects it northwestward along the Adriatic coast (contrast figure 5.5a with figure 5.5b). The band of warmer – in terms of θ_e – air coincides with the one of BWs.

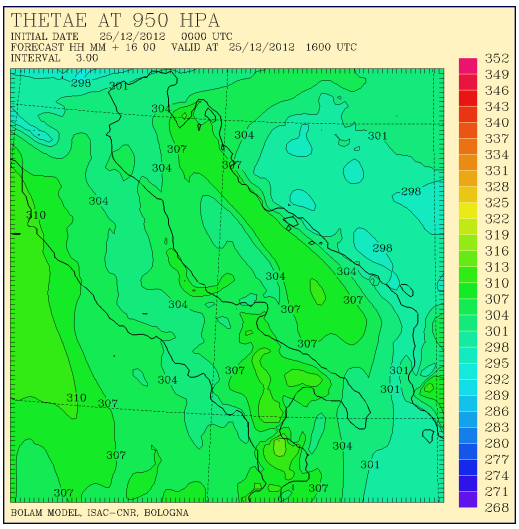

(a) θ_e (K) at 16 UTC on December 25 (zoom over the Ligurian Sea).

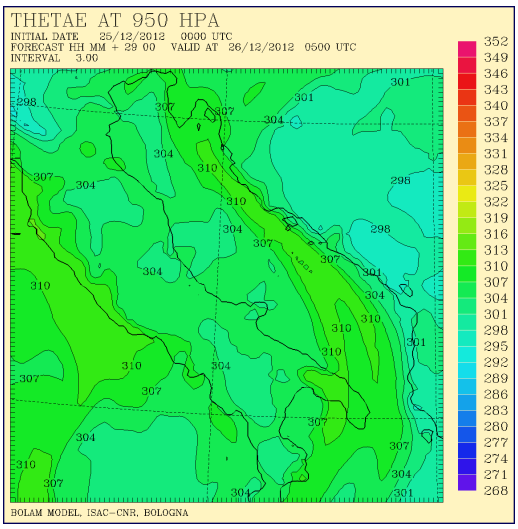

(b) θ_e (K) at 05 UTC on December 26 (zoom over the Ligurian Sea).

Figure 5.5: BOLAM run, equivalent potential temperature θ_e at 950 hPa at two instants.

5.1.2 MOLOCH simulation

A 38-hours simulation with MOLOCH has been performed, from 04 UTC on December 25 to 18 UTC on December 26, nesting the model into the BOLAM run as for the previous case study. MOLOCH integration domain is displayed in figure 5.6. All model settings are the same as for the previous case study (see subsection 4.1.2), except for domain size which is now 262 points in longitude and 370 in latitude.

BOLAM and MOLOCH results are slightly different for this case study as concerns low-level winds: see figure 5.7 (the two charts are to be contrasted with figures 5.2a and 5.2b, respectively). As we can notice in figure 5.7a, BOLAM predicts a wider and slightly stronger barrier wind than MOLOCH: 75 km width against 55 km and 18 m/s against 17 m/s; BOLAM forecasts a longer event as well: BWs are still visible in figure 5.2b, while they are not in figure 5.7b – according to MOLOCH the event ends at 09 UTC on December 26.

The same difference in both intensity and duration is detectable for wind at 10 meters, although the gap in width is less pronounced. An analogous dissimilarity is found for wind at the 900 hPa level, where there is no BW though a “pseudo” one, with winds nearly parallel to the mountains, is formed for just a few hours farther downstream than at lower levels (see figure 5.10 and section 2.1 for criteria of defining BWs). BOLAM forecasts a greater deflection of the incoming flow and a wider “pseudo BW” than MOLOCH. No significant differences are found between the two models at higher levels.

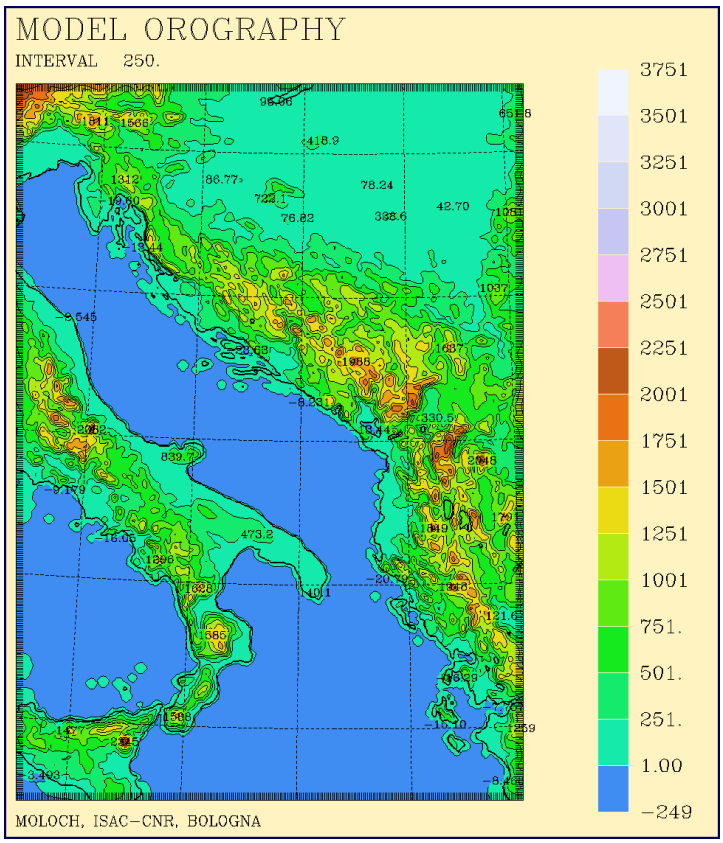

Figure 5.6: MOLOCH main run integration domain.

The major differences between the two forecasts concern the very barrier flow, with small or no dissimilarities in other areas and instants. Essentially, we can assert that BOLAM predicts a stronger BWs episode than MOLOCH.

As for other quantities, such as relative humidity, temperature, pressure and geopotential, there are no significant dissimilarities between BOLAM and MOLOCH forecasts, just as for the previous case study.

5.2 Sensitivity tests: reduced-orography simulations

Sensitivity tests have been conducted on this case study in the same fashion as for the previous one, by gradually lowering the orography up to the point that no BW is predicted anymore. The lowering function $s_3(i, j)$ (see equation 4.2) has been employed to lower the southern portion of the Dinaric Alps, which the incoming flow impinges on; since they are obliquely oriented with respect to parallels and meridians, a coordinate transformation has been applied to the basic form of $s_3(i, j)$ to obtain the *rotated* lowering function, which has an analogous shape to that in figure 4.26 while being oriented from north-west to south-east. The angle between parallels and the Dinaric Alps has been

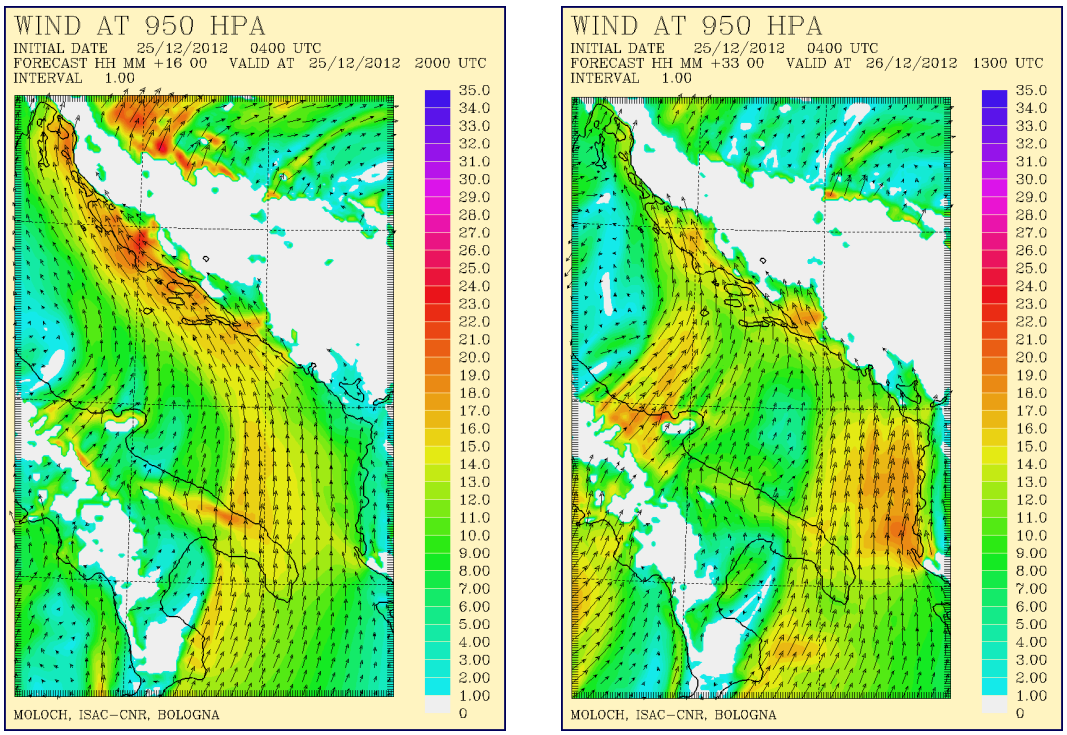

(a) Wind at 950 hPa (m/s) at 20 UTC on December 25.

(b) Wind at 950 hPa (m/s) at 13 UTC on December 26.

Figure 5.7: MOLOCH run, wind at 950 hPa (m/s) at two instants (zoom over the Adriatic Sea).

estimated at 40°.

Five simulations have been performed with BOLAM, with scaling factors of 0.1 to 0.5 (mountains lowered by 10% to 50%). A MOLOCH simulation has been nested into each of the BOLAM ones, with equally lowered orography. An example of reduced orography, relative to the simulation with scale factor 0.3, is displayed in figure 5.8.

As in the Alpine case, the BW extent, intensity and duration all decrease as the orography is progressively reduced; the BW completely disappears for 50% reduction – in this case the incoming flow crosses the mountains. The 950 hPa wind chart for the case of 40% reduction is displayed in figure 5.9, together with the one for the simulation with realistic orography. It is noteworthy that while the incoming winds are deflected less than in the real case, there is another contributor to the generation of BWs which remains unchanged: *föhn*-like downslope winds coming from the central Apennines and impinging on the central portion of the Dinaric Alps. As this part of the orography has been lowered to a lesser extent than the southern one, the effect of these winds is quite independent of the orography reduction we chose. This apparent heterogeneous nature

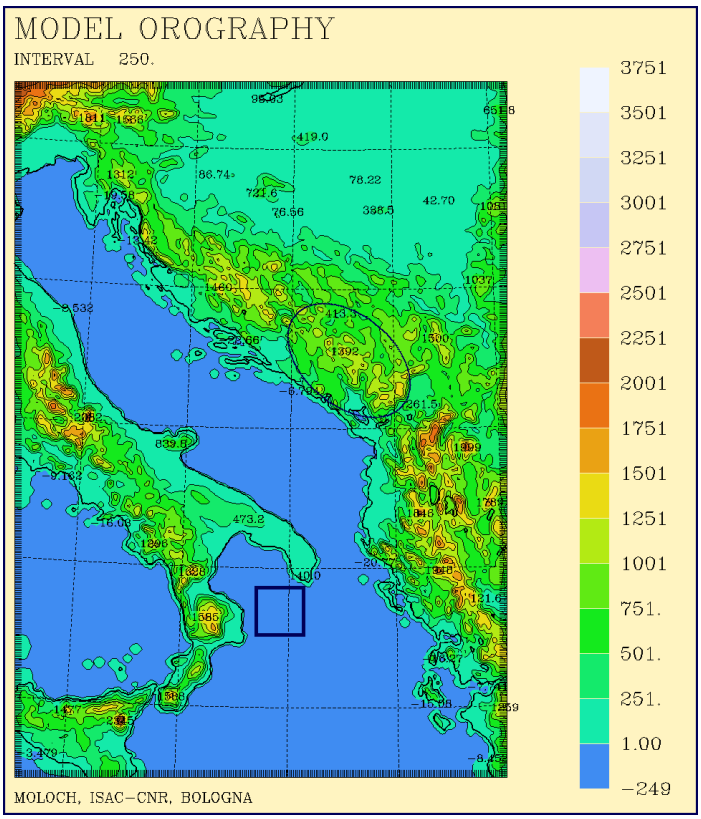

Figure 5.8: MOLOCH simulation with scale factor 0.3, integration domain; the portion of the orography that was reduced by more than 15% (half the scale factor) is that within the blue ellipse; U, N and the NMH have been computed within the region in the blue square.

of the BW could result in an overestimation of its extent.[3]

Nonetheless, we deemed it unnecessary to lower the entire model representation of the Dinaric Alps, as the greatest part of the incoming flow impinges on their southern portion: the above-mentioned wind coming from the central Apennines is a somewhat separate feature. This assumption is corroborated by the 900 hPa wind charts shown in figure 5.10. As we can see, in the real case (figure 5.10a) intense southeasterly winds are found on the northern half of the Adriatic coast. Although they cannot be defined as BWs according to the criteria discussed in section 2.1, their orientation and pattern are similar to those of BWs to the point that they can be referred to as "pseudo BWs", as already observed. In the simulation with 40% reduced orography (figure 5.10b) these winds are nearly absent, being much weaker than in the realistic-orography case while their orientation is even less parallel to the mountains and their duration is smaller as well. However, the contribution of winds coming from the central Apennines is identical in the two simulations. Therefore we conclude that their impact in generating BWs is not as significant as that of winds blowing over southern Italy.

[3]We tried to overcome this issue by measuring BW parameters via a weighted average, with weights decreasing moving northward so that the southernmost portion of the BWs, being the "purest" one – that is, the one featuring the least contribution from winds coming from the central Apennines – accounts for the major part of the calculation.

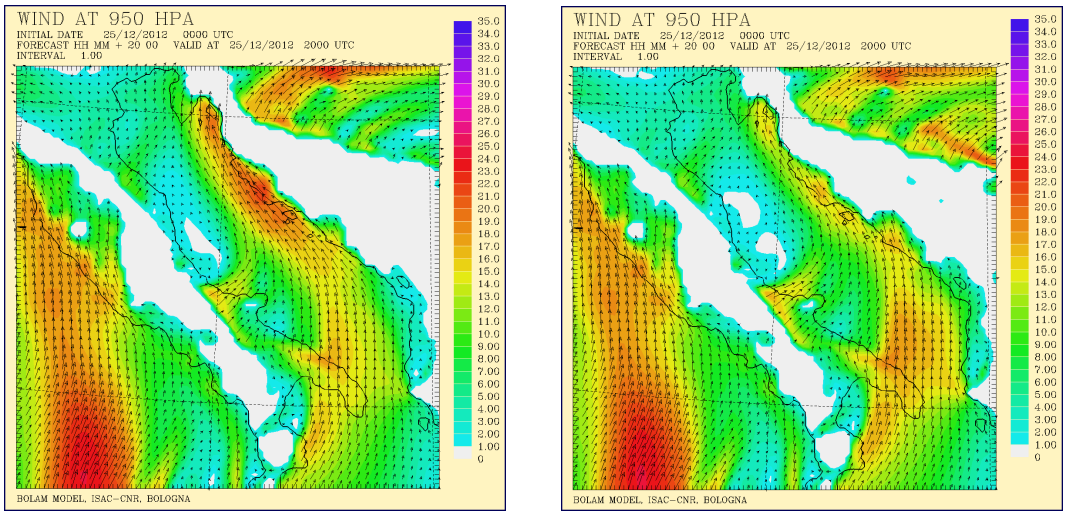

(a) Realistic-orography simulation. **(b)** Simulation with 40% reduced orography.

Figure 5.9: Comparison between the realistic-orography simulation and the one with 40% reduced orography, MOLOCH forecast for 950 hPa wind (m/s) at 20 UTC on December 25.

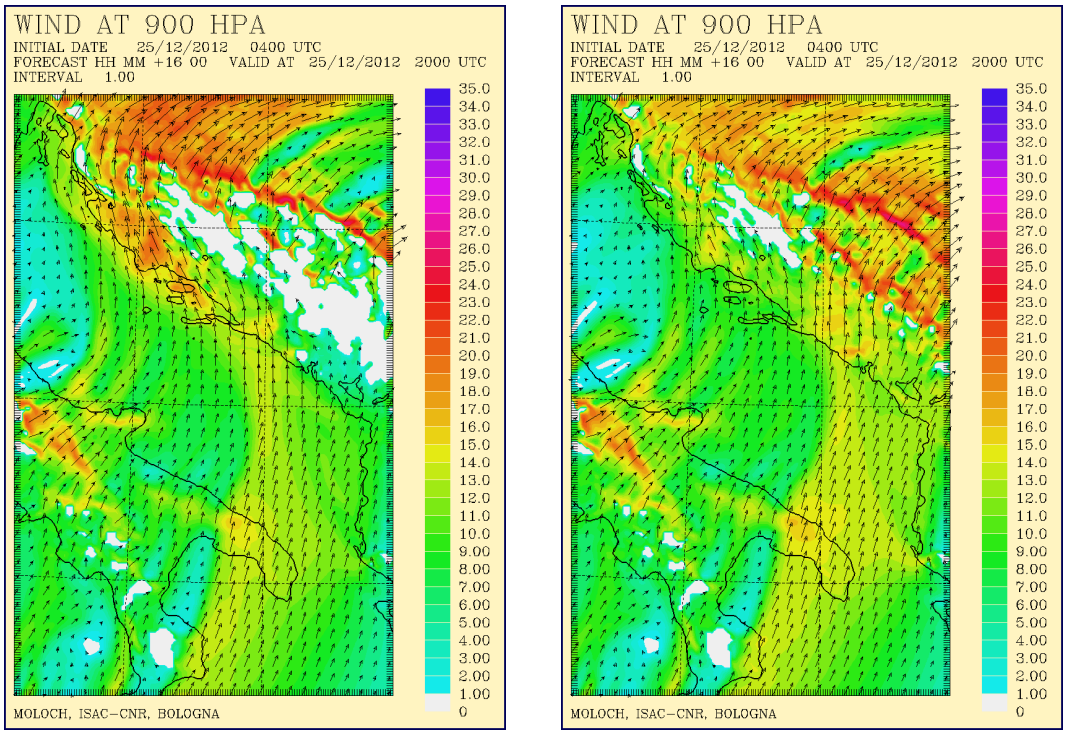

(a) Real case. **(b)** Simulation with orography reduced by 40%.

Figure 5.10: Wind at 900 hPa (m/s) at 20 UTC on December 25 (zoom over the Adriatic Sea), for the real case and the simulation with orography reduced by 40%.

The intensity and duration of BWs decrease as well with decreasing orography: see also table 5.1. There are not any significant differences in temperature, humidity and precipitation patterns and distributions between the various simulations. Nonetheless, the coastal regions on the side of the southern Dinaric Alps are slightly warmer and moister (by roughly 0.5 °C and 5% relative humidity, respectively) in the simulation with 40% reduced orography with respect to the real case. This small difference is due to the fact that the incoming flow advects more effectively heat and humidity towards the mountains when it is not deflected into a BW.

5.3 The Barrier Wind Index

The incoming flow average speed U and the Brunt-Väisälä frequency N were computed for each simulation via the same routine we employed for the previous case study, operating within a square region of 25×25 grid points about 200 km upstream of the Dinaric Alps (see figure 5.8). The height of the Dinaric Alps H to be used in the calculation of the NMH has been estimated in the same way as we did for the Alpine case study (see section 4.4) and subsequently rounded to 1500 m (so in the case of 10% reduction, it is 1350 m and so on). The lower eight levels of MOLOCH, up to a height of roughly 1200 m, have been employed for the calculation. As already noted in the previous Chapter, this choice is arbitrary. This case study also featured a further difficulty in accurately calculating the BW extension, as there is no sharp separation between the low-level incoming flow and the upper-level one. Wind is quite uniform in the vertical in both intensity and direction, varying very little up to 3000 m altitude. Since it would not make sense to calculate the Froude number within a layer that is higher than the mountain, we chose to maintain roughly the same ratio of the layer depth to the mountain height for all case studies.

A comparison of the major features for all the simulations is displayed in table 5.1 (the one with 50% reduced orography has been excluded as it does not feature any BW). BW average speed, width and depth have been calculated in an analogous way to the previous case study. In this case the transition from the BW to the surrounding wind circulation is not as sharp as for the Alpine event, as winds vectors vary in a smoother fashion. In order to overcome this issue, we set two "softer" thresholds of 20° and 60% of the maximum speed for variation in wind direction and speed, respectively: the BW boundary has been placed where at least one of the two thresholds is surpassed.

A plot of the BWI versus the NMH for this case study is displayed in figure 5.11. The blue crosses are not strictly error bars, though they are large in size to visually account for the uncertainties associated with the Non-dimensional Mountain Height and the Barrier Wind Index, which may be cautiously estimated at 0.1, as we commented at the end of the previous Chapter. Contrasting this plot with the one for the Alpine case study (figure

Orography	v_u [m/s]	v_b [m/s]	W [km]	D [m]	NMH	BWI
Real	10.8	15.3	60	700	2.09	2.39
10% red.	10.9	14.3	49	650	1.86	1.68
20% red.	11.0	13.0	42	610	1.64	1.21
30% red.	11.1	11.7	35	560	1.42	0.83
40% red.	11.2	9.7	28	510	1.21	0.49

Table 5.1: Principal features for all simulations: v_u is the upstream wind average speed, v_b is the BW average speed, W is its average width and D is its average depth. The NMH is the Non-dimensional Mountain Height, the BWI is the Barrier Wind Index.

4.34), we can notice that the two plots are very similar, exhibiting a nearly linear profile (we have to keep in mind that the determination of BW parameters was less accurate in this case than in the Alpine one). A more detailed discussion about this will be provided in Chapter 7.

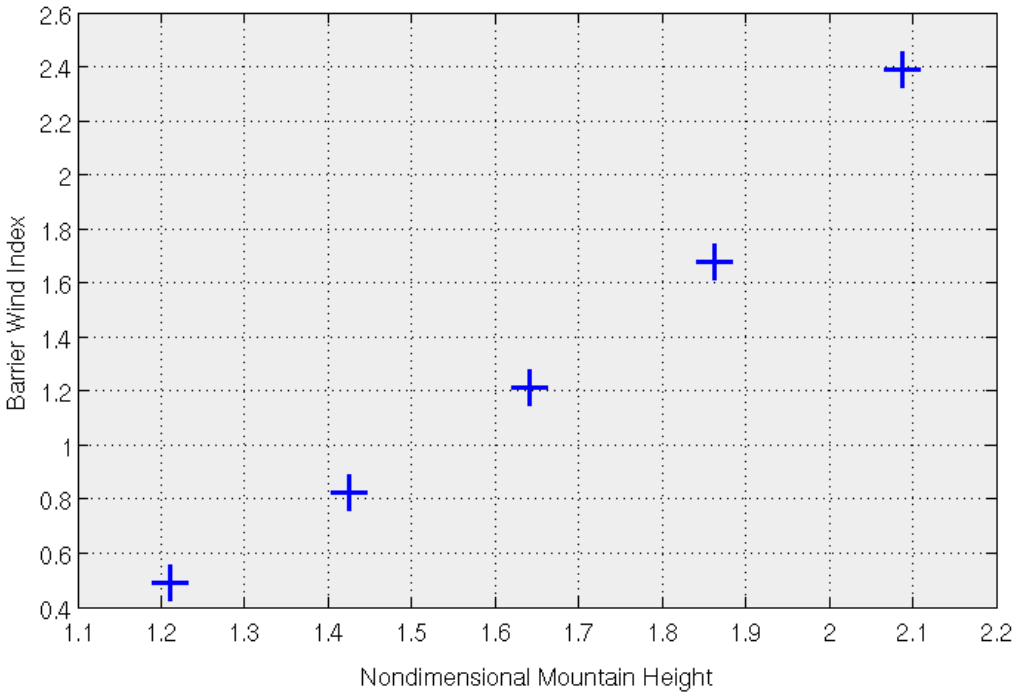

Figure 5.11: Plot of the BWI versus the NMH for the Dinaric case study.

Chapter 6

The 2012 Ligurian case study

The third case study we selected is a Ligurian event that occurred from October 18 to October 21, 2012. It lasts over 3 days and features extensive barrier winds off the western Ligurian and Provence coast. This event also exhibits a totally different upstream flow from those of the previous case studies, as it consists of the weaker branch of an intense southeasterly flow, separated from its major part by Sardinia and Corsica. No precipitation at all occurs throughout the event.

6.1 Event simulations

6.1.1 BOLAM simulation

The first simulation we performed is a 96-hours BOLAM run, from October 18, 2012, 00 UTC to October 22, 2012, 00 UTC. The integration domain is displayed in figure 6.1. All model settings are the same as for the previous case studies (see subsection 4.1.1), except for domain size which is now 202 points in longitude and 150 in latitude. The accuracy of the simulation was not affected by the initial condition adjustment period, as the core of the event starts several hours after the initialization.

The synoptic situation producing this Ligurian event is displayed in figure 6.2, concerning the central part of the event. A deep trough situated off the Atlantic coast has caused a marked elongated ridge to move northwards and settle over Italy and Central Europe (figure 6.2a). M.s.l. pressure over Italy is moderately high and uniform, with a stronger gradient over the Tyrrhenian Sea and the western Mediterranean Sea (figure 6.2b). This pattern remains nearly unchanged for over 3 days and generates intense southerly (southwesterly to southeasterly) winds blowing over the Mediterranean Sea.

The core of the BWs event lasts from 06 UTC on October 18 to 10 UTC on October 21: wind at the 950 hPa level is displayed at four instants in figure 6.3. As we can see,

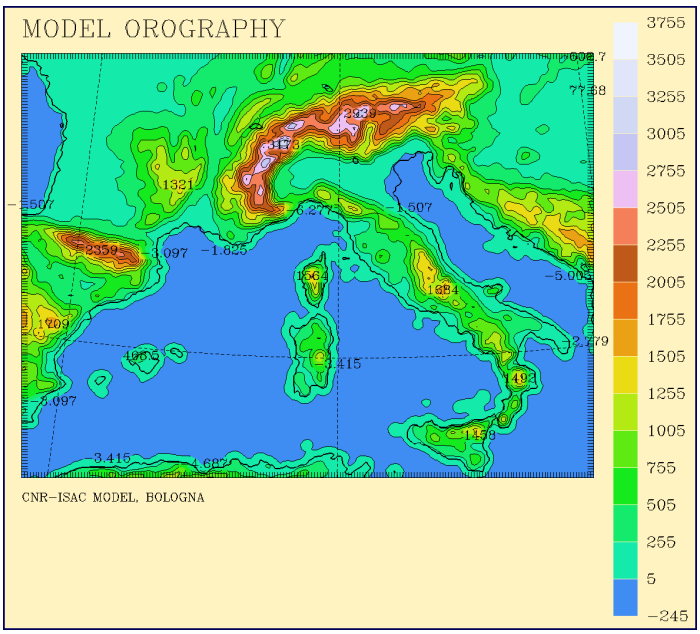

Figure 6.1: BOLAM main run integration domain.

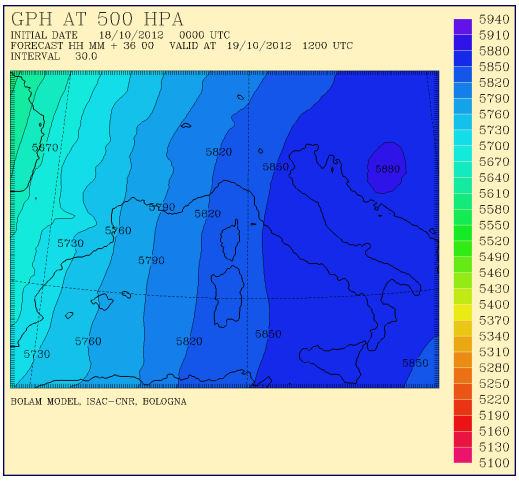

(a) 500 hPa geopotential height (dam).

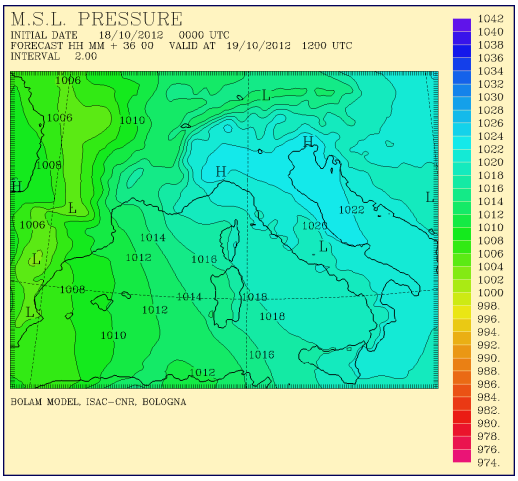

(b) M.s.l. pressure (hPa).

Figure 6.2: Synoptic situation, BOLAM forecast for 500 hPa geopotential height and m.s.l. pressure at 12 UTC on October 19.

the incoming flow consists of a wide band of southeasterly winds (figure 6.3a) which are more intense in its left part (facing downstream) and weaker in its right (eastern) part, which is the one directly headed towards the Maritime Alps. The flow is heavily impacted by the topography of Sardinia and Corsica – two minima are found on their leeward side, a maximum is found in the outflow from the Strait of Bonifacio; it is also shaped by the Corsican and Ligurian topography which guides it through the Corsica Channel into the Ligurian Sea and deflects it westward. A moderate BW, exceeding 10 m/s throughout

the event and peaking at 20 m/s at the 950 hPa level, is thus established in front of the Maritime Alps (wind near the surface is slightly weaker). The considerable duration of the event is most likely a result of the topographic conformation of the area as well as of the persistence of the pressure and flow pattern. The BW speed and width vary over time (see figures 6.3b, 6.3c and 6.3d), being larger during the first half of the event until 12 UTC on October 19, and decreasing afterwards.

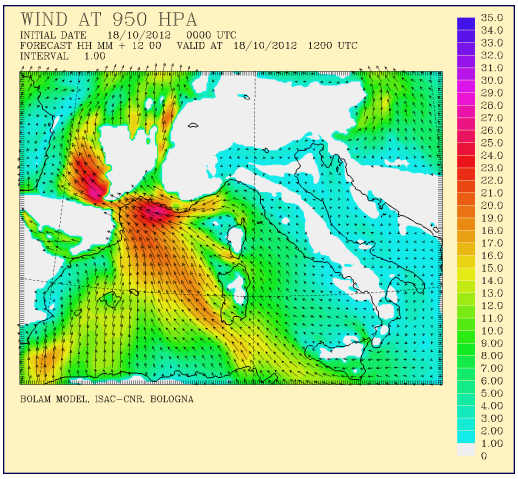

(a) 950 hPa wind (m/s) at 12 UTC on October 18.

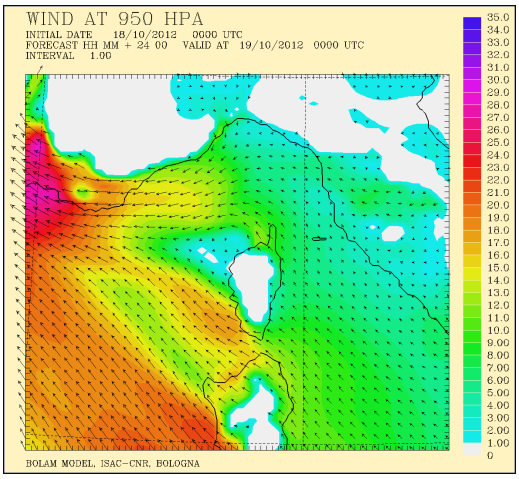

(b) 950 hPa wind (m/s) at 00 UTC on October 19 (zoom over the Ligurian Sea).

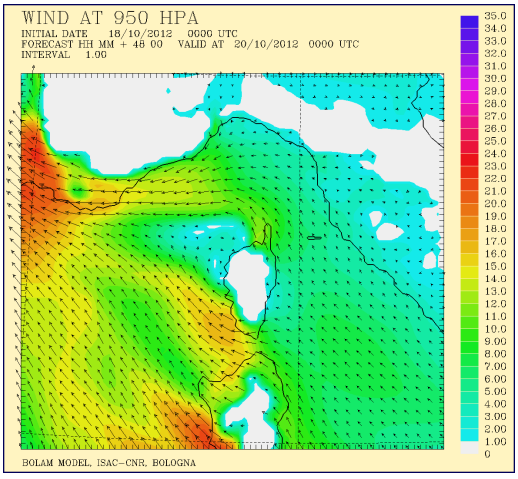

(c) 950 hPa wind (m/s) at 00 UTC on October 20 (zoom over the Ligurian Sea).

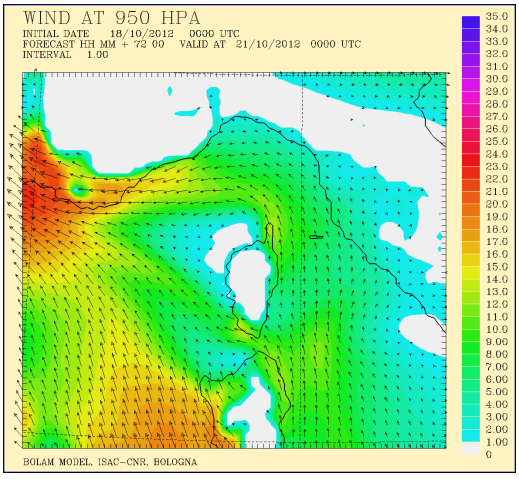

(d) 950 hPa wind (m/s) at 00 UTC on October 21 (zoom over the Ligurian Sea).

Figure 6.3: BOLAM run, wind at 950 hPa at four instants.

The outflow from the Po Valley is a significant contribution to BW in this case especially for wind near the surface, as we can observe in figure 6.4, showing wind streamlines at 950 hPa (6.4a) and at 10 meters (6.4b) (we can assume that the streamlines represent

wind trajectories with fair accuracy, as the circulation is quite steady around the instant shown). The outflow is the result of the inflow from the eastern border of the Po Valley. It is a typical occurrence in this area and a determinant factor in triggering intense precipitation over Liguria (see, for instance, Buzzi et al., 2013). In this case, the Po Valley outflow is a significant contributor for wind at 10 meters, which does not exhibit a clear BW pattern – the upstream wind is not even normal to the Maritime Alps, albeit being directed towards them. Strong vertical shear is predicted for the incoming flow over the Tyrrhenian Sea, with wind veering in the lower levels as altitude increases. At the 950 hPa level the outflow influence is smaller than near the surface, nonetheless the wind speed maximum off the Ligurian and French coasts visible in figure 6.4a is most likely the result of both barrier and outflow effects. The Po Valley outflow is visible also in figure 6.5, which displays relative humidity at 950 hPa, as a streak of drier air located immediately off the western Ligurian and French coasts.

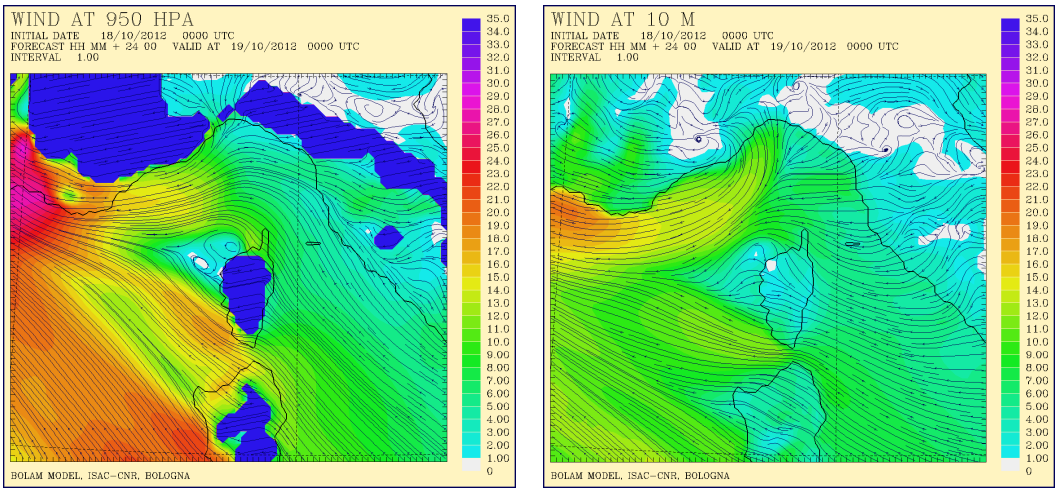

(a) Streamlines of wind at 950 hPa. **(b)** Streamlines of wind at 10 meters.

Figure 6.4: BOLAM run, streamlines of low-level wind at 00 UTC on October 19 (zoom over the Ligurian Sea).

At the 900 hPa level, the barrier wind is present for just a few hours: compare figure 6.6a, which relates to the beginning of the event, with figure 6.6b, relating to the second part; the incoming flow is still deflected at this height, though not as much as below, and a wide band of intense low-level winds blowing parallel to the mountains is not enduringly attained. At higher levels there is no BW.

This event is completely rainless according to the BOLAM model, as no precipitation is predicted over the whole region where BWs occur. M.s.l. pressure remains nearly steady around 1018 hPa throughout the event. A pressure "nose" is present, though it is weaker than the one of the previous case studies (roughly 1 hPa difference between

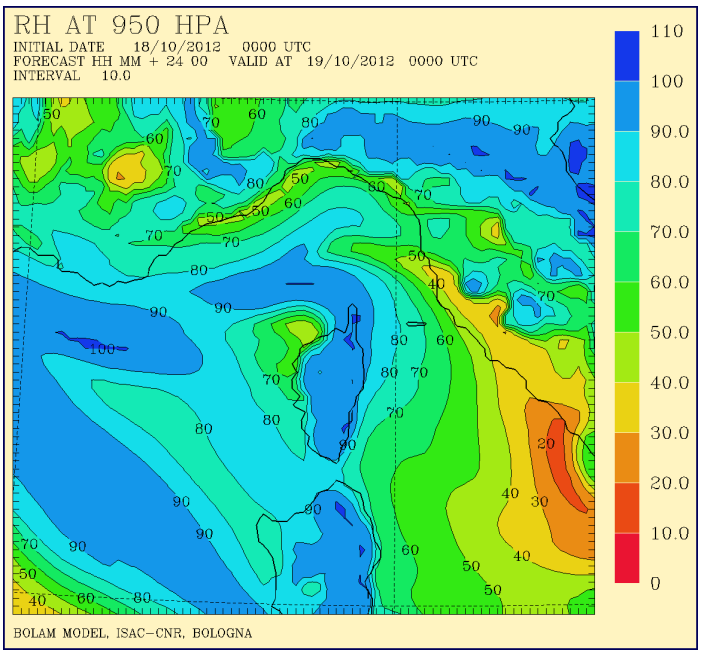

Figure 6.5: BOLAM run, relative humidity (%) at 950 hPa at 00 UTC on October 19 (zoom over the Ligurian Sea).

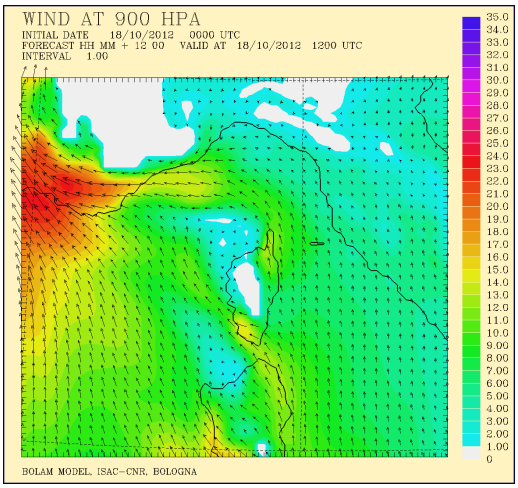

(a) Wind at 900 hPa (m/s) at 12 UTC on October 18.

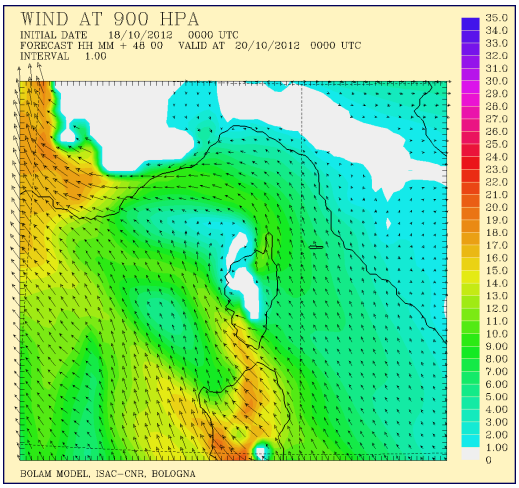

(b) Wind at 900 hPa (m/s) at 00 UTC on October 20.

Figure 6.6: BOLAM run, wind at 900 hPa at 12 UTC on October 18 and at 00 UTC on October 20 (zoom over the Ligurian Sea).

upstream and downstream locations). This is most likely connected with the “mixed nature” of the event, as in this case the deflection of the airflow is produced by both the conformation of the topography, as said before, and the effect of pressure increase, and it is favoured by the outflow from the Po Valley.

6.1.2 MOLOCH simulation

A 84-hours simulation with MOLOCH has been performed, from 06 UTC on October 18 to 18 UTC on October 21, nesting the model into the BOLAM run as for the previous case studies. The integration domain is displayed in figure 6.7. All model settings are the same as for the previous case studies (see subsection 4.1.2), except for domain size which is now 218 points in longitude and 258 in latitude.

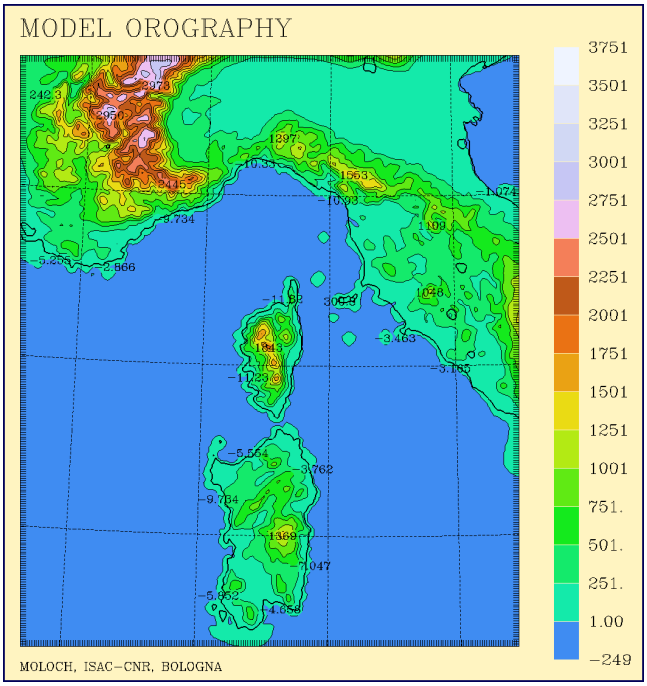

Figure 6.7: MOLOCH main run integration domain.

As for low-level wind, BOLAM and MOLOCH are in good agreement: see figure 6.8, where the two models' output for the same instant (00 UTC on October 19) is compared for wind at 950 hPa and at 10 m. There is very little difference between the two forecasts, apart from small-scale features such as localized wind maxima produced by katabatic winds on the northern Sardinian coast (figure 6.8b) and on the western side of the Maritime Alps (figure 6.8d), which are better resolved by MOLOCH due to its larger resolution.[1]

Other quantities, such as pressure and geopotential, relative humidity and temperature, show no significant dissimilarities between BOLAM and MOLOCH forecasts (see, for instance, figure 6.9 where a comparison is drawn for m.s.l. pressure and 950 hPa temperature forecasts).

[1]However, as already pointed out while discussing the previous case studies, we cannot be completely confident that these features are real and have not been artificially introduced by the model.

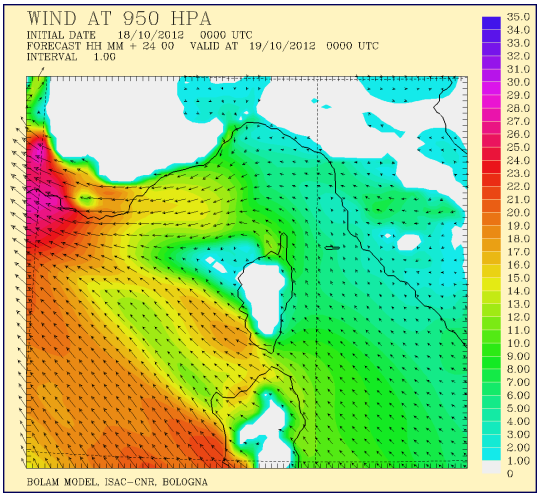

(a) 950 hPa wind (m/s), BOLAM forecast (zoom over the Ligurian Sea).

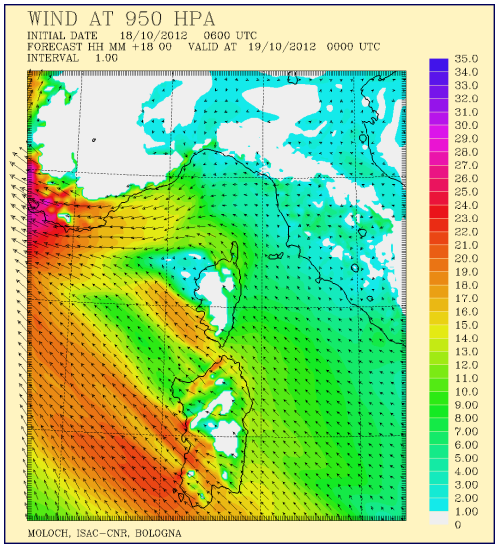

(b) 950 hPa wind (m/s), MOLOCH forecast.

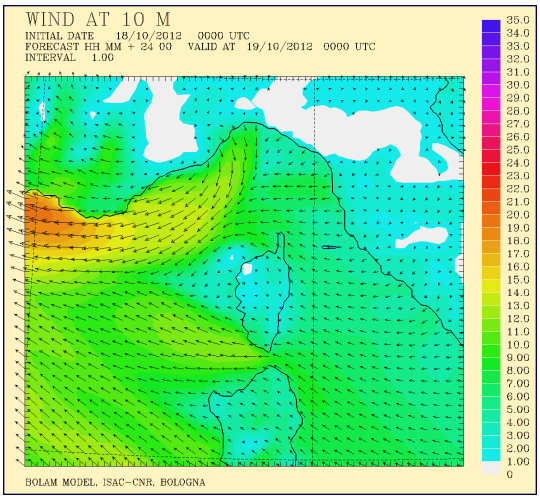

(c) 10 m wind (m/s), BOLAM forecast (zoom over the Ligurian Sea).

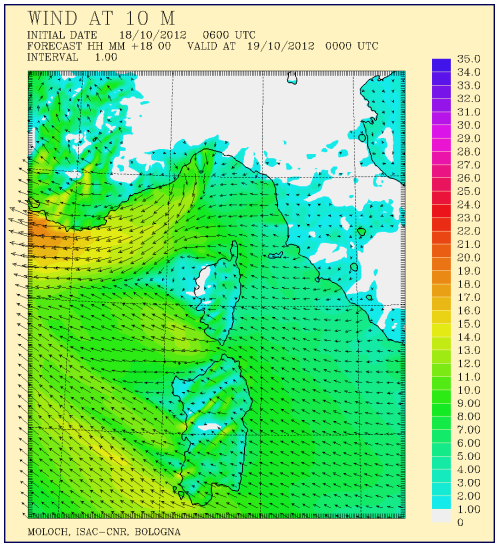

(d) 10 m wind (m/s), MOLOCH forecast.

Figure 6.8: Wind at 950 hPa and at 10 m, BOLAM and MOLOCH forecasts for 00 UTC on October 19.

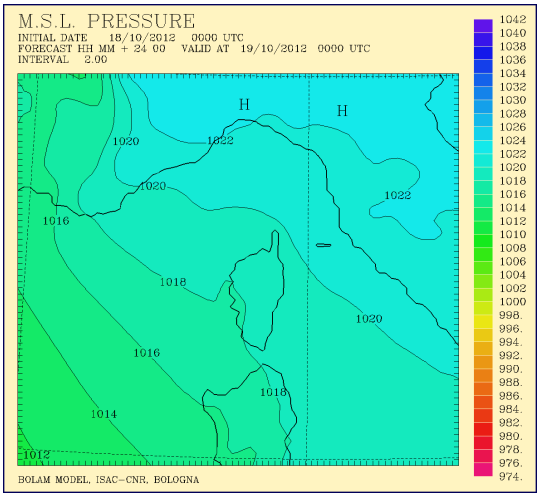

(a) M.s.l. pressure (hPa), BOLAM forecast (zoom over the Ligurian Sea).

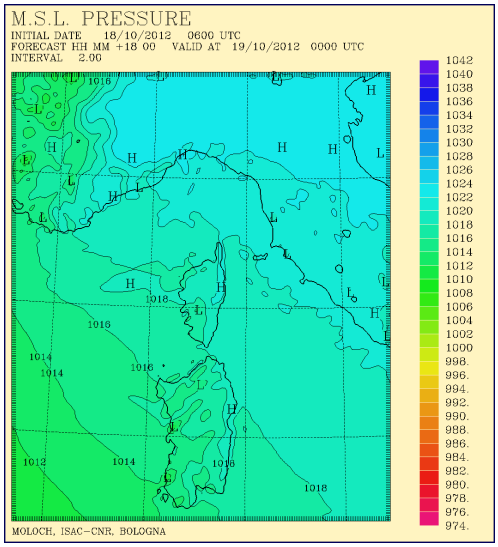

(b) M.s.l. pressure (hPa), MOLOCH forecast.

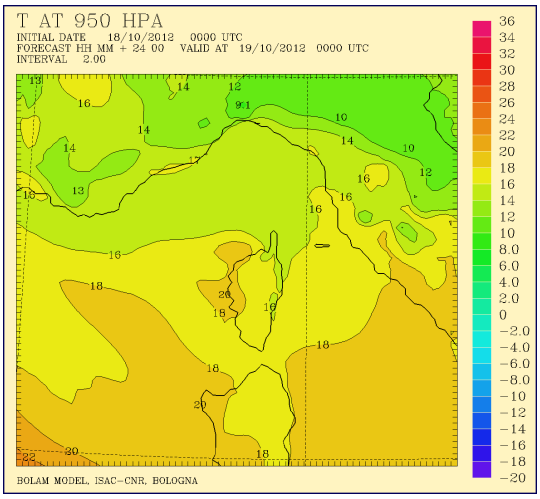

(c) Temperature at 950 hPa (°C), BOLAM forecast (zoom over the Ligurian Sea).

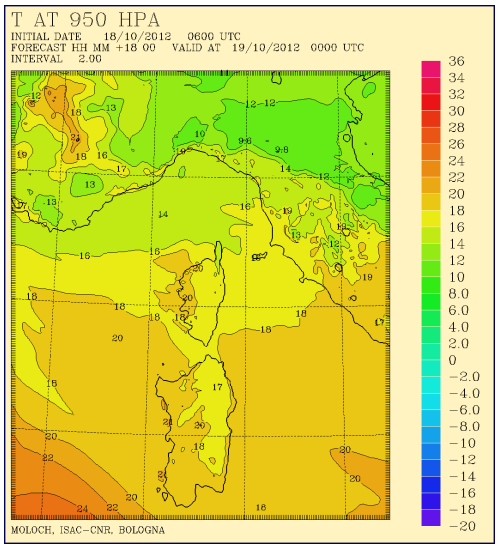

(d) Temperature at 950 hPa (°C), MOLOCH forecast.

Figure 6.9: M.s.l. pressure and temperature at 950 hPa, BOLAM and MOLOCH forecasts for 00 UTC on October 19.

6.2 Sensitivity tests: reduced-orography simulations

Sensitivity tests have been conducted on this case study as for the previous ones. The lowering function $s_4(i, j)$ (see equation 4.2) has been employed to lower the Maritime Alps, which the incoming airflow impinges on. Six simulations have been performed with BOLAM, with scaling factors of 0.1 to 0.6 (mountains lowered by 10% to 60%).

A MOLOCH simulation has been nested into each of the BOLAM runs, with equally lowered orography. The MOLOCH domain relative to the simulation with scale factor 0.4 (orography reduced by 40%) is displayed in figure 6.10 as an example.

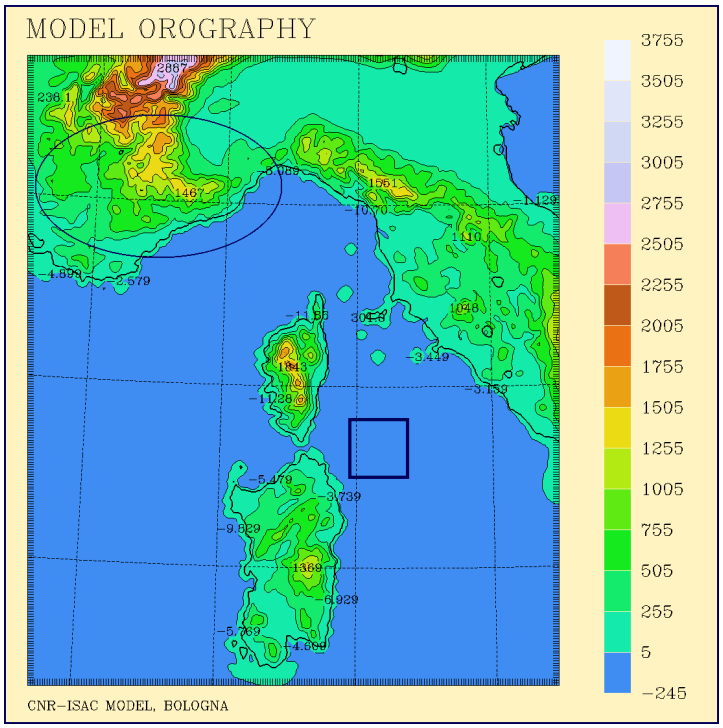

Figure 6.10: MOLOCH simulation with scale factor 0.4, integration domain; the portion of the orography that was reduced by more than 20% (half the scale factor) is that within the blue ellipse; U, N and the NMH have been computed within the region in the blue square, measuring 25×25 grid points or approximately 70×70 kilometers.

Wind at the 950 hPa level is displayed in figure 6.11 for the simulation with real orography and the ones with 20%, 40% and 60% reduced orography, respectively. The same comparison is drawn for wind at 10 meters in figure 6.12. As we can see, the BW is displaced downstream (with respect to the incoming flow) though its intensity and width do not reduce as much as for the previous case studies; this is also valid for other instants.

The strong persistence of the BW pattern, even in the simulations with drastically reduced orography, suggests that the influence of the surrounding topography on wind circulation is quite marked in this case, so that the low-level flow tends to be guided into the Ligurian Sea and then deflected in any case. As the outflow from the Po Valley appears to decrease with reduced orography,[2] it can be excluded from being the principal cause of the BW persistence. A further conceivable cause of the deflection of the incoming flow is the northwestern portion of the Alps, to the north of the Maritime Alps, which is not lowered. However, its effect is most likely marginal for two reasons: it is too far from the region – the western Ligurian Sea – where the flow is deflected, being over 100 km to

[2]One of the reasons for this is most likely the fact that as mountains have been lowered, there are further ways for low-level air in the Po Valley to flow out other than the Ligurian valleys.

the north; this region does not shift much as the Maritime Alps are lowered, whereas we would expect it to be considerably displaced northwards if the northwestern Alps had a marked impact on the deflection.

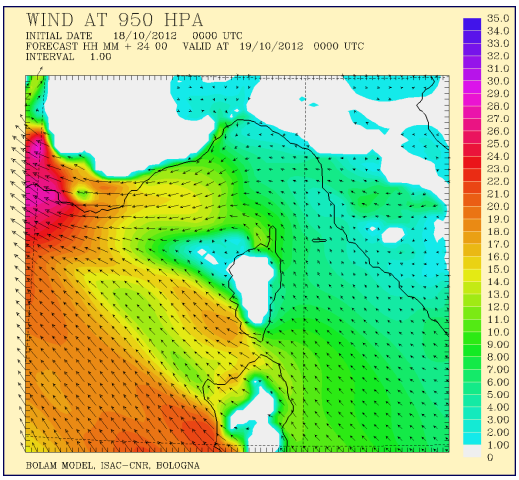

(a) Real-orography simulation.

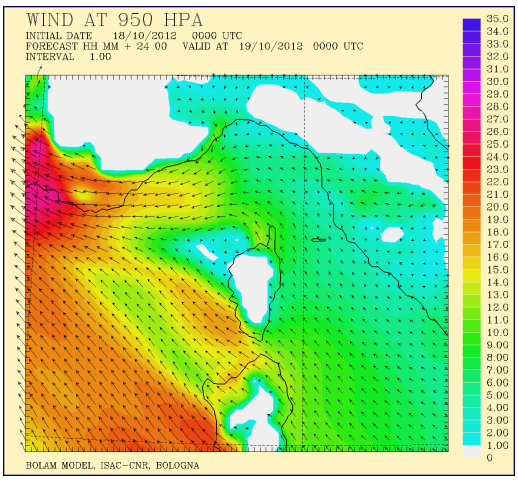

(b) Simulation with 20% reduced orography.

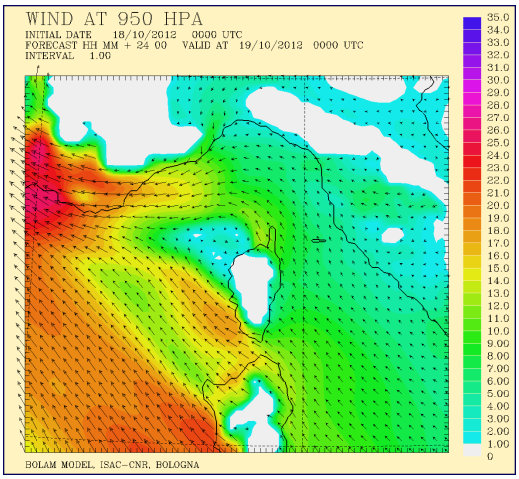

(c) Simulation with 40% reduced orography.

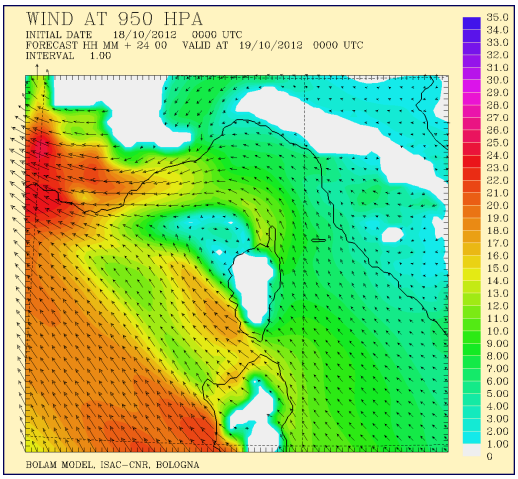

(d) Simulation with 60% reduced orography.

Figure 6.11: Comparison between BOLAM real-orography and reduced-orography simulations, wind at 950 hPa (m/s) at 00 UTC on October 19.

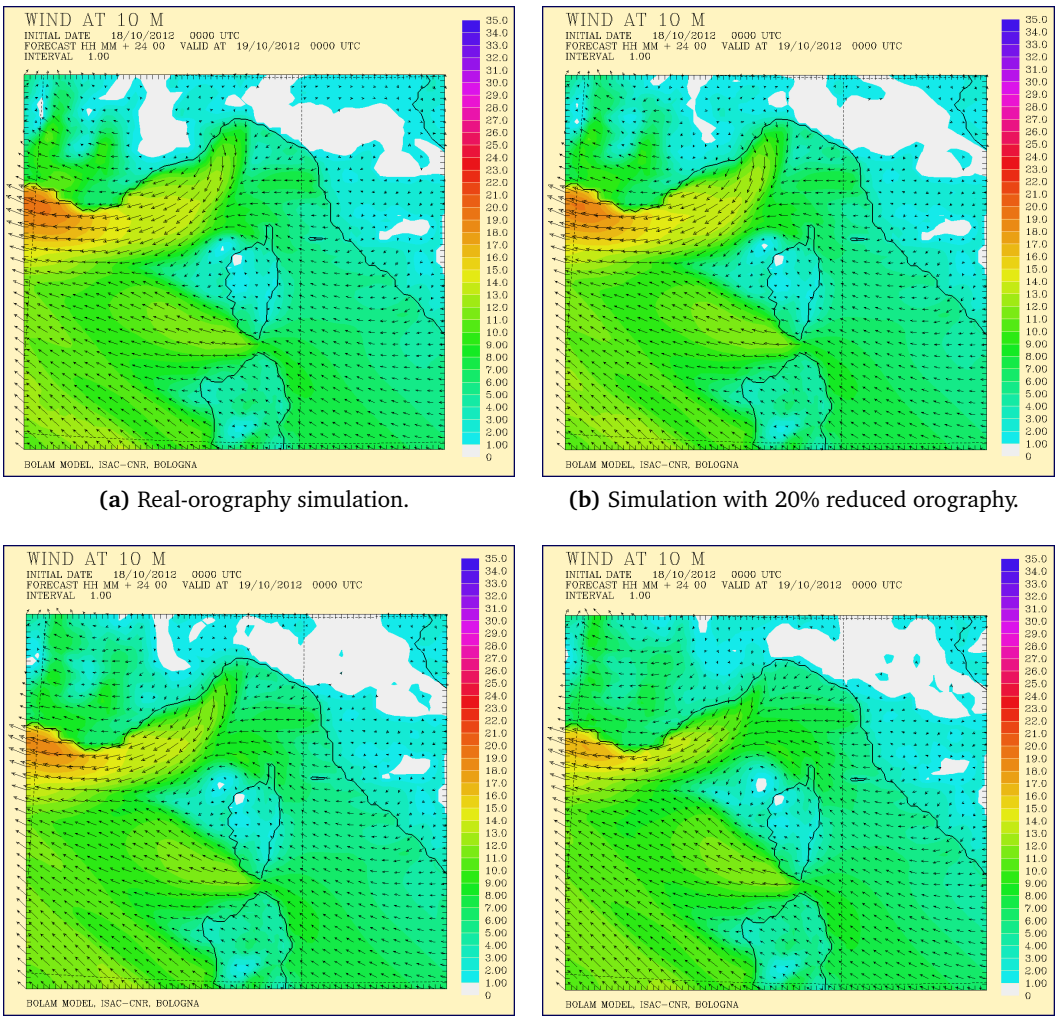

(a) Real-orography simulation.

(b) Simulation with 20% reduced orography.

(c) Simulation with 40% reduced orography.

(d) Simulation with 60% reduced orography.

Figure 6.12: Comparison between BOLAM real-orography and reduced-orography simulations, wind at 10 meters (m/s) at 00 UTC on October 19.

There are no significant differences in pressure between the various simulations: see, for instance, figure 6.13 where a comparison is drawn for m.s.l. pressure between the realistic-orography case and the one with 60% reduced orography. Pressure is slightly higher over the Ligurian Sea in the former case than in the latter, as we expect because of the accumulation effect. Temperature and humidity patterns also do not show any visible variations between the simulations.

There is good agreement between BOLAM and MOLOCH reduced-orography simulations, as well as for the realistic-orography case.

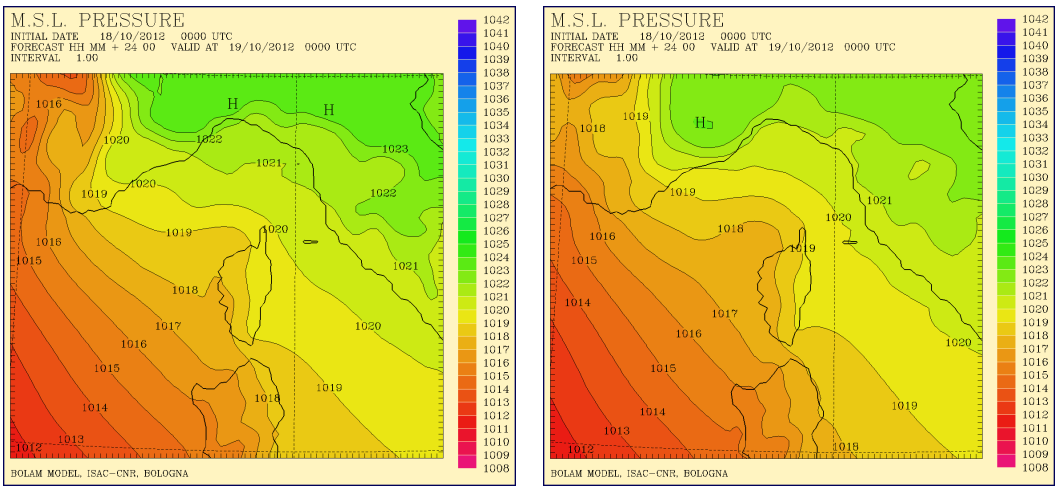

(a) Real-orography simulation. **(b)** Simulation with 60% reduced orography.

Figure 6.13: Comparison between BOLAM real-orography and reduced-orography simulations, m.s.l. pressure (hPa) at 00 UTC on October 19.

6.3 The Barrier Wind Index

The incoming airflow average speed U and the Brunt-Väisälä frequency N have been computed for each simulation via the dedicated routine we employed for the previous case studies, operating within a square region of 25×25 grid points (roughly 70×70 kilometers) situated about 250 km upstream of the Maritime Alps (see figure 6.10). The height of the Maritime Alps H to be used in the calculation of the NMH has been estimated in the same way as we did for the previous case studies (see section 4.4) and subsequently rounded to 1500 m (so in the case of 10% reduction, it is 1350 m and so on). As we did for the Dinaric case study – the estimated height for the Dinaric Alps being also 1500 m – the lower 8 levels of MOLOCH, up to a height of roughly 1200 m, have been employed for the calculation, thereby maintaining approximately the same ratio of the layer depth to the mountain height.

A comparison of the major features for all the simulations is displayed in table 6.1. BW average speed, width and depth have been calculated in a similar way to the Alpine case study (see subsection 4.4). Since in this case, as well as in the Dinaric case study, the transition from the BW to the surrounding wind is not sharp, we used the same "soft" thresholds of 20°for variation in wind direction and 60% of the maximum for wind speed (see subsection 5.3).

A plot of the BWI versus the NMH for this case study is displayed in figure 6.14. As in the previous case studies, the blue crosses are not error bars, though they are large in size to visually account for the uncertainties associated with the Non-dimensional

Orography	v_u [m/s]	v_b [m/s]	W [km]	D [m]	NMH	BWI
Real	7.7	12.9	59	650	2.33	2.57
10% red.	7.8	12.8	57	640	2.08	2.39
20% red.	7.8	12.8	55	630	1.84	2.27
30% red.	7.9	12.7	53	630	1.60	2.15
40% red.	8.0	12.7	50	620	1.35	1.97
50% red.	8.1	12.6	47	600	1.12	1.75
60% red.	8.2	12.5	45	590	0.89	1.62

Table 6.1: Principal features for all simulations: v_u is the upstream wind average speed, v_b is the BW average speed, W is its average width and D is its average depth. The NMH is the Non-dimensional Mountain Height, the BWI is the Barrier Wind Index.

Mountain Height and the Barrier Wind Index, which can be cautiously estimated at 0.1, as we already commented. This plot exhibits a nearly linear profile, as the ones for the other case studies. However, the BWI values are much larger here than in any other case, most likely due to the topographic effect on the incoming flow. This difference will be discussed in detail in the next Chapter.

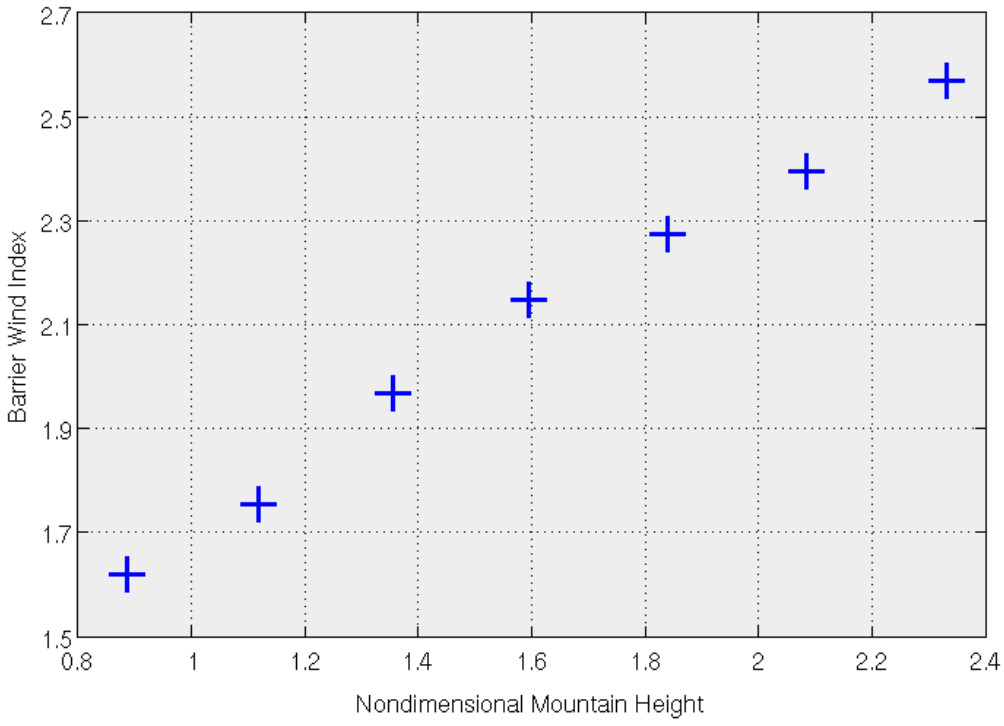

Figure 6.14: Plot of the BWI versus the NMH for the Ligurian case study.

Chapter 7

Results

7.1 Results of the application of the BWI

In the present work we tried to apply the idealized theory of the low Froude number flow over an obstacle to realistic situations, employing mesoscale meteorological models to simulate BWs episodes in order to better understand the role of the Froude number in determining the flow pattern. Although theory works satisfactorily in several cases, it cannot account for the complexity and variability typical of real weather, having been developed for idealized flows in idealized conditions. Furthermore, the same theory may yield an adequate representation of some aspects of the flow, while failing to explain or to account for other aspects. For instance, Pierrehumbert and Wyman (1985) pointed out that the theory of a hydrostatic, inviscid, rotating, continuously stratified flow over a three-dimensional mountain, albeit acceptable for several respects, does not reproduce the sharpness of vertical wind shear associated with barrier winds in cases of upstream blocking. Smolarkiewicz and Rotunno (1990) observed that the same phenomenon of flow reversal and upstream blocking is erroneously explained as a consequence of the parcel's loss of kinetic energy against the mountain barrier by the theory of Sheppard (1956), while Smith (1980, 1988) correctly associates it to the positive density anomaly on the windward side of the mountain.

The Barrier Wind Index, as defined in subsection 4.4, is a non-dimensional parameter indicative of the extent attained by the barrier wind during an episode of low-level blocking. It has been defined on the basis of the idealized theory, attempting to find a common ground between idealized flow regimes, in which we have full control of the flow features and parameters (such as upstream wind, stratification etc.), and realistic flow regimes, in which the whole complexity, heterogeneity and variability of the real atmosphere is introduced. The BWI equals 1 when the BW has 50 km width, 500 m depth and an average speed equal to the average speed of the incoming low-level airflow

during the steady-state stage of the event. The BWI can be a useful diagnostic tool for estimating the significance of BW events and thereby for characterizing, in terms of the presence and extent of BWs, a severe weather episode or a climatology, for instance.

Several issues arise due to the arbitrariness associated to the calculation of the BWI:

- the areas where the average speed of both the incoming flow and the barrier wind are computed can be positioned anywhere, as there is no precise criterion for determining where they should be placed;
- the numerical criteria for determining the BW boundaries are also arbitrary: as every case is different from any other, the same thresholds cannot be employed for all cases.[1]

These problems can be solved to some extent by repeating the calculation of the BWI several times, each time varying the position of the areas and/or the thresholds, and then averaging the result over the sample. Naturally, there must not be too much variability between the various cases, otherwise the averaging technique would not make sense. Such an issue can be prevented by placing the areas as far as possible from strong wind gradients, though this might not be enough in some cases.

Just as for the BWI, several issues arise for the estimation of the NMH:

- the area in which the incoming wind U and the Brunt-Väisälä frequency N are computed can be placed anywhere in principle, as already noted[2];
- the vertical depth of the layer where U and N are computed (or the number of levels) is arbitrary as well;
- in case of complex orography structure, there is no precise criterion to determine the mountain height H;
- in moist (saturated) cases the *moist Brunt-Väisälä frequency* N_m is to be used instead of the dry one.

These problems can be tackled in various ways (the first two are especially important when a strong horizontal and/or vertical variability is found within the incoming flow). The calculation can be repeated multiple times, each time varying slightly the position of the area, and then U and N can be averaged over the sample, just as for the BWI. An

[1] For instance, there are events with a sharp and well-defined BW, such as the Alpine one in Chapter 4, which is separated from the surrounding flow by an abrupt variation in wind speed and direction; on the other hand, there are episodes in which the BW boundary is smooth and steady, such as the Dinaric one and the Ligurian one in Chapters 5 and 6, respectively.

[2] Provided that the distance from the mountains is kept larger than 100 km, which is a scale length representative of the boundary between upstream and near-orography flow.

analogous approach can be employed for the vertical depth of the layer, though in this case it is difficult to obtain a large sample. It is preferable to choose the layer depth so as to satisfy some criterion about wind shear: for instance, two thresholds can be set for wind speed and direction and the layer upper boundary can be placed where one of them is exceeded; or, alternatively, a ratio of the layer depth to the mountain height can be decided *a priori* for all cases. The mountain height H can be calculated as an average over the range (or over a selected portion of it, for instance the one where the highest peaks are found); or, alternatively, it can be computed as the average over a sample of vertical cross sections of the maximum mountain height within each cross section (the so-called "silhouette orography"), as we did for our case studies.

A plot of the Barrier Wind Index vs the Non-dimensional Mountain Height is displayed in figure 7.1 for all three case studies.

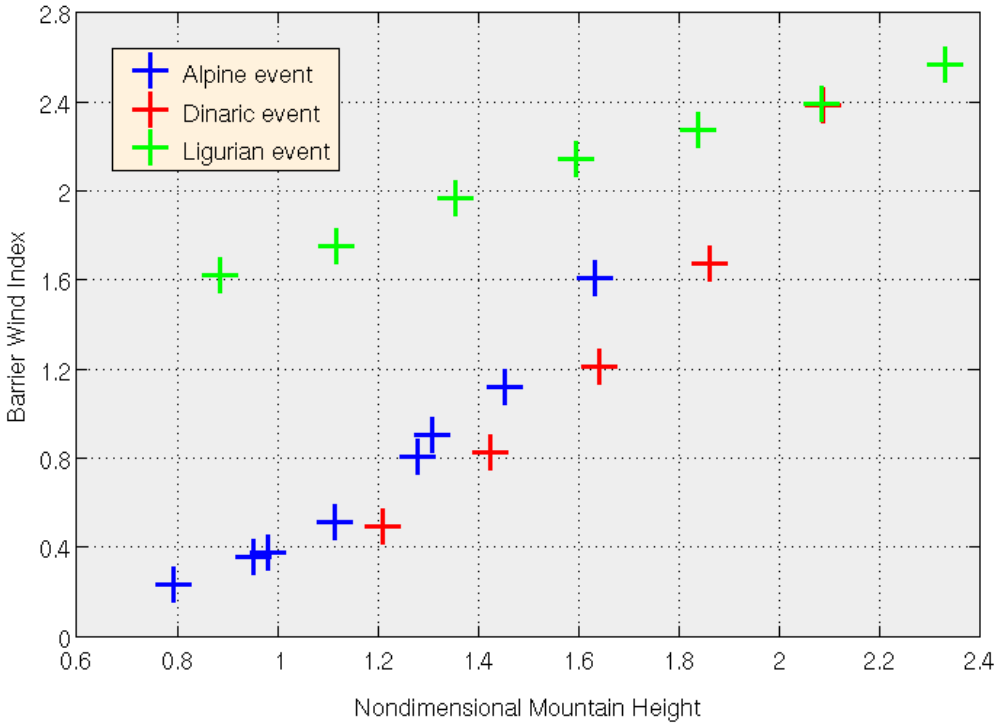

Figure 7.1: Plot of BWI versus NMH for all case studies.

First of all, we have to keep in mind that the crosses in figure 7.1 are not error bars, but they are large in size to account for the uncertainty associated with both the BWI and the NMH. As discussed in subsection 4.4, a cautious estimate of this uncertainty could be 10% relative error or 0.1 for both the BWI and the NMH (0.05 for smaller values).

All three plots show a roughly linear increase of the BWI as the NMH gets larger. The Alpine curve and the Dinaric curve are similar to each other, whereas the Ligurian curve

is completely dissimilar from the other two for both its gradient, which is smaller, and its values, which are much larger than those of the other two curves. Such a dissimilarity can be at least partially explained by the strong difference in the nature of the incoming flow between the Ligurian event and the other two. In the former case the flow is heavily influenced by the presence of several mountains on both its sides, that is the Sardinian and Corsican orography to the west and the Tuscan and Ligurian orography to the east; this topography is distributed in such a pattern that the flow is channelled through the Corsica Channel and then diverted westwards along the Ligurian coasts; the deflection produced by the barrier effect is thereby enhanced. The Alpine and Dinaric events feature a much more unconfined incoming flow, travelling all the way over the sea (and over the flat topography of Apulia as well, in the Dinaric case) until it impinges against the mountains and is eventually deflected. This could explain the large difference between the BWI of the Ligurian case and that of the others.

The Alpine and Dinaric curves appear to be more consistent with the theory of a low Froude number flow over an obstacle enounced, for instance, by Drazin (1961), Smith (1980, 1988) and later by Smolarkiewicz and Rotunno (1989, 1990), approaching to 0 as the NMH tend to 1, just as we would expect given that BW is a nonlinear phenomenon pertaining to the $\mathrm{Fr} < 1$ regime (naturally it would not be realistic to expect that the two curves tend exactly to 0, due to the numerous uncertainties associated with both the abscissa and the ordinate). The Ligurian curve appears to have an offset of at least 1.5 and its difference from the other curves reduces as the NMH increases, possibly due to the predominant barrier effect in the high-orography simulations. The offset suggests that for the Ligurian case, other factors – that is, the topographic influence and also the outflow from the Po Valley (see Chapter 6) – contribute to produce low-level blocking so that it does not disappear as the orographic barrier effect vanishes.

Naturally, we have to consider also model errors when discussing the significance of the BWI vs NMH plot, as they can considerably alter both parameters. Consider, for instance, the slight misplacement of the BW boundary by the MOLOCH model in the Alpine case (see subsection 4.2): such an error could have brought to an overestimation of the BWI in that case. Humidity have to be accounted for as well, as latent heat release can play an important role in shifting nonlinear patterns to higher values of the NMH, even cancelling them in some cases (see, for instance, Miglietta and Buzzi, 2004). The dry Brunt-Väisälä frequency N should then be replaced with the moist one N_m which accounts for latent heat release effects.

7.2 Barrier winds in the Italian region

As we saw in Chapter 2 through our climatology, BWs episodes occur with noticeable frequency in the Italian region, due to the presence of numerous high mountain ranges.

The mountain range which most frequently produces BWs is the Apennines one, because of its considerable height and the fact that cold northeasterly winds often blow over the Adriatic Sea, constituting the ideal incoming flow to be deflected through barrier effect. On the other hand, winds coming from the Tyrrhenian Sea are warmer and moister than those coming from the Balkans, so that a smaller number of BWs episodes occurs on the western side of the Apennines.

Several reasons can explain this difference. Latent heat release effects play a significant role, as already noted. Nonetheless, we deem baroclinicity effects to be noteworthy as well: when airflow impinges on a mountain range that is roughly oriented along a meridian and is deflected due to the orographic barrier effect, a southerly or northerly BW will originate depending on whether the incoming flow is westerly or easterly; assuming a negative meridional temperature gradient is present, this will advect warmer air northwards in the former case, colder air southwards in the latter. Since, as we saw, the presence of a low-level cold pool can reinforce the barrier effect, thereby prolonging the duration of the BWs episode, an advection of colder air southwards would tend to increase the duration of BWs episodes and to favour their occurrence; conversely, the advection of warmer air northwards would hinder the formation and/or the development of BWs. This reasoning is valid for temperature gradients oriented in any way: what is relevant in affecting the development of BWs events in a certain region is the average orientation of temperature gradients over time.

Baroclinicity effects could explain the considerable difference between the number of Adriatic events and that of Tyrrhenian events. Indeed, we already pointed out how significant is temperature advection by BWs while discussing the Alpine case study in Chapter 4. A similar phenomenon has been analyzed by van den Broeke and Gallee (1996), who commented about the possibility that BWs off the western coast of Greenland advect warm and moist air northwards, thereby boosting the melting of the ice sheet.

The Alps are the highest and most extensive Italian mountain range, although they do not frequently produce BWs. This is due to several factors, such as meteorological variability and the relative infrequency of intense southerly low-level winds blowing over the Adriatic Sea. The first factor can be explained as follows: since the low-level incoming flow required to produce BWs on the southern side of the Alps is usually associated with a cyclone over northwestern or northern Italy, it often happens that BWs are generated but a “steady state” is hardly attained, as the rapid movement of the cyclone breaks the development of the event; such an occurrence has been observed several times while

analyzing weather for the climatology in Chapter 2, with weak, short or intermittent BWs that were not included in it. As for the second factor, strong southerly winds over the Adriatic Sea are also associated with flow over the Alps, with intense orographic precipitation. In this case, there is no upstream blocking and low-level winds are not brought to rest even in the immediate vicinity of the mountains.

The Dinaric Alps also generate frequently BWs, possibly due to their compact distribution, with high peaks continuously distributed from Albania to Slovenia. This shape and distribution, together with the presence of high topography in Albania, enhances the low-level convergence over the southern Adriatic Sea and the pressure increase caused by the barrier effect, making Dinaric events quite frequent, much more than Tyrrhenian ones which feature a much more unconfined incoming flow.

Finally, Ligurian episodes are quite noteworthy for the great topographic contribute to the deflection of southerly to southeasterly low-level winds blowing over the Tyrrhenian Sea. Such a deflection is so common that pseudo barrier winds are quite frequently observed over the western Ligurian Sea – naturally they were not included in our climatology due to their short duration or their being weak.

Both our climatology and our case studies simulations are in good agreement with previous observations and simulations (Parish, 1982; Marwitz, 1983; O'Connor et al., 1994; Buzzi et al., 1997) as far as wind speeds and the BW extent are concerned. The BW largest speeds, that in the Alpine case (see Chapter 4) were predicted to exceed 30 m/s, have been found in all cases between 500 m and 1000 m altitude, that is halfway between mountain foot and mountain top or slightly below, just as previously observed.

7.3 The impact of BWs on weather patterns

As we discussed earlier in Chapter 1, BWs can have a significant influence on weather patterns in the region where they occur, dramatically altering weather conditions with respect to those that would be found in their absence.

A first example of this impact has been shown in Chapter 4 while discussing the Alpine case study: we pointed out the presence of strong gradients in both wind and temperature over the Veneto plains and, to a certain extent, over the whole Po Valley. It is not simple for meteorological models to perform adequately accurate forecasts in these cases, as a small overestimation or underestimation of the BW extent can yield large errors in the predicted wind speed and/or direction, as we observed in section 4.2.

The key role of the BW in advecting moisture and temperature, thereby reinforcing the upstream blocking, was also highlighted in Chapter 4, as well as the importance of the cold pool in producing and prolonging the BWs event. In the Alpine case the cold pool is also responsible for a remarkable shift in the precipitation distribution, which features

maxima more upstream with respect to the mountain peaks, while the presence of the BWs enhances the low-level convergence, generating intense rainfall. The combined effect of the cold pool and the BWs was, in that particular day (February 11, 2013), the generation of a moderate to intense snowfall over the Veneto plains and the northeastern Po Valley.

For these reasons the barrier wind is quite a "complete" mesoscale phenomenon, being able to profoundly modify the surrounding circulation and hence weather conditions over a large area. The Alpine event analyzed in Chapter 4 is quite a significant episode, featuring intense low-level winds with sharp vertical shear associated, a marked cold pool and intense (non-convective) rainfall. The Alpine case study is also the only *first-type* event we performed a dedicated simulation on. This type of episodes is particularly interesting in that it features a separated low-level flow, with BWs found all the way in front of the incoming flow and thereby strong horizontal shear present throughout.

The Ligurian case study (Chapter 6) is also remarkable for its duration and for the considerable influence that the topography of the area has on the incoming flow, which is channelled and deflected also in reduced-orography simulations. As a result, intense low-level easterly winds have been predicted for over 72 hours off the eastern Ligurian and Provençal coasts.

Through the analysis of the three case studies in Chapters 4, 5 and 6, we deduced that a relatively low resolution – like the one we set for BOLAM, 9 km – is sufficient to adequately simulate BWs episodes in the Italian region. A higher-resolution, non-hydrostatic model, like MOLOCH, seems necessary in cases of strong convection, which was not present in any of our case studies. Small-scale orographic effects – such as lee waves generation – are better resolved by a non-hydrostatic model, although it is sufficient to use a hydrostatic one, like BOLAM, when the horizontal scale of the orography is large enough.

Chapter 8

Conclusions and future perspectives

In the present work, the dynamics of BWs in the Italian region has been analyzed. A first characterization of them has been developed in a two-year climatology in which BWs events have been classified with respect to their speed and frequency of occurrence and to their upstream Froude number, which has been estimated from the low-level temperature profile, the upstream wind speed and the average mountain height. The daily forecast archive of the BOLAM and MOLOCH meteorological models, developed within the CNR–ISAC institute in Bologna, have been employed to carry out the climatology. The distribution of the events with respect to the Froude number has been subsequently analyzed.

Afterwards, three case studies – an Alpine one, a Dinaric one and a Ligurian one – have been selected from the climatology and dedicated simulations have been performed on them, using again BOLAM and MOLOCH models. The simulations have been analyzed and a detailed characterization of BWs in the three regions has been carried out. For the Alpine episode, model forecasts have been contrasted with observational data obtained from Veneto agency ARPAV (*Agenzia Regionale per la Prevenzione e Protezione Ambientale del Veneto*, Veneto Environmental Preservation and Protection Regional Agency).

Sensitivity tests were subsequently performed on the three case studies by gradually lowering the mountains up to the point that BWs were not predicted anymore. In this way, the influence of the orography on wind circulation has been investigated with respect to the upstream Froude number, which is modified together with the height of the mountains. A Barrier Wind Index (BWI) has been devised in order to assess the BW extent.

Both our climatology and our dedicated simulations are in good agreement with idealized theory of low Froude number flow over an isolated orography. However, the applicability of the theory to the real(istic) atmosphere is limited by the considerable complexity, heterogeneity and variability that characterizes it with respect to an idealized

atmosphere. The presence of strong horizontal wind shear has been found to be the most complex feature to be simulated via meteorological models, and theory does not account for it as previously noted by Pierrehumbert and Wyman (1985) and by Smolarkiewicz and Rotunno (1990).

Barrier winds have been found to be quite an interesting phenomenon, capable of influencing the surrounding circulation over a large area and of modifying markedly weather patterns. The Barrier Wind Index (BWI) has been shown to constitute a useful diagnostic tool for assessing the BW extent and connecting it to other features of the associated upstream blocking event.

In perspective, a further analysis of the formation, development and evolution of barrier winds is required for a better comprehension of their nature and features. A noteworthy aspect that is worth investigating is the separation of the BW from the surrounding circulation, which is found in some cases only – that we referred to as *first-type events*.

A worthwhile approach would be that of undertaking idealized simulations, in order to isolate the most significant factors which influence the formation, development and persistence of BWs. Just as we performed sensitivity tests by lowering the realistic orography, the role of stratification, latent heat release effects, vertical wind shear, the shape of the mountain, the presence of a pre-existing or advected *cold pool* etc. are all significant factors that are worth being investigated by altering parameters within the frame of an idealized simulation, in which it is possible to control every aspect of the incoming flow, the orography and the evolution of meteorological quantities.

Finally, after having isolated the most important factors, it is necessary to identify their role in the occurrence of BWs episodes in selected regions by developing a detailed climatology, possibly using both meteorological models and observational data so as to ascertain as accurately as possible the data reliability.

The present study has large economic, societal and meteorological applicability: from assessing the frequency of barrier winds episodes over a selected region in order to devise, for instance, wind turbine functioning time policies or maritime routes optimization; to the study of the influence of coastal barrier winds in polar regions on weather and climate in the surroundings; to the forecasting of air quality or severe weather over certain regions where strong gradients could be found, resulting in sharp differences in weather between close locations.

Acknowledgements

I would like to gratefully thank my advisor, prof. Andrea Buzzi, for his valuable advice and precious help throughout this work; all members of the Dynamic Meteorology Research Group of the CNR–ISAC institute in Bologna, who made my time spent there interesting and worthwhile; dr. Massimo Ferrario and dr. Marco Dianin from ARPAV Veneto, who provided me with fundamental meteorological data and were greatly kind and helpful when I needed their assistance.

I would like to thank all my friends and colleagues at the University of Bologna for having supported me and for having donated so many enjoyable moments to me during these years. A special and huge thank goes to Michela and Olimpia, whose support has been inestimable and whose friendship has been, is and will always be precious to me.

The greatest thank is for my parents and sister, who have always been there for me and will never stop accompanying me through the delights and predicaments of life.

References

Bertò, A., et al., 2004: Back-tracking water vapour contributing to a precipitation event over Trentino: a case study. *Meteorologische Zeitschrift*, **13 (3)**, 189–200.

Bousquet, O. and B. F. Smull, 2003: Observations and impacts of upstream blocking during a widespread orographic precipitation event. *Quarterly Journal of the Royal Meteorological Society*, **129 (588)**, 391–409.

Buzzi, A. and S. Tibaldi, 1977: Inertial and frictional effects on rotating and stratified flow over topography. *Quarterly Journal of the Royal Meteorological Society*, **103 (435)**, 135–150.

Buzzi, A. and S. Tibaldi, 1978: Cyclogenesis in the lee of the Alps: A case study. *Journal of the Royal Meteorological Society*, **104 (440)**, 271–287.

Buzzi, A., et al., 1997: Low-level jet simulation over the Southern Ocean in Antarctica. *Tellus Series A*, **49 (2)**, 263–276.

Buzzi, A., et al., 1998: Numerical simulations of the 1994 Piedmont flood: Role of orography and moist processes. *Monthly Weather Review*, **126 (9)**, 2369–2383.

Buzzi, A., et al., 2013: Heavy rainfall episodes over Liguria of autumn 2011: numerical forecasting experiments, submitted to NHESS; published online.

Chen, W. D. and R. B. Smith, 1987: Blocking and deflection of airflow by the Alps. *Monthly Weather Review*, **115 (11)**, 2578–2597.

Clausen, H. B., et al., 1979: Surface accumulation on Ross Ice Shelf. *Antarctic Journal of the United States*, **14 (5)**, 68–72.

Drazin, P. G., 1961: On the steady flow of a fluid of variable density past an obstacle. *Tellus*, **13 (2)**, 239–251.

Ficker, H. v., 1906: *Der Transport kalter Luftmassen ueber die Zentral-Alpen*. Denkschriften der Math.-Naturwiss. Klasse der K. Akad. der Wiss., Wien, 200 pp.

King, J. C. and J. Turner, 2007: *Antarctic Meteorology and Climatology*. Cambridge University Press, 424 pp.

Kozo, T. L., 1980: Mountain barrier baroclinity effects on surface winds along the Alaskan Arctic Coast. *Geophysical Research Letters*, **7 (5)**, 377–380.

Loescher, K. A., et al., 2006: Climatology of barrier jets along the Alaskan coast. Part I: Spatial and temporal distributions. *Monthly Weather Review*, **134 (2)**, 437–453.

Long, R. R., 1953: Some aspects of the flow of stratified fluids: I. A theoretical investigation. *Tellus*, **5 (1)**, 42–58.

Long, R. R., 1954: Some aspects of the flow of stratified fluids: II. Experiments with a two-fluid system. *Tellus*, **6 (2)**, 97–115.

Long, R. R., 1955: Some aspects of the flow of stratified fluids: III. Continuous density gradients. *Tellus*, **7 (3)**, 341–357.

Marwitz, J. D., 1983: The kinematics of orographic airflow during Sierra storms. *Journal of the Atmospheric Sciences*, **40 (5)**, 1218–1227.

Marwitz, J. D., 1987: Deep orographic storms over the Sierra Nevada. Part I: Thermodynamic and kinematic structure. *Journal of the Atmospheric Sciences*, **44 (1)**, 159–173.

Miglietta, M. M. and A. Buzzi, 2004: A numerical study of moist stratified flow regimes over isolated topography. *Quarterly Journal of the Royal Meteorological Society*, **130**, 1749–1770.

Moore, G. W. K. and I. A. Renfrew, 2005: Tip jets and barrier winds: A QuikSCAT climatology of high wind speed events around Greenland. *Journal of Climate*, **18 (18)**, 3713–3725.

O'Connor, W. P., et al., 1994: Cyclonically forced barrier winds along the Transantarctic Mountains near Ross Island. *Monthly Weather Review*, **122**, 137–150.

Orlanski, I. and B. D. Gross, 1994: Orographic modification of cyclone development. *Journal of the Atmospheric Sciences*, **51 (4)**, 589–611.

Parish, T. R., 1982: Barrier winds along the Sierra Nevada mountains. *Journal of Applied Meteorology*, **21 (7)**, 925–930.

Parish, T. R., 1983: The influence of the Antarctic Peninsula on the wind field over the western Weddell Sea. *Journal of Geophysical Research: Oceans*, **88**, 2684–2692.

Pierrehumbert, R. T. and B. Wyman, 1985: Upstream effects of mesoscale mountains. *Journal of the Atmospheric Sciences*, **42 (10)**, 977–1003.

Queney, P., 1948: The problem of air flow over mountains: A summary of theoretical studies. *Bulletin of the American Meteorological Society*, **29**, 16–26.

Rotunno, R. and R. Ferretti, 2001: Mechanisms of intense Alpine rainfall. *Journal of the Atmospheric Sciences*, **58 (13)**, 1732–1749.

Schwerdtfeger, W., 1974: Mountain barrier effect on the flow of stable air north of the Brooks Range. *Proceedings of the 24th Alaska Science Conference*, University of Alaska, 204–208.

Schwerdtfeger, W., 1975: The Effect of the Antarctic Peninsula on the temperature regime of the Weddell Sea. *Monthly Weather Review*, **103 (1)**, 45–51.

Schwerdtfeger, W., 1979: Meteorological aspects of the drift of ice from the Weddell Sea toward the mid-latitude westerlies. *Journal of Geophysical Research: Oceans*, **84**, 6321–6328.

Schwerdtfeger, W., 1984: *Weather and Climate of the Antarctic*. Elsevier Sciences Publisher, 261 pp.

Scorer, R. S., 1955: Theory of airflow over mountains: IV. Separation of flow from the surface. *Quarterly Journal of the Royal Meteorological Society*, **81**, 340–419.

Sheppard, P. A., 1956: Airflow over mountains. *Quarterly Journal of the Royal Meteorological Society*, **82 (354)**, 528–529.

Simpson, G. C., 1919: *Meteorology: British Antarctic Expedition 1910-13*. Thacker, Spink, Calcutta, 464 pp.

Smith, R. B., 1979: The influence of mountains on the atmosphere. *Advances in Geophysics*, **21**, 87–230.

Smith, R. B., 1980: Linear theory of stratified hydrostatic flow past an isolated mountain. *Tellus*, **32 (4)**, 348–364.

Smith, R. B., 1982: Synoptic observations and theory of orographically disturbed wind and pressure. *Journal of the Atmospheric Sciences*, **39 (1)**, 60–70.

Smith, R. B., 1988: Linear theory of hydrostatic flow over an isolated mountain in isosteric coordinates. *Journal of the Atmospheric Sciences*, **45**, 3889–3896.

Smolarkiewicz, P. K. and R. Rotunno, 1989: Low Froude number flow past three-dimensional obstacles. Part I: Baroclinically generated lee vortices. *Journal of the Atmospheric Sciences*, **46 (8)**, 1154–1164.

Smolarkiewicz, P. K. and R. Rotunno, 1990: Low Froude number flow past three-dimensional obstacles. Part II: Upwind flow reversal zone. *Journal of the Atmospheric Sciences*, **47 (12)**, 1498–1511.

van den Broeke, M. R. and H. Gallee, 1996: Observation and simulation of barrier winds at the western margin of the Greenland ice sheet. *Quarterly Journal of the Royal Meteorological Society*, **122**, 1365–1383.

Wegener, A., 1911: *Thermodynamik der atmosphäre*. Verlag J. A. Barth, Leipzig, 331 pp.

BOLAM and MOLOCH references

Arakawa, A. and V. R. Lamb, 1977: Computational design of the basic dynamical processes of the UCLA general circulation model. *Methods in Computational Physics*, **17**, 173–265.

Billett, S. J. and E. F. Toro, 1997: On WAF-type schemes for multidimensional hyperbolic conservation laws. *Journal of Computational Physics*, **130**, 1–24.

Blackadar, A. K., 1962: The vertical distribution of wind and turbulent exchange in a neutral atmosphere. *Journal of Geophysical Research*, **67 (8)**, 3095–3102.

Bougeault, P. and P. Lacarrere, 1989: Parameterization of orography-induced turbulence in a mesobeta-scale model. *Monthly Weather Review*, **117 (8)**, 1872–1890.

Buzzi, A., et al., 1994: Validation of a limited area model in cases of mediterranean cyclogenesis: Surface fields and precipitation scores. *Meteorology and Atmospheric Physics*, **53 (3-4)**, 137–153.

Buzzi, A., et al., 1998: Numerical simulations of the 1994 Piedmont flood: Role of orography and moist processes. *Monthly Weather Review*, **126 (9)**, 2369–2383.

Buzzi, A. and L. Foschini, 2000: Mesoscale meteorological features associated with heavy precipitation in the southern Alpine region. *Meteorology and Atmospheric Physics*, **72**, 131–146.

Buzzi, A., et al., 2003: A case study of an orographic cyclone south of the Alps during the MAP SOP. *Quarterly Journal of the Royal Meteorological Society*, **129 (591)**, 1795–1818.

Buzzi, A., et al., 2011: High-resolution short-range wind forecasts with the ISAC model MOLOCH. *Proceedings of the COST Action ES1002 "WIRE" Workshop, 22–23 March 2011, Nice, France*.

Cavaleri, L., et al., 2010: Predictability of extreme meteo-oceanographic events in the Adriatic Sea. *Quarterly Journal of the Royal Meteorological Society*, **136**, 400–413.

Charnock, H., 1955: Wind stress on a water surface. *Quarterly Journal of the Royal Meteorological Society*, **81 (350)**, 639–640.

Chessa, P. A., et al., 2004: Application of a limited-area short-range ensemble forecast system to a case of heavy rainfall in the Mediterranean region. *Weather and Forecasting*, **19**, 566–581.

Corazza, M., et al., 2003: Simulating extreme precipitation with a mesoscale forecast model. *Meteorology and Atmospheric Physics*, **83**, 131–143.

Davolio, S., et al., 2006: Orographic influence on deep convection: case study and sensitivity experiments. *Meteorologische Zeitschrift*, **15 (2)**, 215–223.

Davolio, S., et al., 2007: High resolution simulations of an intense convective precipitation event. *Meteorology and Atmospheric Physics*, **95 (3-4)**, 139–154.

Davolio, S., et al., 2009a: High resolution simulations of a flash flood near Venice. *Natural Hazards and Earth System Sciences*, **9**, 1671–1678.

Davolio, S., et al., 2009b: Numerical forecast and analysis of a tropical-like cyclone in the Ionian Sea. *Natural Hazards and Earth System Sciences*, **9**, 551–562.

Davolio, S., et al., 2009c: Orographic triggering of long-lived convection in three dimensions. *Meteorology and Atmospheric Physics*, **103**, 35–44.

Diomede, T., et al., 2008: Discharge prediction based on multi-model precipitation forecasts. *Meteorology and Atmospheric Physics*, **101**, 245–265.

Drofa, O. and P. Malguzzi, 2004: Parameterization of microphysical processes in a non-hydrostatic prediction model. *Proceedings of the 14th International Conference on Clouds and Precipitation (ICCP), Bologna, Italy*.

Fantini, M. and P. Malguzzi, 2008: Numerical study of two-dimensional moist symmetric instability. *Advances in Geosciences*, **17**, 1–4.

Fantini, M., et al., 2012: Numerical study of slantwise circulations in a strongly-sheared pre-frontal environment. *Quarterly Journal of the Royal Meteorological Society*, **138**, 585–595.

Georgelin, M., et al., 2000: The second COMPARE exercise: A model intercomparison using a case of a typical mesoscale orographic flow, the PYREX IOP3. *Quarterly Journal of the Royal Meteorological Society*, **126**, 991–1030.

Gyakum, J. R., et al., 1996: A regional model intercomparison using a case of explosive oceanic cyclogenesis. *Weather and Forecasting*, **11**, 521–543.

Kain, J. S. and J. M. Fritsch, 1990: A one-dimensional entraining/detraining plume model and its application in convective parameterization. *Journal of the Atmospheric Sciences*, **47**, 2784–2802.

Kain, J. S. and J. M. Fritsch, 2004: The Kain-Fritsch convective parameterization: an update. *Journal of Applied Meteorology*, **43 (1)**, 170–181.

Lagouvardos, K., et al., 2003: The meteorological model BOLAM at the National Observatory of Athens: Assessment of two-year operational use. *Journal of Applied Meteorology*, **42**, 1667–1678.

Lehmann, R., 1993: On the choice of relaxation coefficients for Davies' lateral boundary scheme for regional weather prediction models. *Meteorology and Atmospheric Physics*, **52 (1-2)**, 1–14.

Malguzzi, P. and N. Tartaglione, 1999: An economical second order advection scheme for explicit numerical weather prediction. *Quarterly Journal of the Royal Meteorological Society*, **125 (558)**, 2291–2303.

Malguzzi, P., et al., 2006: The 1966 "century" flood in Italy: A meteorological and hydrological revisitation. *Journal of Geophysical Research: Atmospheres*, **111 (D24)**.

Malguzzi, P., et al., 2010: Numerical study of a banded precipitation event over Italy. *Advances in Geosciences*, **26**, 19–23.

Miglietta, M. M. and A. Buzzi, 2004: A numerical study of moist stratified flow regimes over isolated topography. *Quarterly Journal of the Royal Meteorological Society*, **130**, 1749–1770.

Mlawer, E. J., et al., 1997: Radiative transfer for inhomogeneous atmospheres: RRTM, a validated correlated-k model for the longwave. *Journal of Geophysical Research: Atmospheres*, **102 (D14)**, 16 663–16 682.

Monin, A. S. and A. M. Obukhov, 1954: Basic laws of turbulent mixing in the surface layer of the atmosphere. *Trudy Geofizicheskogo Instituta, Akademiya Nauk SSSR*, **151**, 163–187.

Morcrette, J. J., 1991: Radiation and cloud radiative properties in the European Centre for Medium Range Weather Forecasts forecasting system. *Journal of Geophysical Research: Atmospheres*, **96 (D5)**, 9121–9132.

Nagata, M., et al., 2001: A mesoscale model intercomparison: A case of explosive development of a tropical cyclone (COMPARE III). *Journal of the Meteorological Society of Japan*, **79**, 999–1033.

Orlandi, E., et al., 2010: A nudging scheme to assimilate satellite brightness temperature in a meteorological model: Impact on representation of African mesoscale convective systems. *Quarterly Journal of the Royal Meteorological Society*, **136 (647)**, 462–474.

Richard, E., et al., 2007: Quantitative precipitation forecasting in mountainous regions: The advances achieved by the Mesoscale Alpine Programme. *Quarterly Journal of the Royal Meteorological Society*, **133**, 831–846.

Ritter, B. and J. F. Geleyn, 1992: A comprehensive radiation scheme for numerical weather prediction models with potential applications in climate simulations. *Monthly Weather Review*, **120 (2)**, 303–325.

Rotach, M. W., et al., 2009: MAP D-PHASE: Real-time demonstration of weather forecast quality in the Alpine region. *Bulletin of the American Meteorological Society*, **90 (9)**, 1321–1336.

Tettamanti, R., et al., 2002: *Numerical simulation of katabatic winds with a non-hydrostatic meteorological model*. Roma, 95 pp.

Zampieri, M., et al., 2005: Sensitivity of quantitative precipitation forecasts to boundary layer parameterization: a flash flood case study in the Western Mediterranean. *Natural Hazards and Earth System Science*, **5 (4)**, 603–612.